Modelling of Hydrogen Electric Propulsion System for Future Regional Aircraft

A study on Bombardier Dash 8-Q300 Aircraft during Go-Around Manoeuvre

Avani Patidar

TU Delft

Modelling of Hydrogen Electric Propulsion System for Future Regional Aircraft

A study on Bombardier Dash 8-Q300 Aircraft during Go-Around Manoeuvre

Thesis report

by

Avani Patidar

submitted to obtain the degree of Master of Science in Aerospace Engineering
at the Delft University of Technology
to be defended publicly on May 23rd, 2024 at 13:00.

Thesis committee

Chair:	Dr. M.D. Pavel
Supervisors:	Dr Ir. M.M. van Paassen
	Dr Ir. Clark Borst
	Ir. O. Stroosma
External examiner:	Dr. Ir. M.F.M. Hoogreef
Place:	Faculty of Aerospace Engineering, Delft
Project Duration:	September, 2023 - May, 2024
Student number:	5719607

Cover Image Credits: De Havilland Aircraft of Canada Limited

An electronic version of this thesis is available at `http://repository.tudelft.nl/`.

Faculty of Aerospace Engineering · Delft University of Technology

Copyright © Avani Patidar, 2024
All rights reserved.

Preface

This document marks the culmination of my eight-month thesis journey as part of my Aerospace Engineering master's programme at TU Delft. It represents my humble contribution towards the advancement and implementation of hydrogen-based propulsion technologies in aviation, which will aid the industry's ongoing energy transition.

The report contains two main sections: a comprehensive literature review that discusses the current research landscape on aviation's energy transition and various aspects of hydrogen-electric propulsion powertrains, and a scientific article outlining a modelling framework for hydrogen-electric powertrains in regional aircraft. This framework aims to assist in the integration of this innovative propulsion system into operational aircraft scenarios by supporting the evaluation of flight procedural changes.

I am immensely grateful to my supervisors, Dr. Ir. M.M. van Paassen, Dr. Ir. Clark Borst, and Ir. O. Stroosma, for providing me with the opportunity to work on this novel project and for their invaluable guidance and suggestions throughout the process. I have greatly appreciated our weekly meetings and the wealth of knowledge I have gained from our discussions. Furthermore, I express my gratitude to Dr. M.D. Pavel and Dr. Ir. M.F.M. Hoogreef for generously volunteering their time to serve on the thesis defence committee.

I extend my sincere appreciation to my friends Aashna and Manini for their assistance in reviewing the technical aspects of the project. I am also thankful to Devashish, Pranshul, Jagadish, Mrunmayee and Shubham for their companionship during lunchtime conversations and walks, offering much-needed respite from the demands of thesis work.

To my cherished friends and family, both near and far, your unwavering support and encouragement have been a constant source of strength and motivation. Finally, I want to express my heartfelt gratitude to my father, mother, and brother. Your love, guidance, and unwavering belief in my abilities have been the driving force behind this journey and the basis of my perseverance, and for that, I am eternally grateful.

Avani Patidar
Delft, May 23rd 2024

Contents

List of Figures v

I Literature Review & Research Definition 1

1 General Introduction 2

2 Literature Review 4
2.1 Sustainable Aviation . . . 4
2.2 Hydrogen-Based Aviation . . . 4
2.3 Hydrogen-Electric Propulsion for Regional Aircraft . . . 7
2.4 Powerplant Components . . . 9
2.5 Powertrain Modeling and Operational Strategy . . . 12
2.6 Go-Around . . . 13

3 Research Questions 15

4 Project Plan 16
4.1 Methodology . . . 16
4.2 Expected Results . . . 17
4.3 Planning . . . 19

References 24

II Scientific Article 25

5 Modelling and Operational Analysis of Hydrogen-Electric Powertrain for Future Regional Aircraft During A Go-Around 26
5.1 Introduction . . . 27
5.2 Background . . . 29
5.3 Methodology . . . 35
5.4 Model Simulation and Operational Envelope Exploration Setup . . . 53
5.5 Results . . . 57
5.6 Discussion . . . 69
5.7 Conclusion . . . 70

III Appendix 77

A Longer Duration Simulation Results 78

B All Graphs from Operational Analysis 80

C Example Input to DIGITAL DATCOM 89

Nomenclature

List of Abbreviations

AC	Alternating Current
APU	Auxiliary Power Unit
BoP	Balance of Plant
BSE	Battery Specific Energy
DC	Direct Current
DOF	Degree of freedom
EOM	Equations of Motion
FAA	Federal Aviation Administration
FC	Fuel Cell
FCSD	Flight Control System Design
HEP	Hydrogen Electric Propulsion
HEPS	Hydrogen Electric Propulsion System
HFC	Hydrogen Fuel Cell
IATA	International Air Transport Association
ICAO	International Civil Aviation Organization
ICCT	International Council of Clean Transportation
LT-PEMFC	Low-Temperature Proton Exchange Membrane Fuel Cell
MCL	Maximum Climb Power
MCR	Maximum Cruise Rating
MSE	Mean Squared Error
MTOM	Maximum Take-off Mass
MTOP	Maximum Take-off Power
MTOW	Maximum Take-off Weight
nMAE	Normalized Mean Absolute Error
NTOP	Maximum Take-off Power
OBM	On-board Model
OEW	Operating Empty Weight
PEMFC	Proton Exchange Membrane Fuel Cell
PMAD	Power Management and Distribution
RMSE	Root Mean Square Error
SAF	Sustainable Aviation Fuel
SHP	Shaft Horse Power
SoC	State of Charge
SOFC	Solid Oxide Fuel Cells
SOP	Standard Operating Procedures
TMS	Thermal Management System
UAV	Unmanned Aerial Vehicle

List of Figures

2.1 Schematic of basic fuel cell [23] . . . 5
2.2 Fuel cell structure of PEMFC [25] . . . 6
2.3 Hybrid-electric propulsion system based on hydrogen-based fuel cells and batteries [6] . . . 9
2.4 Example of a go-around manoeuvre [74] . . . 14

4.1 Proposed Architecture of the Powertrain . . . 17
4.2 Planning Gantt Chart [Updated: Mid-Term Review Meeting] . . . 18

A.1 Simulation Results of the HEPS Powertrain Engine: Longer Duration . . . 79

B.1 Battery Initial SoC Sensitivity Analysis Graphs . . . 81
B.2 Battery Nominal Capacity Sensitivity Analysis Graphs . . . 82
B.3 Aircraft Mass Sensitivity Analysis Graphs . . . 83
B.4 Go-Around Speed Sensitivity Analysis Graphs . . . 84
B.5 Propeller Efficiency Sensitivity Analysis Graphs . . . 85
B.6 Fuel Cell Operating Temperature Sensitivity Analysis Graphs . . . 86
B.7 Battery Thermal Mass Sensitivity Analysis Graphs . . . 87
B.8 Hybridization factor Sensitivity Analysis Graphs . . . 88

Part I

Literature Review & Research Definition

*Main deliverable for the Research Proposal Review meeting (week 7)
**This section serves as an interim deliverable and was created before the development of the scientific article. As such, it has not been edited for consistency with the article.

1

General Introduction

In 2020, the International Council of Clean Transportation (ICCT) published a report that casts light on the environmental impact of regional air transport. It revealed that regional aviation contributes to 5% of global aviation emissions and, more alarmingly, mass of CO_2 emitted increased by 9% from 2013 to 2019 [1]. The increase in emissions was primarily attributed to the slow advancements in fuel efficiency for regional aircraft, as the number of flights remained relatively steady during the period. Notably, even two of the top 10 regional aircraft, the De Havilland Dash 8-Q400 and the ATR 72-600, celebrated for their fuel efficiency, recorded concerning emissions spikes between 2013 and 2019 [1]. These disconcerting figures underscore the pressing need for the implementation of fuel-efficient and environmentally friendly propulsion systems in the regional aviation sector.

In response to the escalating carbon emissions within the aviation sector, hydrogen-based propulsion systems have gained significant momentum as a viable alternative to conventional fossil fuel-based mechanisms. Both the European Union, through its "Fly the Green Deal" initiative [2], and the International Air Transport Association (IATA), with its "Aircraft Technology Net-Zero Roadmap" [3], have set a clear timeline for the introduction of hydrogen-based regional aircraft into active service by 2035.

In contrast to hydrogen combustion, hydrogen fuel cells present an appealing alternative for propulsion due to their negligibly low-emission operation. Hydrogen fuel cells, unlike traditional combustion engines, don't release harmful pollutants. Instead, they produce water because of their lower operating temperature [4], making them an eco-friendly choice for powering aircraft. This inherent advantage of hydrogen fuel cells serves as the foundation for the development of hydrogen-electric propulsion systems (HEPS) in the aviation industry.

The utilisation of hydrogen fuel cells in HEPS capitalises on their high energy density and environmentally friendly attributes. These attributes have spurred a surge in efforts aimed at creating efficient and sustainable hydrogen-electric propulsion systems for aviation. However, it is essential to acknowledge that while hydrogen fuel cells offer remarkable benefits, their application for high-power requirements necessitates a more intricate and extensive balance of plant (BoP) [4, 5]. The BoP comprises diverse systems, encompassing power conditioning units, thermal management, control systems, pumps, and supplementary components. These components govern inputs, outputs, and environmental conditions, ensuring the optimal and secure operation of the fuel cell system. An intricate Balance of Plant (BoP) increases the size of the fuel cell system (FCS), leading to a higher maximum take-off mass (MTOM) for the aircraft. This heightened MTOM can potentially diminish the aircraft's overall efficiency, impacting aircraft operations and pilot procedures.

Therefore, in the pursuit of optimising hydrogen-electric propulsion systems (HEPS) for aviation, there is an increasing consensus among researchers regarding the integration of batteries as auxiliary power sources [6–8]. This integration serves as a peak power-shaving strategy to complement hydrogen fuel cells. Batteries play a crucial role in supplying additional power during high-demand flight phases. Simultaneously, they contribute to a reduction in aircraft mass by alleviating the load on the full cell system (FCS). This highlights the multifaceted nature of powertrain architecture in hydrogen-electric propulsion systems, which encompasses various critical subsystems. These include the fuel cell stack, responsible for electricity generation; the thermal management system, vital for temperature regulation; and power management, ensuring efficient energy distribution, among other components.

The successful integration of Hydrogen Electric Propulsion Systems (HEPS) into real aircraft settings necessitates an in-depth understanding of how this sophisticated system operates and interacts with human pilots across a spectrum of conditions and scenarios. Among these critical aviation phases, the go-around stands out, involving a rapid shift from approach to takeoff thrust—an essential juncture in flight operations. The reliability and performance of the propulsion system during this manoeuvre profoundly impact not only safety measures but also the overall efficiency and performance benchmarks of the aircraft. Hence, it becomes imperative to conduct a comprehensive examination of the Hydrogen-Electric Propulsion System (HEPS). Understanding the nuances of HEPS performance and functionality, especially during pivotal flight operations like go-around manoeuvres, requires detailed modelling of its intricate dynamics. This study aims to construct an HEPS model specifically designed to evaluate and analyse alterations in human interaction and flight procedures within the go-around operational phase.

2

Literature Review

This chapter presents a thorough examination of the existing body of knowledge in the field of hydrogen-electric propulsion (HEP) systems, and go-arounds. By synthesising and analysing existing literature, this chapter will lay a solid foundation for the following chapters, in which a comprehensive model for the HEP systems will be developed and simulated.

2.1. Sustainable Aviation

The aviation industry has grown steadily over the last few decades. This expansion also resulted in aviation accounting for 2% of global energy-related CO_2 emissions in 2022, with growth outpacing that of rail, road, or shipping in recent decades [9] . In fact, as stated to a report by the Advisory Council for Aviation Research and Innovation in Europe (ACARE), aviation contributes to up to 4% of total carbon emissions in Europe [2] . According to a study by Environmental and Energy Study Institute (EESI) commercial aviation contributed to around 5% of world's total climate impact which includes the non-CO_2 emissions such as aircraft contrails and NO_x etc.[10] . The research also predicts that with the current trend of growth, these emissions could triple by 2050. To address the challenge of carbonising the aviation industry, various international organisations, such as the International Air Transport Association (IATA) [11] , the International Civil Aviation Organization (ICAO) [12] , and the ICCT, have committed to achieving net-zero CO_2 emission goals by 2050. In light of these policy changes, the aviation industry is actively exploring low-carbon emitting fuel alternatives, including Sustainable Aviation Fuel (SAF), batteries, and liquid hydrogen solutions.

According to IATA, Sustainable Aviation Fuel, being derived from non-fossil sources, has the potential to reduce greenhouse gas emissions by 65% in 2050 [11] . However, it may not entirely eliminate emissions from aviation [13] . Batteries, on the other hand, pose challenges due to their low energy density, making them heavier and potentially less efficient for installation on commercial aircraft as stated by Eisenhut *et al.*[14] and Finger *et al.* [15] . Consequently, there is a substantial focus on hydrogen-based solutions, which encompass hydrogen combustion and hydrogen fuel cells (HFC).

2.2. Hydrogen-Based Aviation

Hydrogen serves as a promising energy storage medium owing to its carbon-free and relatively pure characteristics. Therefore, to counter the environmental concern caused by Jet A-1 fuel as well depletion of fossil fuels, hydrogen is actively being considered as a long-term replacement solution. According to a 2020 report by the European Commission [16], hydrogen combustion has the potential to reduce the climate impact of flight (CO_2 and non-CO_2 effects) by approximately 50% to 75%, while fuel-cell propulsion could offer even more substantial reductions, ranging from 75% to 90%.

Von Ohain was the first to use hydrogen as a fuel for his turbojet engine derivative, the HeS-1, in an innovative approach in 1937 [17]. Later, in the late 1950s, the United States Air Force tested the feasibility of using liquid hydrogen as a fuel for aero-engines [17] . Fast forward two decades to the oil crisis, and Brewer suggested the potential of liquid hydrogen (LH_2) as a viable commercial aircraft fuel [18]. Brewer emphasised the critical importance of a concerted effort from the aviation and scientific communities to pave the way for LH_2-fuelled aviation to become a reality. In the subsequent decades, numerous researchers and organisations explored hydrogen as a potential fuel source. In 1990, Victor conducted

research on hydrogen's potential to reduce CO_2emissions [19] . A study conducted by Hagling *et al.* in 2006 [20] highlighted that while hydrogen combustion could eliminate CO_2 emissions, it still resulted in the generation of water vapor and nitrogen oxides (NO_x), which could contribute to the greenhouse effect. Hence, it can be argued that a LH_2 combustion engine might not be the optimal choice in the pursuit of sustainable aviation propulsion systems.

2.2.1. Hydrogen Fuel Cells (HFC)

The first crude hydrogen fuel cells were developed in 1838 by William Grove, who documented his findings in an article [21] . Almost a century later, in 1932, Francis Thomas Bacon invented hydrogen-oxygen fuel cells [22] , paving the way for fuel cell technology to be commercialised. According to Li [23] , a fuel cell is an electrochemical device that directly converts the chemical energy resulting from the fuel-oxidant reaction into electrical energy. The process of breaking and forming bonds during the the fuel-oxidant reaction can be seen at the atomic level as electron rearrangement. As a result, there is an opportunity to capture electrical energy by capturing electrons as they transition to form new, lower-energy bonds. This is the primary function of fuel cells [5].

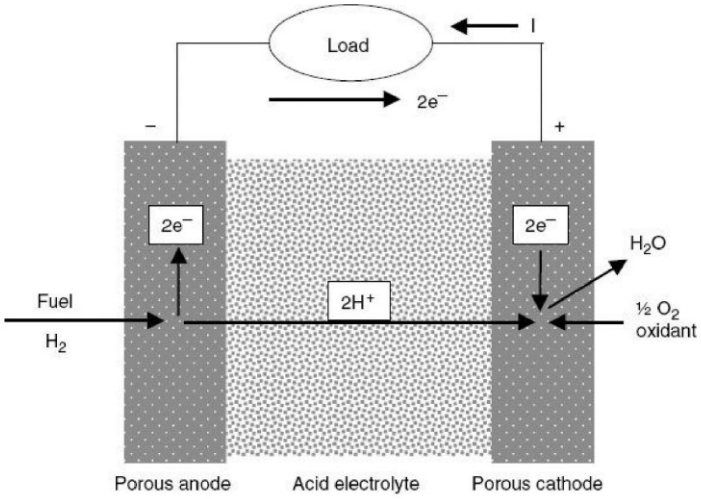

Figure 2.1: Schematic of basic fuel cell [23]

In a fuel cell, there are three primary components: a fuel electrode (anode), an oxidant electrode (cathode), and an electrolyte situated between them. The operational principle of typical acid fuel cells involves the following steps [5, 23]:

1. Molecular hydrogen is delivered from a gas flow stream to one of the electrodes, often referred to as the anode (or fuel electrode). At the anode, hydrogen (fuel) undergoes oxidation at the interface of the anode and the electrolyte:

   Anode half-cell reaction: $H_2 \Rightarrow 2H^+ + 2e^-$
2. The protons migrate through the acidic electrolyte, while the electrons are directed through an external circuit. Both protons and electrons eventually reach the cathode (or oxidant electrode).
3. At the cathode, protons and electrons combine with oxygen supplied from an external gas flow stream, leading to the formation of water:

   Cathode half-cell reaction: $\frac{1}{2}O_2 + 2H^+ + 2e^- \Rightarrow H_2O$

As seen in Figure 2.1, the completion of the circuit and the provision of electric current to the load are achieved through proton transfer within the electrolyte and the flow of electrons through the wire. In addition, the electrochemical reactions and the migration of protons result in the generation of waste heat. Thus, the comprehensive reaction within the fuel cell can be described as:

$$H_2 + \frac{1}{2}O_2 \Rightarrow H_2O + \Delta + \epsilon$$

where Δ and ϵ represent waste heat and useful electrical energy respectively.

HFCs, employing a redox reaction between hydrogen and oxygen to produce electrical current, present themselves as a remarkably promising choice for advanced and sustainable propulsion systems for aircraft. While various types of fuel cells are available today, the Proton Exchange Membrane Fuel Cell (PEMFC) stands as the top contender for fuel cell-based propulsion systems.

Proton Exchange Membrane Fuel Cell (PEMFC)
The Proton Exchange Membrane Fuel Cell (PEMFC), alternatively referred to as the Polymer Electrolyte Membrane Fuel Cell, was originally conceived in the 1960s by General Electric engineers. Its development aimed to address the limitations of solid-oxide fuel cells (SOFCs), which were characterised by the use of costly materials and restricted to stationary applications [24].

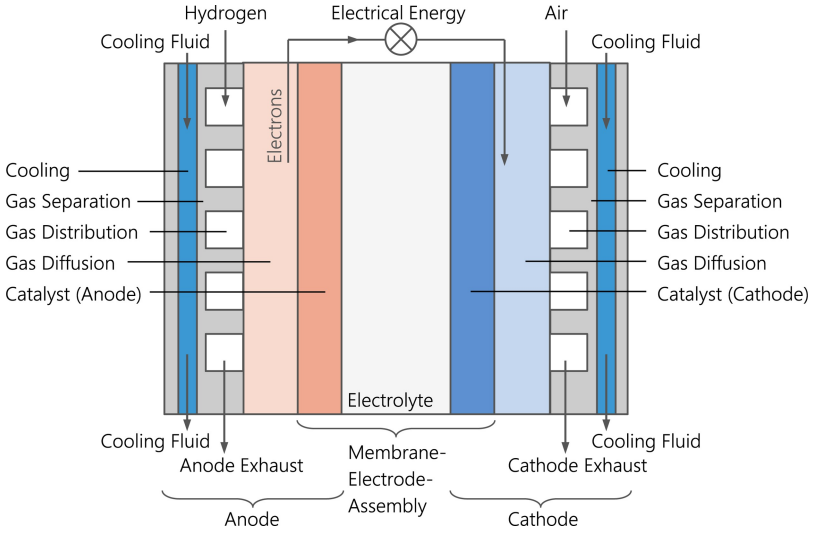

Figure 2.2: Fuel cell structure of PEMFC [25]

In their analytical study on fuel cells [26], Mekhilef *et al.* detailed the key components of a PEMFC. These components comprise bipolar plates and a membrane electrode assembly (MEA), which encompasses a catalyst layer, a gas diffusion layer, and the central Proton Exchange Membrane (PEM). The PEM's notable characteristics include low penetrability and high proton conductivity, enabling it to transport protons from the anode to the cathode while impeding the passage of electrons and reactants [26]. The PEM must be kept consistently hydrated with liquid water to ensure continuous conductivity. As a result, the temperature inside the cell must be closely monitored because water evaporation could cause the membrane to dry out. The gas diffusion layer is also mentioned as being crucial for ensuring uniform fuel access, which allows electrons to flow through the external circuit and generate electricity at the anode [5, 26]. Figure 2.2 provides a visual representation of a PEMFC fuel cell's general structure.

In their book on fuel cells [5], O'Hayre *et al.* emphasised that the PEMFC currently has the highest power density compared to all other fuel cell types, with power densities ranging from $500\,\mathrm{mW\,cm^{-2}}$ to $2500\,\mathrm{mW\,cm^{-2}}$. Furthermore, it excels in rapid start-up and shut-down capabilities, as well as the ability to operate at relatively low temperatures, typically below $90\,^{\circ}\mathrm{C}$ [5]. These distinguishing features make it particularly well-suited for a wide range of applications, including potential replacement of combustion-based propulsion systems.

2.2.2. Fuel Cell Applications for Aviation

Fuel cell systems (FCSs) have garnered considerable attention in the scientific community in recent years due to their remarkable efficiency and lack of emissions during operation. This has resulted in numerous publications focusing on their potential applications in aircraft. As Friedrich *et al.* [27] and Kadyk *et al.* [28] have noted, fuel cells offer several advantages over liquid hydrogen combustion. These advantages include durability, reliability, quiet operations, zero emissions and increased efficiency, which in turn lowers fuel requirements. Additionally, the integration of fuel cells into aircraft systems that utilise byproducts like water, heat, or exhaust air facilitates vital functions such as de-icing, cabin air conditioning, and water supply [28].

In the context of fuel cell applications in aircraft, investigations by Scholz *et al.* [29] and Kazula *et al.* [25] have highlighted the advantages of PEMFC. These advantages include high specific power, good efficiency (ranging from 40% to 60%), rapid start-up capabilities, and operation at low temperatures. Similar conclusions were drawn by Rendón in their paper on aircraft hybrid-electric propulsion [30], where it was noted that PEMFCs fuelled by hydrogen exhibit lower weight compared to SOFCs. Additionally, PEMFCs offer characteristics such as high current densities, and high energy density. Due to its advanced technology readiness level, PEMFC has already found practical application in the propulsion systems of small aircraft [25, 31].

Numerous fuel cell unmanned aerial vehicles (UAVs) and demonstrator aircraft have effectively showcased the practical application of fuel cell technology in aviation. Prominent examples encompass the Boeing Fuel Cell Demonstrator [32], Antares DLR-H2 [33], ENFICA-FC Rapid 200-FC [34], as well as several smaller UAVs [35–37]. Collaborating with H2Fly, the German Aerospace Center (DLR) transitioned from the Antares DLR-H2 and Antares-H3 to world's first hydrogen-electric passenger aircraft, the HY4. In September 2016, the HY4 aircraft took its inaugural flight [38]. In January 2023, a significant milestone was achieved in the domain of hydrogen-electric propulsion systems (HEPS) when ZeroAvia accomplished a successful flight using HEPS technology with a Dornier 228 [39]. Within just six weeks, in March 2023, Universal Hydrogen achieved another remarkable feat by flying a modified Dash-8 Q300 equipped with HEPS for a duration of 15 minutes, setting a record as the largest hydrogen-powered aircraft to date [40].

It is important to note that despite these achievements, the application of cutting-edge fuel cell technology to larger aircraft remains challenging, primarily due to the substantial power requirements at low weight, which currently exceed its capabilities, as stated in an investigation on fuel cell based aircraft by Scholz *et al.* [29]. Nonetheless, it's worth emphasising that several companies, including ZeroAvia[1] and Conscious Aerospace[2], are actively dedicated to the development of commercial hydrogen-electric aircraft. These endeavours are anticipated to result in commercial offerings in the vicinity of 2027-2028.

With anticipated advancements in fuel cell technology on the horizon, concept studies have been undertaken across various aircraft categories, as collected by Sahoo, Zhao and Kyprianidis in their research [41]. These studies encompass commuter aircraft [42–44], regional aircraft [6, 8, 45], and short-to-mid-range aircraft [46, 47]. Concepts of larger aircraft are also being investigated by NASA and Boeing [48]. These investigations aim to explore the feasibility and potential applications of fuel cell technology in diverse aviation scenarios. This research will focus on the application of HEPS on regional aircraft.

2.3. Hydrogen-Electric Propulsion for Regional Aircraft

The European Union's commitment to achieving net-zero emissions includes ambitious plans to introduce hydrogen and hybrid electric solutions for regional and short-to-medium-range (SMR) aircraft by 2030, with the possibility of these solutions entering into operational service by 2035 [2]. As a result, there has been a significant increase in research efforts dedicated to novel propulsion systems for regional aircraft in recent years. Hydrogen fuel cells (HFCs) have emerged as a point of interest in the area of innovative regional aircraft propulsion systems, and they have been integrated to varying degrees in these research efforts defined by the powertrain topology.

Zamboni *et al.* introduced a method for the conceptual design of hybrid-electric aircraft in their paper[49]. While this particular paper assumed the use of batteries rather than fuel cells, it did lay the groundwork for the conceptual design of hybrid systems that use HFCs. Palladino *et al.* [45] conducted research focusing on a parallel hybrid propulsion system, which combines a conventional gas turbine with a fuel cell system. This approach is considered a short-to-medium-term solution due to its perceived energy efficiency and lightweight characteristics, as supported by studies conducted by Zamboni *et al.* [49].

Palladino *et al.*'s paper involved retrofitting the hybrid propulsion system onto the ATR72 aircraft. Each propeller was powered by both the electric motor and the gas turbine, with the balance between the two power sources determined by the power hybridisation factor (ratio between the power supplied by the electric motor and the total power delivered to the propeller). After evaluating the weight and volume requirements for a fully hybrid flight, the paper opted to use electrical power exclusively during the climb and cruise phases of flight. The investigation then assessed emission reductions for hybridisation

[1] https://zeroavia.com/about-us/

[2] https://www.consciousaerospace.com/company

factors ranging from 0.1 to 0.5. The paper found that the highest emission reduction was achieved with a hybridisation factor of 0.45, corresponding to an electric power output of $800\,\text{kW}$ per side. The paper's conclusion highlighted the potential of hydrogen-based electric propulsion to significantly reduce aircraft emissions, even with the state-of-the-art technological capabilities available today. Other studies with similar hybrid-electric propulsion with gas turbines were conducted by Orefice et al [50] and Pastra *et al.* [51].

A fully electric powertrain based on HFCs has also been explored as a propulsion system option. This powertrain configuration features a single power path that starts at the fuel tank and through the fuel-cell system, the Power Management and Distribution Unit (PMAD), connects to the electric motor responsible for driving the aircraft's propeller.

Kazula, Staggat, and Graff conducted a comprehensive investigation into the functional and safety challenges associated with HFC systems in their research [7]. The study primarily focuses on PEMFCs as the primary energy source for electrified aircraft propulsion, identifying potential shortcomings and safety considerations. The research included a Functional Hazard Analysis and a safety assessment process following the guidelines of ARP4761 and ARP4754A, respectively. The study's key findings highlighted that, before the widespread implementation of HFCs in commercial aviation, certain design challenges must be addressed. These challenges encompass functional independence, solutions for cold start conditions, heat transfer mechanisms, and lightweight design considerations. Furthermore, the research underscored that safety concerns may arise due to the substantial amount of electric energy involved in the process.

In another research by Pontika *et al.* [8], an analysis of the mission performance characteristics of a Fuel Cell (FC) regional aircraft system was conducted, contrasting it with a conventional regional aircraft and a retrofit of a hydrogen gas turbine regional aircraft. The baseline aircraft shared geometrical similarities with the ATR72, featured twin turboprop engine models, each rated at 2 MW and had 8-propellers. The study comprehensively modelled the entire fuel cell system and assessed the aircraft's performance.

Notably, when performing the same mission as its counterparts, the fuel cell aircraft weighed more due to the additional weight of the FC system, and thus, it necessitated increased thrust requirements. The fuel consumption of the FC aircraft was significantly lower compared to that of the conventional aircraft, resulting in a slower reduction in weight over the mission duration compared to the conventional aircraft, which could affect the landing mass. According to the research, FC efficiency was lower at higher power settings, such as take-off and climb, but significantly higher at lower power settings, such as taxi and descent. In the research's conclusion, Pontika *et al.* pointed out that, despite a potential increase in propulsion system mass, an FC aircraft retrofit results in lower emissions and overall improved propulsion efficiency compared to the hydrogen gas turbine aircraft, owing to the FC's lower fuel consumption. They suggested that future efforts should focus on the design of a hybrid propulsion system by optimising the FC configuration for cruise conditions, where it excels in efficiency, and integrating it with batteries to meet take-off and climb requirements. Additionally, careful consideration was recommended in selecting the maximum FC net power to ensure sufficient power under a variety of cruise and ambient conditions, as well as accounting for potential efficiency drops in the electric power system.

2.3.1. Battery Supported Hydrogen-Electric Propulsion

Marciello *et al.* conducted a comprehensive investigation into the design of three hybrid-electric aircraft configurations [6], taking into account technology forecasts, including the usage of battery-backed PEMFC propulsion systems, in the context of the EU's GENESIS (Gauging the ENvironmEntal Sustainability of electrIc and hybrid aircraft Systems) project. Figure 2.3 depicts an energy architecture scenario in which a fuel cell system is the primary power source and batteries are used as a backup. To model distributed electric propulsion, the paper's writers used a secondary propulsion line. This research emphasises that determining the best point for maximum fuel savings is dependent on the battery usage strategy used during the flight mission. Specifically, using batteries during longer phases reduces the amount of energy drawn from the fuel cell system(s).

The study included an examination of aircraft with hybrid propulsion systems, with a Supplied Power Ratio taken into account at various stages such as take-off and climb. Under nominal conditions, this ratio represents the proportion of power supplied by the battery system relative to the total source power, which includes fuel-cell system and batteries. It was assumed that no battery power was used during the descent, landing, taxiing, alternate, and holding phases. The findings indicated that battery-backed Fuel

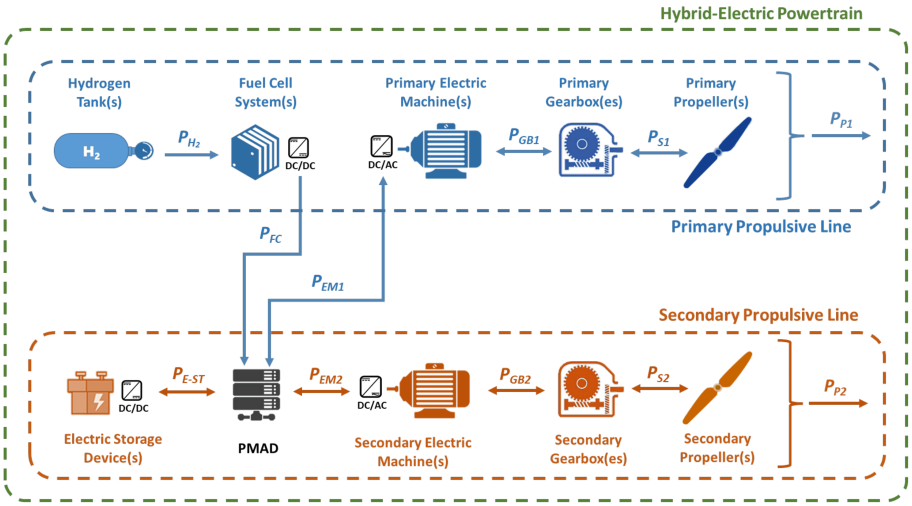

Figure 2.3: Hybrid-electric propulsion system based on hydrogen-based fuel cells and batteries [6]

Cell configurations for an aircraft similar to the ATR, designed for a range of 600 nautical miles, could yield fuel consumption reductions over 85% for a typical 200-nautical-mile mission and over 70% for a 600-nautical-mile mission.

In another research conducted by Gao *et al.* [52], research was focused on hydrogen electric hybrid aircraft. The study discussed a multiple-propeller, fixed-wing airplane that incorporated an FC/lithium battery hybrid power source system. Within this configuration, the FC system was identified as the primary power source, while the lithium batteries were seen to play a crucial role in buffering transient loads.

The paper highlighted that FC regional aircraft with a range of 1,000 kilometres could potentially achieve an 8% reduction in energy consumption and significantly decrease climate impact by 80-90% with an 15% increase in MTOM compared to conventional aircraft. To realise these benefits, the paper emphasised the importance of implementing energy management strategies in FC aircraft operations. They suggest that these strategies should be designed to accomplish various objectives, including minimising hydrogen consumption, extending the FC's operational lifespan, maximising overall system efficiency, and maintaining a narrow range for battery state-of-charge (SoC). Additionally, effective FC electric hybrid control functions were deemed essential for appropriately distributing power and torque between the FC and the electric powertrain.

2.4. Powerplant Components

In the context of a HEPS, the powerplant, like a traditional internal combustion engine, is dependent on a number of supporting subsystems to maintain optimum state of operation and ensure the reliability of the entire system. These critical subsystems, include the Balance of Plant (BoP) components which manage functions such as fuel and oxidiser supply, waste heat management, water management, power distribution, and fuel cell monitoring. Thus, these subsystems are important to consider when modelling HEPS [37].

2.4.1. Fuel Cell Stack

Accoding to Larminie and Dicks [4], a single fuel cell typically produces only 0.8 to 1.0 volts. To achieve higher voltage output, multiple fuel cells are often connected in series, forming what is known as a fuel cell stack [53]. The primary PEMFC stack configuration is known as 'bipolar plate stacking', named after the conductive plate that interconnects adjacent cells. This arrangement simplifies electrical connections between cells and reduces ohmic losses [43]. In an effort to address the voltage requirements for powering regional aircraft, Zaghari *et al.* [54] explored multi-stack configurations to enhance power output. For their research, they considered two fixed 2000V DC-bus systems for a 4MW fully electrified (retrofit) aircraft. The paper underscores that the choice of FC configurations and architecture significantly influences system weight and power loss in the event of failure, ultimately concluding that a configuration with 4 stacks

connected in series proved to be the most reliable.

2.4.2. Hydrogen Supply: Fuel Tank

Storing hydrogen on board poses a significant challenge for hydrogen-based powertrains. Even with a superior weight energy density, hydrogen has a disadvantage in terms of volumetric energy density in comparison to conventional hydrocarbon fuels making it difficult to store [4].

One prominent storage method in hydrogen-powered aircraft applications is the use of cryo-compression tanks. Verstraete *et al.* [55] discuss design of twin LH_2 tanks for regional aircraft. These tanks feature approximately 12 to 13 cm of insulation, operate at low pressures ranging from 1.7 to 3 bar, and maintain cryogenic temperatures at around 20.3 K. The hydrogen boil-off from the tank is warmed up to the operating temperatures before entering the fuel cell stack. This technology represents a promising avenue for enhancing hydrogen storage in aviation. Additionally, Larminie and Dicks [4] also suggest various chemical storage methods for hydrogen.

2.4.3. Air Supply: Compressor

The fuel cell's oxygen supply differs from onboard storage, relying instead on filtered ambient air. However, this approach introduces challenges related to oxygen concentration at the cathode, particularly at high altitudes due to low ambient pressure, which can impede fuel cell performance.

To address this, compressors are employed to elevate the air pressure within the fuel cell [4] generally between ambient pressure, and maximally around 2 bar gauge pressure [42]. While this addition of compressor enhances the fuel cell's open circuit voltage and oxygen supply, it also adds extra weight and power demands, ultimately impacting the overall aircraft performance. Nevertheless, air compression remains an appealing choice for aircraft applications of HFCs [4]. The compression process can be regarded as adiabatic, meaning that it occurs without the transfer of heat into or out of the system. As a result of this compression, high temperatures can be attained at the compressor outlet and thus there might be need to cool down the air to operating temperatures [53].

2.4.4. Water Management

Low Temperature PEM Fuel Cells (LT-PEMFC) necessitate precise control of water content within the electrolyte membrane for optimal performance. While proton conductivity in the membrane is directly tied to its water content, excessive water within the fuel cell can lead to electrode flooding, potentially clogging the porous gas diffusion [4, 5]. As per Ji and Wei, maintaining this delicate equilibrium is vital to prevent fuel cell degradation and ensure high performance, representing the core challenge of water management [56].

To tackle this challenge, researchers have explored various approaches. Some researchers, like Buchi and Srinivasan [57], and Hogarth and Benziger [58], have delved into self-humidifying fuel cells that use water produced at the cathode to keep the membrane hydrated, while excess water is removed by the oxygen supply. However, achieving the right balance in this auto-humidification process can be challenging, particularly when high currents may dry out the cathode faster than water production can replenish it. Consequently, the most widely adopted solution involves passing the reactant gases (oxygen and hydrogen) through a humidifier before entering the fuel cell stack. The water produced within the cell can be utilised in this humidification process, as well as for thermal management purposes [4].

2.4.5. Thermal Management System

In an ideal PEMFC operating at temperatures around $80\,°C$, approximately 80% of the chemical energy undergoes conversion into electrical energy. The remaining 20% is dissipated as thermal energy, commonly referred to as waste heat [4]. Hence, most larger PEMFC systems necessitate active cooling for temperature control. They also require provisions for cold starts and substantial cooling, all while accommodating only minor temperature variations within the stack. As a result, this leads to the development of robust and weighty thermal management systems (TMS) [5].

Numerous researchers emphasize the significance of TMS in the fuel cell balance of plant (BoP). For instance, Réndon *et al.* [30] argued that TMS for electrical components are necessary and may be included in HEP design, with corresponding additional weight and Chen *et al.* [59] offer valuable insights into potential cooling strategies for PEM Fuel Cells' thermal management systems, such as liquid cooling, air

cooling, evaporative cooling, and flow boiling.

In their evaluation of fuel cell aircraft, Scholz *et al.* [29], highlight a critical aspect: fuel cells and the components of the electrical powertrain lack a natural heat rejection system, akin to the exhaust flow in conventional internal combustion engine (ICE) aircraft powered by gas turbines. As a result, alternative methods for heat dissipation become imperative. The utilisation of convection-based heat transfer can introduce various challenges, including anti-icing, cabin heating, and component overheating, potentially leading to operational failures, especially under hot weather conditions. Adding to this complexity is the observation made by Rheaume and Lentsii [60] that the heat loads of these components are at their peak during take-off, presenting a distinctive challenge. As a conventional solution, ram air-based Thermal Management Systems (TMS) are employed, where ambient air serves as the primary heat sink. As a result, further research was conducted on ram-air-based thermal management systems [60, 61]. In a separate study, Kellerman *et al.* [62] proposed a comprehensive approach to ram-air-based thermal management for hybrid aircraft, emphasising the efficient dissipation of heat to the surrounding ambient air. This approach can also be adapted for fuel cell-powered aircraft. Additionally, Kellerman *et al.* [63] conducted a study in which they assessed various cooling systems for Battery Thermal Management Systems (TMS). Ultimately, they developed a battery TMS model that includes a Thermoelectric module, a finned ram air heat exchanger (HEX) serving as a heat sink, and a simplified heat pipe for heat acquisition.

In a recent study conducted by Kösters *et al.* [64], a novel phase-change-heat-pump (PCHP) cooling strategy was proposed and compared to conventional liquid cooling through a model-based analysis. This innovative approach involved using water as a coolant, which is evaporated within cooling channels inside the fuel cell. Subsequently, the water vapour is compressed to high pressures (5 bar) by a compressor and directed to a condenser. The condenser, in turn, is cooled using ram air. The liquid water is then throttled through an expansion valve and circulated back into the fuel cell. An intriguing aspect of this method is that it raises the temperature of the steam entering the condenser to 324°C, resulting in significantly higher heat transfer potential due to the increased temperature difference with the surrounding air. Consequently, this approach leads to the use of smaller heat exchangers, offering a more efficient cooling solution.

Recent theses from TU Delft, such as those authored by Scoccimarro [53] and Hoogerdijk [65], also delved deeply into the intricacies of thermal management systems for hydrogen-electric propulsion. Furthermore, various TMS architectures and the factors influencing TMS selection were explored in a literature review by Coutinho *et al.* [66]. The majority of TMS topologies examined in this literature review, particularly for hypothetical aircraft, saw the use of liquid cooling loops as their primary transport systems. The use of ram air was also noted to be a prevalent and well-established technology at the aircraft level. The review emphasised that one of the primary challenges in TMS design was the integration of diverse heat transfer technologies to ensure the necessary heat transfer functionality while minimising adverse effects on overall aircraft efficiency and performance. Lastly, Scholz *et al.* [29] also pointed out that thermal management system design is closely linked to the design of the propulsion system due to the high level of interdependencies and interactions between them.

2.4.6. Power Management and Distribution

Power Management and Distribution (PMAD) serves as a crucial subsystem within the overall framework, primarily tasked with the efficient management and distribution of electric power. This encompassing system is comprised of various components, including cables, protection switches, inverters, and converters. PMAD's primary function revolves around the redundant and protected distribution of electric power from diverse sources, such as the hydrogen fuel cell (HFC) stack and the battery, to the myriad electrical loads throughout the aircraft. These electrical loads encompass a wide spectrum, including propulsion systems, avionics, lighting, and various other critical electrical components.

Notably, the fuel-cell stack produces electric power in the form of direct current (DC), and this output voltage is influenced by factors like stack architecture and current density. PMAD, therefore, takes on the vital role of ensuring that the voltage and frequency align seamlessly with the specific requirements of each load. In instances where electric motors necessitate alternating current (AC) power, PMAD incorporates inverters. Furthermore, PMAD systems include monitoring and control functions to ensure the safe and efficient distribution of power. When designing aircraft models, it is crucial to carefully consider both the mass and efficiency of this system to optimise overall performance and efficiency [4, 67].

2.4.7. Electric Motors and Propellers

The electric motors play a pivotal role in the conversion of electric power into shaft power, which is the force responsible for turning the aircraft's propellers. An insightful comparative analysis conducted by Hayes and Goodarzi [67] underscores the superior suitability of AC motors for electric vehicle (EV) applications. The efficiency of these electric motors is intricately linked to two key variables: motor torque and motor RPM. The interplay between these factors significantly influences the overall efficiency of the electric motors.

Subsequently, the propellers act as the final link in the chain, responsible for the transformation of the shaft power generated by the electric motors into thrust. This thrust, as the ultimate outcome of this process, serves as the driving force for propelling the aircraft forward. It's worth noting that well-optimised propellers can achieve impressive propulsive efficiencies, with typical values typically reaching around 0.8 [42].

2.4.8. Battery

Batteries function as electrochemical storage devices, delivering direct current (DC). In a hydrogen-electric powertrain, batteries serve as auxiliary power sources, typically composed of multiple lithium-ion cell-based battery packs. These batteries are primarily utilised during take-off and climb phases, when additional power is needed, and are recharged during other flight phases by harnessing excess power generated by the fuel cell.

According to insights from Vratny, Kuhm, and Hornung [68], the battery's output voltage is predominantly determined by two key factors: the current discharge rate and the state of charge (SOC). Their research emphasises that "*the lower the SOC, the lower is the nominal/operating voltage of a battery [...] at a given SOC, the higher the discharge current, the higher is the decrease of the available output voltage*." Moreover, the paper highlights the significance of considering both SOC and discharge rate effects, even when the power demand remains constant. This consideration is necessary because the varying output voltage of the battery significantly influences the efficiency of any connected converter, thus affecting the overall efficiency of the powertrain and, consequently, the required output power from the battery, especially as the discharge rate fluctuates.

A study by Finger, Braun, and Bil [15] emphasises the critical significance of taking the discharge C-rate, along with specific power, into account. This importance is particularly pronounced in the context of hybrid-electric aircraft that are designed with peak-load shaving operational strategies in mind. These factors are shown to be just as essential, if not more so, than specific energy when optimising the performance and efficiency of battery systems in such applications. Additionally, it is essential to recognise that maintaining a certain SOC margin is crucial for battery protection.

2.5. Powertrain Modeling and Operational Strategy

In recent years, multiple research studies have delved into powertrain modelling and architecture within the realm of hydrogen-electric propulsion systems (HEPS). For instance, Hales *et al.* [69], representing GKN Aerospace[3], introduced the Hybrid Hydrogen Electric Architecture (H2GEAR) program. This initiative aims to demonstrate the technological advancements required to create a certifiable power and propulsive system based on fuel cell-driven hydrogen electric powertrains. The paper emphasises the significance of technology development in the fuel cell power system, with a focus on enhancing fuel cell stack operating temperature, efficiency, and specific power.

Vietze and Weiland [70] conducted a comprehensive modelling study of a hydrogen-electric aircraft powertrain, focusing on its functional characteristics and component behaviour. The research employed the DAHER TBM850 as a reference aircraft and involved modelling the entire hydrogen circuit, from the storage tank through various sub-systems to the consumption of hydrogen by the fuel cell. This encompassed modelling the tank, motor, heat exchanger, fuel cell, and mission profile. The study also incorporated a sensitivity analysis to identify two critical factors significantly impacting the system's functional behaviour and fundamental design characteristics: the minimum inlet pressure of the fuel cell (FC) and the initial condition of the liquid/vapour thermodynamics. In addition, Vietze and Weiland also derived specific powertrain requirements, including maximum tank pressure and tank volume. Simultaneously, Swannet [71] in the pursuit of designing control and energy management for hybrid aircraft, contributed to the field

[3] https://www.gknaerospace.com/en/about-us/

by modelling the electric powertrain in his thesis. Swannet's modelling extended to components like the battery, electric motor, and propeller, enhancing the overall understanding of powertrain dynamics for hybrid aircraft.

In a recent publication by Staggat *et al.* [72], the focus was on modelling a powertrain topology for a regional aircraft that combines a fuel cell with battery support. The chosen regional aircraft for this study was the ATR 72-600, and the assumed flight mission encompassed takeoff, climb, cruise, and descent phases. The aircraft featured two propulsor units, one on each wing, each comprising a propeller, an electric motor with a gearbox, a motor controller, a fuel cell system, its respective thermal management system (TMS), and a battery. The hydrogen was assumed to be stored in a liquid hydrogen (LH_2) tank.

The fuel cell system incorporated high-temperature proton exchange membrane (HTPEM) fuel cell stacks and a compressor driven by fuel cell power. The auxiliary power source was a lithium-ion battery with a 20% state of charge (SoC) margin. The operational strategy drew inspiration from a battery energy strategy introduced in Hoelzen *et al.*'s work on conceptual operational strategies [73]. This strategy involved using the battery stack to support the fuel cell system only during peak power loads, enabling the downsizing of the fuel cell system. Additionally, surplus fuel cell system power during less power-demanding flight phases (such as cruise and descent) were used to recharge the battery for later high-power manoeuvres, such as a go-around.

The temperature control for the fuel cell system, gearbox, motor, inverter, and converter was actively managed by a TMS, while the battery pack was assumed to be passively cooled. The different temperature levels and levels of waste heat for dissipation led to separate modelling of the TMS for the power electronics, electric motors, and gearboxes compared to that of the fuel cell system. The TMS management system model included components like heat exchangers, coolants, coolant pumps, pipes, and air fans. Electric components such as converters, inverters, and motors were individually modelled.

The component sizes and the maximum take-off mass (MTOM) of the aircraft were to be determined using an iterative sizing methodology. The powertrain model was then subjected to simulations varying the hybridisation factor (HF) from 0.2 to 0.8 and the assumed battery pack's specific energy (BSE) from 300 Wh/kg to 1000 Wh/kg, aiming for a weight-advantageous fuel cell-battery configuration. The results revealed a global minimum of MTOM at an HF of approximately 0.5 and the highest BSE investigated of 1000 Wh/kg. The resulting MTOM of approximately 24,000 kg closely aligned with the ATR 72-600's MTOM of 22,800 kg. The study's conclusion emphasised that, for the investigated aircraft, achieving the best results in terms of maximum take-off mass (MTOM) required a higher specific energy (BSE). As a result, future aircraft of similar weight and size would necessitate highly advanced battery technology with a specific energy (BSE) significantly surpassing currently available state-of-the-art solutions.

Having explored the nuances of modelling the Hydrogen Electric Propulsion System (HEPS), the attention now shifts to a specific mission profile namely, the go-around phase. As this phase has been selected for closer examination within the context of HEPS behaviour, it becomes pertinent to delve into a discussion about it and its significance within flight operations.

2.6. Go-Around

Runway excursions or overruns, responsible for 33 percent of all commercial aviation accidents, often stem from unstable approaches and a failure to execute a go-around, as Michael Coker highlighted in his article [74] (see Figure 2.4). When the safety of a landing is in question, a go-around manoeuvre should be initiated without hesitation. Several circumstances necessitate a go-around, including requests from air traffic control (ATC), unexpected events like wind shear, an unstable approach, or when landing within the touchdown zone seems improbable.

According to the Federal Aviation Administration (FAA) [75], a go-around represents a standard protocol utilised in instances where approach and landing conditions deviate from expected norms or when safety is compromised. However, executing go-around manoeuvres presents significant challenges. These procedures, crucial for safety occur at low altitudes and speeds, in close proximity to the ground. Pilots executing a go-around must navigate through a series of actions, including adjustments in attitude, thrust, aircraft configuration, and pitch trim [76]. These specific actions are outlined in the aircraft operating manual as part of Standard Operating Procedures (SOPs) – the go-around/missed approach checklist.

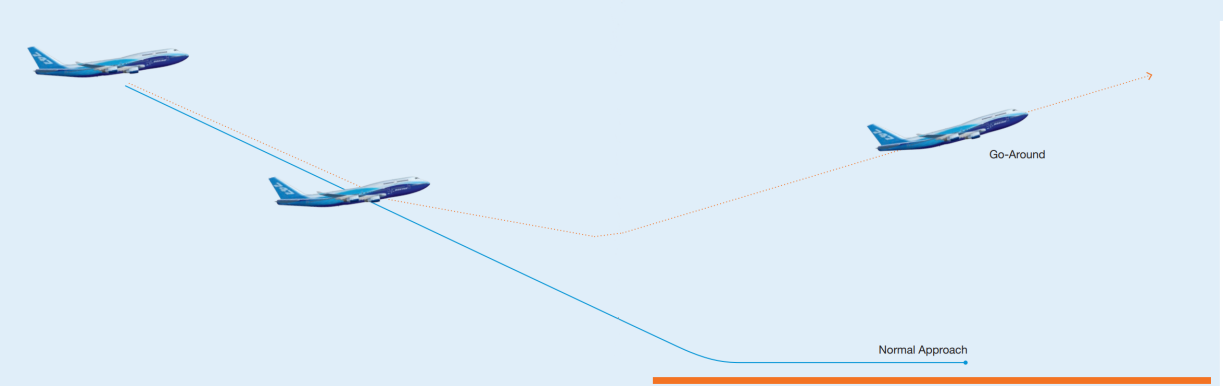

Figure 2.4: Example of a go-around manoeuvre [74]

The Federal Aviation Administration (FAA) underscores [75] that careful monitoring of available thrust and the thrust required to maintain flight is critical during the approach. If a go-around manoeuvre is initiated, pilots must swiftly apply full or maximum allowable takeoff power, commonly referred to as takeoff/go-around (TOGA) thrust. This application of thrust demands a sufficient energy reserve to ensure the aircraft remains in control and attains a desired speed to move towards a safe altitude. Furthermore, it's essential to understand that the go-around manoeuvre itself is not inherently dangerous. Its safety depends on prompt execution and proper handling. To this end, Rosenkrans [77] reinforces FAA's guidance by emphasising that any approach or landing may result in a go-around, so the pilots should be prepared to execute a go-around in the presence of unstabilised elements during an approach or landing. Delays or incorrect execution can introduce potential risks. According to Flight Safety Foundation (FSF) [78], the crew is advised to review the fundamental elements of the go-around manoeuvre and the missed approach procedure at an appropriate moment during the final approach.

Consequently, executing a go-around represents a high-workload scenario where pilots may need to manage various aspects of energy control. When integrating a novel propulsion system such as HEPS, the procedural dynamics of executing a go-around may diverge from the established practices associated with conventional propulsion systems. Pilots may encounter altered performance characteristics or response times, necessitating a thorough understanding of how the new system influences critical manoeuvres like the go-around. Consequently, pilots might need to incorporate additional preparatory steps to ensure that the operational conditions specific to HEPS are conducive to a safe and effective go-around procedure.

3

Research Questions

For the prospective integration of hydrogen-based flights, understanding the modifications in flight operations and the interplay between humans and machines due to the new propulsion system is essential. This study primarily aims to explore the behaviour of HEPS specifically during the crucial go-around phase, an integral element within flight operations. Achieving an in-depth comprehension of HEPS behaviour is contingent upon employing modelling and simulation techniques. This pivotal exploration forms the core objective of this research endeavour:

Research Objective

To model and simulate a hydrogen-electric propulsion system for regional turboprop aircraft, during a representative go-around phase.

The specific research questions are then given as,

Research Question 1

What components of the Hydrogen-Electric Propulsion System must be modelled in the event of a go-around procedure for future turboprop regional aircraft?

1.1 What factors contribute to the selection of these components for inclusion in the model?
1.2 What impact do the modelled components have on the power demand of the HEP system?

Research Question 2

To what extent is the model influenced by the initial parameters?

2.1 What is the impact of the initial settings and/or assumptions on the output behaviour of the HEPS model?
2.2 What implications do variations in initial settings and assumptions have on go-around flight procedures?

4

Project Plan

Advancing the comprehension of hydrogen-electric propulsion system (HEPS) behaviour, especially in challenging scenarios like the critical go-around phase of regional turboprop aircraft, is the central objective of this study. This chapter outlines the strategic plan designed to fulfil this overarching goal.

4.1. Methodology

To construct the system model effectively, a comprehensive understanding of system requirements, expected outputs, and operational conditions is essential. This initial research phase involves gathering fundamental data from industry references and literature sources. This includes details on the aircraft, fuel cell, powertrain configuration, component specifications, and operational parameters. Additionally, mission profile requirements will be established to define critical factors such as thrust levels, desired altitude, and specific manoeuvring characteristics.

The focal point of this research lies in developing a Hydrogen-Electric Propulsion (HEP) system model using the MATLAB/Simulink platform. Simulink's versatile interface and extensive component library make it well-suited for modelling HEPS. For complex powertrain components, like fuel cell stacks, SimScape toolboxes will be utilized. Leveraging real-time simulation capabilities and MATLAB toolbox integration, the model will efficiently analyse HEPS integration into practical aviation scenarios. This comprehensive model, constructed from a wealth of data and mission profile requisites, will integrate mathematical models of various powertrain components sourced from existing literature. Initially, these individual component models will be formulated to align with the specific requirements and functionalities of the powertrain. Subsequently, these models will be intricately interconnected, amalgamating to form a holistic Hydrogen-Electric Propulsion System (HEPS) model. It aims to provide crucial data to cockpit systems, yielding outputs such as thrust, fuel flow, power usage, and powertrain temperatures. The model will undergo thorough examination, particularly emphasising critical components and their performance in mission-specific scenarios, notably the go-around maneuver.

Post extensive model development, simulation will evaluate its applicability and validity under diverse initial conditions. This sensitivity analysis ensures the model accurately represents real-world behaviour, particularly concerning human interactions during the mission-critical go-around phase. This rigorous verification and validation process establish the model's fidelity in representing the Hydrogen-Electric Propulsion system, forming the groundwork for a comprehensive system evaluation.

4.1.1. Background Information

The chosen aircraft for this modelling initiative is the Dash 8-Q300, presently equipped with two Pratt & Whitney Canada PW1 turboprop engines. However, the plan involves retrofitting the existing engine configuration with a Hydrogen-Electric Propulsion (HEP) system to replace these engines. The primary mission profile entails executing a go-around manoeuvre for an ILS approach at Runway 06 of Schiphol Airport. The intended model will represent a 2MW powertrain operating at an approximate 2000V bus voltage.

To thoroughly comprehend the aircraft's operational dynamics, critical aerodynamic and operational parameters have been methodically considered. The system will be powered primarily by Proton Exchange Membrane Fuel Cells (PEMFC), arranged in a multi-stack setup. In addition, Lithium-ion (Li-ion) batteries

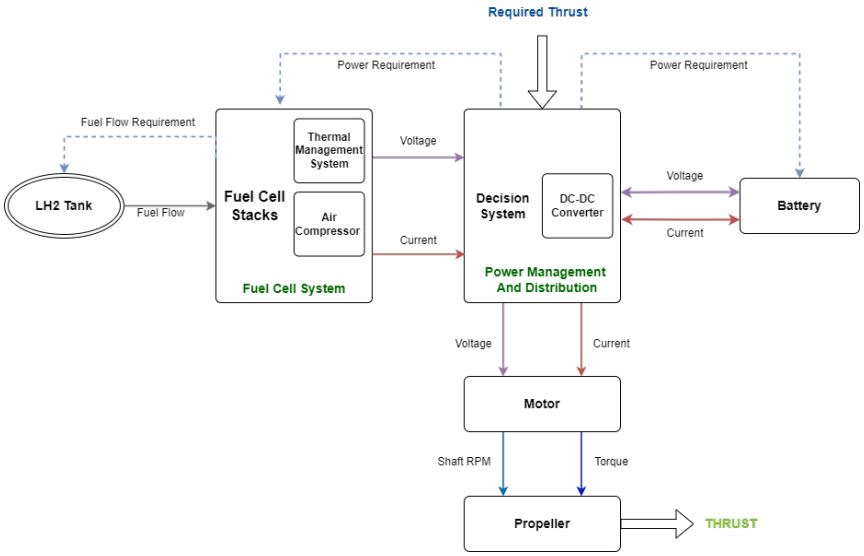

Figure 4.1: Proposed Architecture of the Powertrain

will provide supplementary power during high-demand phases such as take-off and climb. Both these power sources will generate electrical output directed to the Power Management and Distribution (PMAD) unit, responsible for optimising the utilisation of this electrical power. Additionally, the fuel cell system will integrate a thermal management system (TMS) and an air compressor. The TMS maintains optimal operating temperatures within the fuel cell stacks, managing heat flow to enhance their efficiency and lifespan. Simultaneously, the air compressor plays a pivotal role in sustaining adequate oxygen levels at the fuel cell's cathode. The motor and propeller systems will be meticulously modelled based on the aircraft's specific requirements, drawing power from the Power Management and Distribution (PMAD) unit within the powertrain. For a visual reference, please see Figure 4.1.

4.1.2. Simulation

To analyze the system comprehensively, alterations in various initial conditions will be introduced. These changes encompass factors such as the initial fuel levels in the tanks, battery State of Charge (SoC), temperature settings, and environmental conditions (such as hot-day take-off). Assessing the impact of these modifications on the model's behaviour will enable a thorough examination to pinpoint potential adjustments required in pilot behaviour and flight operations.

The simulation will take place within the DUECA (Delft University Environment for Communication and Activation) environment, utilising the SIMONA Research Simulator at TU Delft. This controlled environment facilitates the exploration of diverse scenarios and their effects on the system's performance.

4.2. Expected Results

The components depicted in the powertrain diagram (Figure 4.1) are anticipated to wield significant influence over the overall behavior of the comprehensive model. Predominantly, the fuel cell stack and the battery serve as the primary power sources, thereby exerting the most substantial impact on the system's dynamics and performance. Moreover, the Balance Of Plant, encompassing the Thermal Management System and the Air Compressor, is expected to contribute notably to the model's power performance. These elements play a pivotal role in utilizing a considerable portion of the available system power, thus potentially influencing overall system efficiency.

Among the varying initial conditions, it is projected that alterations in the initial fuel levels and battery State of Charge (SoC) will have a more pronounced effect on the behaviour of the model compared to changes in other operational conditions. These adjustments are likely to significantly influence the system's power management and performance, potentially necessitating adaptations in operational procedures and pilot behaviour.

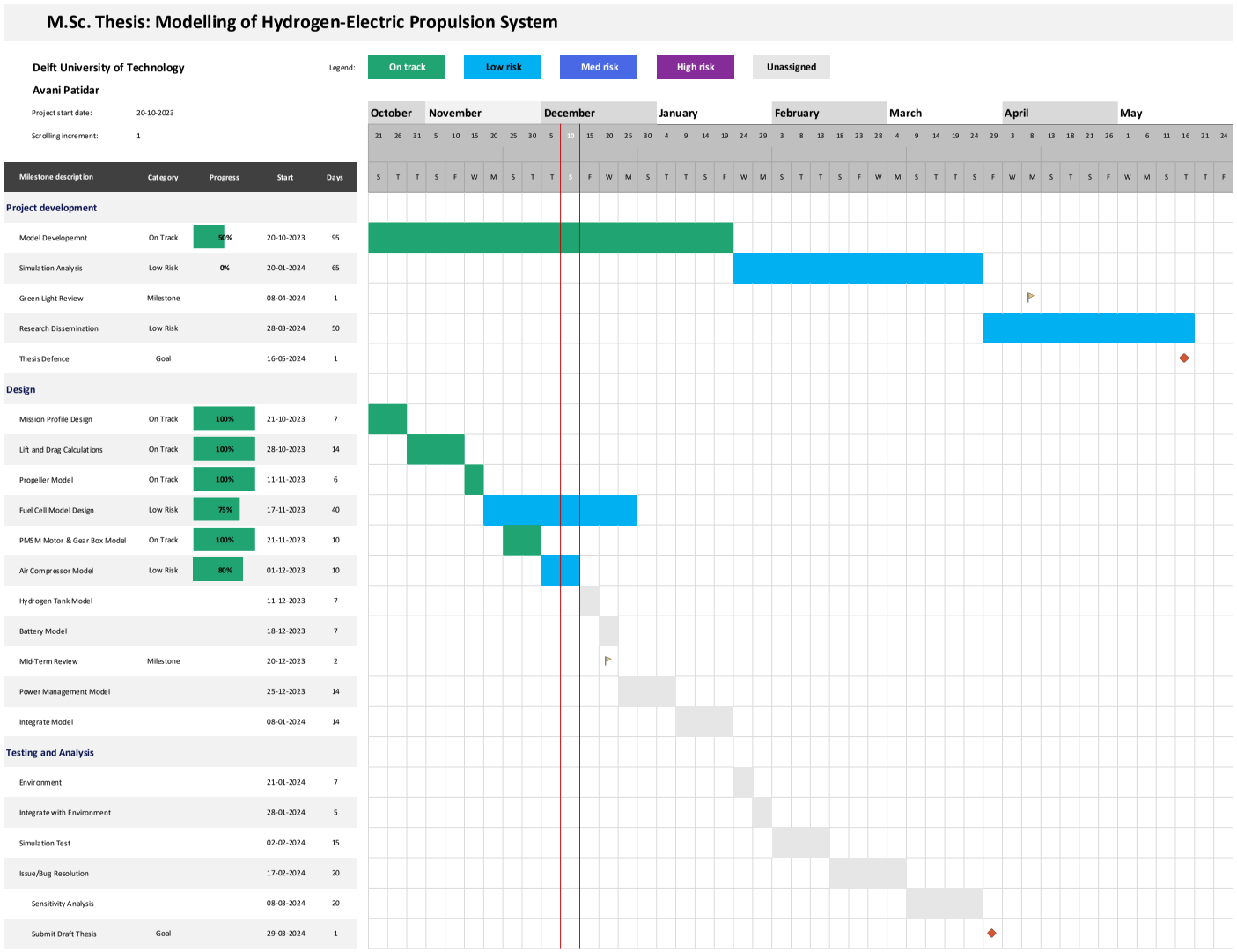

Figure 4.2: Planning Gantt Chart [Updated: Mid-Term Review Meeting]

4.3. Planning

The project planning comprises two pivotal phases: Model Development and Simulation Analysis. In the Model Development phase, individual component models will be formulated and integrated to culminate in a comprehensive system model. Subsequently, in the Simulation Analysis phase, this model undergoes rigorous testing, refinement, and various simulations to conduct sensitivity analysis under diverse conditions. A detailed breakdown of this plan is visualised in the Gantt Chart depicted in Figure 4.2.

References

[1] Brandon Graver et al. “CO2 emissions from commercial aviation: 2013, 2018, and 2019”. In: (2020). URL: https://theicct.org/wp-content/uploads/2021/06/CO2-commercial-aviation-oct2020.pdf.

[2] Directorate-General for Research & Innovation et al. *Fly the Green Deal – Europe’s vision for sustainable aviation*. Publications Office of the European Union, 2022. DOI: doi/10.2777/732726. URL: https://data.europa.eu/doi/10.2777/732726.

[3] International Air Transport Association (IATA). *Aircraft Technology Net Zero Roadmap*. URL: https://www.iata.org/contentassets/8d19e716636a47c184e7221c77563c93/aircraft-technology-net-zero-roadmap.pdf.

[4] James Larminie et al. *Fuel Cell Systems Explained (2nd Edition)*. John Wiley & Sons, 2003. URL: https://app.knovel.com/hotlink/toc/id:kpFCSEE002/fuel-cell-systems-explained/fuel-cell-systems-explained.

[5] Ryan O’Hayre et al. *Fuel Cell Fundamentals*. John Wiley & Sons Ltd., Apr. 2016. DOI: 10.1002/9781119191766.

[6] Valerio Marciello et al. “Design Exploration for Sustainable Regional Hybrid-Electric Aircraft: A Study Based on Technology Forecasts”. In: *Aerospace* 10 (2 Feb. 2023). DOI: 10.3390/AEROSPACE10020165.

[7] Stefan Kazula et al. “Functional and Safety Challenges of Hydrogen Fuel Cell Systems for Application in Electrified Regional Aircraft”. In: *Journal of Physics: Conference Series* 2526 (1 2023). DOI: 10.1088/1742-6596/2526/1/012063.

[8] Evangelia Pontika et al. “Integrated Mission Performance Analysis of Novel Propulsion Systems: Analysis of a Fuel Cell Regional Aircraft Retrofit”. In: American Institute of Aeronautics and Astronautics (AIAA), Jan. 2023. DOI: 10.2514/6.2023-0840. URL: doi.org/10.2514/6.2023-0840.

[9] Internation Energy Agency (IEA). *Aviation - IEA*. URL: https://www.iea.org/energy-system/transport/aviation#tracking.

[10] Environmental & Energy Study Institute (EESI). *The Growth in Greenhouse Gas Emissions from Commercial Aviation; Part 1 of a Series on Airlines and Climate Change*. Oct. 2019. URL: https://www.eesi.org/files/FactSheet_Climate_Impacts_Aviation_1019.pdf.

[11] International Air Transport Association (IATA). *Net-Zero Carbon Emissions by 2050*. 2021. URL: https://www.iata.org/en/pressroom/pressroom-archive/2021-releases/2021-10-04-03/.

[12] International Civil Aviation Organization (ICAO). *Long term global aspirational goal (LTAG) for international aviation*. URL: https://www.icao.int/environmental-protection/Pages/LTAG.aspx.

[13] Eduardo Cabrera et al. “Use of Sustainable Fuels in Aviation – A Review”. In: *Energies* 15.7 (2022). DOI: 10.3390/en15072440. URL: https://www.mdpi.com/1996-1073/15/7/2440.

[14] Dominik Eisenhut et al. “Aircraft Requirements for Sustainable Regional Aviation”. In: *Aerospace* 8 (3 Feb. 2021), p. 61. DOI: 10.3390/AEROSPACE8030061.

[15] D. Felix Finger et al. “Impact of Battery Performance on the Initial Sizing of Hybrid-Electric General Aviation Aircraft”. In: *Journal of Aerospace Engineering* 33 (3 May 2020). DOI: 10.1061/(ASCE)AS.1943-5525.0001113.

[16] Clean Sky 2 et al. *Hydrogen-powered Aviation*. May 2020. DOI: 10.2843/471510.

[17] John L Sloop. *Liquid hydrogen as a propulsion fuel, 1945-1959*. Vol. 4404. Scientific, Technical Information Office, National Aeronautics, and Space Administration, 1978.

[18] G. D. Brewer. “Aviation usage of liquid hydrogen fuel-prospects and problems”. In: *International Journal of Hydrogen Energy* 1 (1 1976), pp. 65–88. DOI: 10.1016/0360-3199(76)90011-2.

[19] D. G. Victor. “Liquid hydrogen aircraft and the greenhouse effect”. In: *International Journal of Hydrogen Energy* 15 (5 1990), pp. 357–367. DOI: 10.1016/0360-3199(90)90186-3.

[20] Fredrik Haglind et al. “Potential of reducing the environmental impact of aviation by using hydrogen Part I: Background, prospects and challenges”. In: *Aeronautical Journal* 110 (Aug. 2006), pp. 533–540. DOI: 10.1017/S000192400000141X.

[21] W. R. Grove. *XXIV. On voltaic series and the combination of gases by platinum*. Feb. 1839. DOI: 10.1080/14786443908649684.

[22] BBC Archive. *The Brits who bolstered the Moon landings*. URL: https://www.bbc.co.uk/archive/the-brits-who-bolstered-the-moon-landings/zfcrscw.

[23] Xianguo Li. *Principles of fuel cells*. CRC press, 2005.

[24] Harold Duane Wallace. “Fuel Cells: A Challenging History”. In: *Substantia* 3.2 (Nov. 2019), pp. 83–97. DOI: 10.13128/Substantia-277.

[25] Stefan Kazula et al. “Review of fuel cell technologies and evaluation of their potential and challenges for electrified propulsion systems in commercial aviation”. In: *Journal of the Global Power and Propulsion Society* 7 (Feb. 2023), pp. 43–57. DOI: 10.33737/JGPPS/158036.

[26] S Mekhilef et al. “Comparative study of different fuel cell technologies”. In: *Renewable and Sustainable Energy Reviews* 16 (2012), pp. 981–989. DOI: 10.1016/j.rser.2011.09.020.

[27] K. A. Friedrich et al. “Fuel Cell Systems for Aircraft Application”. In: *ECS Transactions* 25 (1 Sept. 2009), pp. 193–202. DOI: 10.1149/1.3210571.

[28] Thomas Kadyk et al. “Analysis and Design of Fuel Cell Systems for Aviation”. In: *Energies* 11 (2 Feb. 2018), p. 375. DOI: 10.3390/EN11020375.

[29] Anna E. Scholz et al. “Fuel Cell Hybrid-Electric Aircraft: Design, Operational, and Environmental Impact”. In: *Journal of Aircraft* 60 (3 May 2023), pp. 606–622. DOI: 10.2514/1.C036952.

[30] Manuel A. Rendón et al. “Aircraft Hybrid-Electric Propulsion: Development Trends, Challenges and Opportunities”. In: *Journal of Control, Automation and Electrical Systems* 32 (5 Oct. 2021), pp. 1244–1268. DOI: 10.1007/S40313-021-00740-X/FIGURES/19.

[31] Ahmad Baroutaji et al. “Comprehensive investigation on hydrogen and fuel cell technology in the aviation and aerospace sectors”. In: (2019). DOI: 10.1016/j.rser.2019.02.022. URL: https://doi.org/10.1016/j.rser.2019.02.022.

[32] N. Lapeña-Rey et al. “First fuel-cell manned aircraft”. In: *Journal of Aircraft* 47 (6 2010), pp. 1825–1835. DOI: 10.2514/1.42234.

[33] Deutsches Zentrum für Luft- und Raumfahrt (DLR). *Antares DLR-H2: Fuel cell-powered aircraft*. URL: https://www.dlr.de/en/images/2013/2/antares-dlr-h2-fuel-cell-powered-aircraft_9601.

[34] Giulio Romeo et al. “ENFICA-FC: Design, realization and flight test of all electric 2-seat aircraft powered by fuel cells”. In: *Proc. of 27th International Congress of the Aeronautical Sciences (ICAS2010)*. 2010.

[35] Taegyu Kim et al. “Design and development of a fuel cell-powered small unmanned aircraft”. In: *International Journal of Hydrogen Energy* 37.1 (2012). 11th China Hydrogen Energy Conference, pp. 615–622. DOI: 10.1016/j.ijhydene.2011.09.051.

[36] Christian Rößler. “Conceptual design of unmanned aircraft with fuel cell propulsion system”. PhD Thesis. Technische Universität München, 2012.

[37] Ó. González-Espasandín et al. “Fuel cells: a real option for unmanned aerial vehicles propulsion”. In: *The Scientific World Journal* 2014 (2014), pp. 1–12. DOI: 10.1155/2014/497642.

[38] Marino Boric. *Maiden Flight of HY4 Hydrogen-Powered Airplane*. 2016. URL: https://www.eaa.org/eaa/news-and-publications/eaa-news-and-aviation-news/news/10-06-2016-maiden-flight-of-hy4-hydrogen-powered-airplane.

[39] Charles Alcock. *ZeroAvia achieves first flight with hydrogen-powered regional airliner*. URL: https://www.futureflight.aero/news-article/2023-01-19/zeroavia-achieves-first-flight-hydrogen-powered-regional-airliner.

[40] Hanneke Weitering. *Universal Hydrogen flies hydrogen-powered Dash 8*. URL: https://www.futureflight.aero/news-article/2023-03-02/universal-hydrogen-flies-hydrogen-powered-dash-8.

[41] Smruti Sahoo et al. “A Review of Concepts, Benefits, and Challenges for Future Electrical Propulsion-Based Aircraft”. In: *Aerospace 2020, Vol. 7, Page 44* 7 (4 Apr. 2020), p. 44. DOI: 10.3390/AEROSPACE7040044.

[42] George Vonhoff. “Conceptual Design of Hydrogen Fuel Cell Aircraft: Flying on hydrogen for a more sustainable future”. Master’s Thesis. Delft University of Technology, 2021. URL: http://resolver.tudelft.nl/uuid:8bd63dec-b67b-496b-92bc-3d5c07ff859f.

[43] Miha Zupanič. “Conceptual Design of Fuel Cell Commuter Aircraft”. Master’s Thesis Thesis. Delft University of Technology, Apr. 2023. URL: http://resolver.tudelft.nl/uuid:d499f4bb-921a-4e3d-a676-614961104172.

[44] V. Marciello et al. “Conceptual Design of a Hydrogen-Propelled Aircraft with Distributed Electric Propulsion”. In: American Institute of Aeronautics and Astronautics Inc, AIAA, 2022. DOI: 10.2514/6.2022-3205.

[45] Vincenzo Palladino et al. “Preliminary studies of a regional aircraft with hydrogen-based hybrid propulsion”. In: *AIAA Aviation and Aeronautics Forum and Exposition, AIAA AVIATION Forum 2021* (2021). DOI: 10.2514/6.2021-2411. URL: http://arc.aiaa.org/doi/10.2514/6.2021-2411.

[46] W. H. Wentz et al. “Preliminary design considerations for zero greenhouse gas emission airplanes”. In: *SAE Technical Paper Series* (2004). DOI: 10.4271/2004-01-1803.

[47] Elias G. Waddington et al. “Impact of LH2 Fuel Cell-Electric Propulsion on Aircraft Configuration and Integration”. In: *AIAA Aviation and Aeronautics Forum and Exposition, AIAA AVIATION Forum 2021* (2021). DOI: 10.2514/6.2021-2409. URL: https://arc.aiaa.org/doi/10.2514/6.2021-2409.

[48] Ralph H. Jansen et al. “Overview of NASA electrified aircraft propulsion research for large subsonic transports”. In: *53rd AIAA/SAE/ASEE Joint Propulsion Conference, 2017* (2017). DOI: 10.2514/6.2017-4701.

[49] Jacopo Zamboni et al. “A method for the conceptual design of hybrid electric aircraft”. In: *AIAA Scitech 2019 Forum* (2019). DOI: 10.2514/6.2019-1587.

[50] F. Orefice et al. “Aircraft conceptual design including powertrain system architecture and distributed propulsion”. In: *AIAA Propulsion and Energy Forum and Exposition, 2019* (2019). DOI: 10.2514/6.2019-4465.

[51] Chrysoula Lydia Pastra et al. “Feasibility and benefit assessments of hybrid hydrogen fuel cell and battery configurations on a regional turboprop aircraft”. In: *AIAA AVIATION 2022 Forum* (2022). DOI: 10.2514/6.2022-3290. URL: https://arc.aiaa.org/doi/10.2514/6.2022-3290.

[52] Yuan Gao et al. “Hydrogen-Powered Aircraft: Hydrogen-electric hybrid propulsion for aviation.” In: *IEEE Electrification Magazine* 10 (2 June 2022), pp. 17–26. DOI: 10.1109/MELE.2022.3165725.

[53] Antonio Scoccimarro. “Preliminary Design Methods for the Thermal Management of Fuel Cell Powered Aeroengines”. Master’s Thesis. Delft University of Technology, 2023. URL: http://resolver.tudelft.nl/uuid:9a16e0f8-722d-4a17-9f79-96cea2de6906.

[54] Bahareh Zaghari et al. “The Impact of Multi-Stack Fuel Cell Configurations on Electrical Architecture for a Zero Emission Regional Aircraft”. In: (Jan. 2023). DOI: 10.2514/6.2023-1593.

[55] D. Verstraete et al. “Hydrogen fuel tanks for subsonic transport aircraft”. In: *International Journal of Hydrogen Energy* 35 (20 Oct. 2010), pp. 11085–11098. DOI: 10.1016/J.IJHYDENE.2010.06.060.

[56] M. Ji et al. “A review of water management in polymer electrolyte membrane fuel cells”. In: *Energies* 2 (4 2009), pp. 1057–1106. DOI: 10.3390/en20401057.

[57] F. N. Büchi et al. “Operating proton exchange membrane fuel cells without external humidification of the reactant gases: fundamental aspects”. In: *Journal of the Electrochemical Society* 144 (8 1997), pp. 2767–2772. DOI: 10.1149/1.1837893.

[58] W. H. Hogarth et al. “Dynamics of autohumidifed pem fuel cell operation”. In: *Journal of the Electrochemical Society* 153 (11 2006), A2139. DOI: 10.1149/1.2344841.

[59] Q. Chen et al. “Thermal management of polymer electrolyte membrane fuel cells: a review of cooling methods, material properties, and durability”. In: *Applied Energy* 286 (2021), p. 116496. DOI: 10.1016/j.apenergy.2021.116496.

[60] J. M. Rheaume et al. “Design and simulation of a commercial hybrid electric aircraft thermal management system”. In: *2018 AIAA/IEEE Electric Aircraft Technologies Symposium* (2018). DOI: 10.2514/6.2018-4994.

[61] J. M. Rheaume et al. “Commercial hybrid electric aircraft thermal management system design, simulation, and operation improvements”. In: *AIAA Propulsion and Energy 2019 Forum* (2019). DOI: 10.2514/6.2019-4492.

[62] H. Kellermann et al. “Design and optimization of ram air–based thermal management systems for hybrid-electric aircraft”. In: *Aerospace* 8 (1 2020), p. 3. DOI: 10.3390/aerospace8010003.

[63] H. Kellermann et al. “Design of a battery cooling system for hybrid electric aircraft”. In: *Journal of Propulsion and Power* 38 (5 2022), pp. 736–751. DOI: 10.2514/1.b38695.

[64] T. L. Kösters et al. “Comparison of phase-change-heat-pump cooling and liquid cooling for pem fuel cells for mw-level aviation propulsion”. In: *International Journal of Hydrogen Energy* 47 (68 2022), pp. 29399–29412. DOI: 10.1016/j.ijhydene.2022.06.235.

[65] T L C Hoogerdijk. “Aircraft Integration of Air-Based Thermal Management Systems for Propulsive Fuel Cell Systems”. Master’s Thesis. Delft University of Technology, May 2023. URL: http://resolver.tudelft.nl/uuid:592ad30f-93b3-4d01-9fec-9786616dd9c4.

[66] Maria Coutinho et al. “A review on the recent developments in thermal management systems for hybrid-electric aircraft”. In: *Applied Thermal Engineering* 227 (June 2023), p. 120427. DOI: 10.1016/J.APPLTHERMALENG.2023.120427.

[67] J.G. Hayes et al. *Electric Powertrain: Energy Systems, Power Electronics and Drives for Hybrid, Electric and Fuel Cell Vehicles*. Wiley, 2018. URL: https://books.google.nl/books?id=tshQDwAAQBAJ.

[68] Patrick C. Vratny et al. “Influences of voltage variations on electric power architectures for hybrid electric aircraft”. In: *CEAS Aeronautical Journal* 8 (1 Mar. 2017), pp. 31–43. DOI: 10.1007/S13272-016-0218-Z/FIGURES/17. URL: https://link-springer-com.tudelft.idm.oclc.org/article/10.1007/s13272-016-0218-z.

[69] Michael O. Hales et al. “H2GEAR Hydrogen Electric Powertrain – System Architecture”. In: American Institute of Aeronautics and Astronautics (AIAA), June 2023. DOI: 10.2514/6.2023-3874.

[70] Marco Vietze et al. “System analysis and requirements derivation of a hydrogen-electric aircraft powertrain”. In: *International Journal of Hydrogen Energy* 47 (91 Nov. 2022), pp. 38793–38810. DOI: 10.1016/J.IJHYDENE.2022.09.052.

[71] Kilian Swannet. “Optimal Control And Energy Management For Hybrid Aircraft”. Master’s Thesis. Delft University of Technology, May 2022. URL: http://resolver.tudelft.nl/uuid:511989dc-0e95-414c-839b-7af0ff5ad7a0.

[72] Martin Staggat et al. “Modelling of a battery supported fuel cell electric power train topology for a regional aircraft”. In: *Journal of Physics: Conference Series* 2526 (1 June 2023), p. 012061. DOI: 10.1088/1742-6596/2526/1/012061.

[73] Julian Hoelzen et al. “Conceptual Design of Operation Strategies for Hybrid Electric Aircraft”. In: *Energies* 11.1 (2018). DOI: 10.3390/en11010217. URL: https://www.mdpi.com/1996-1073/11/1/217.

[74] Michael Coker. “Why and When to Perform a Go-Around Maneuver”. In: *Boeing Aero* (2014), pp. 05–11.

[75] Federal Aviation Administration (FAA). “Chapter 9: Approaches and Landings”. In: 2023.

[76] David Carbaugh et al. “Performing Safe Go-Around Maneuvers”. In: *Boeing Aero* (2014), pp. 13–17.

[77] Wayne Rosenkrans. “Go-Around Risks”. In: *Aero Safety World* (2015), pp. 16–20.

[78] Flight Safety Foundation. “Being Prepared to Go Around”. In: *Approach and Landing Accident Reduction Tool Kit* (2009).

Part II

Scientific Article

Modelling and Operational Analysis of Hydrogen-Electric Powertrain for Future Regional Aircraft During A Go-Around

Avani Patidar *
Delft University of Technology, Delft, The Netherlands, 2629 HS

The aviation industry's shift towards sustainable propulsion, notably hydrogen-electric propulsion (HEPS), underscores the need to grasp its effects on flight procedures and pilot duties. This research aims to develop a HEPS engine powertrain model for evaluating its influence on flight procedures, especially during critical phases like go-around for regional turboprop aircraft. The HEPS engine powertrain model was constructed by selecting powertrain components important for modelling based on their relevance to important HEPS system outputs like the thrust generation, battery discharge, and fuel left in the tank. Subsystems such as the fuel cell system, battery, motor, propeller etc. were modelled using MATLAB/Simulink and integrated to form a holistic representation of the HEPS engine. The model underwent testing through a simulated go-around mission, followed by an analysis of its operational envelope, which unveiled significant parameters influencing system behaviour during such manoeuvres. Among the critical parameters identified were the initial battery state of charge (SoC), nominal battery capacity, and propeller efficiency. Thrust generation limitations were identified for heavier aircraft configurations, as well as the relatively low impact of go-around speed on the system's power path. For a HEPS-based Dash 8 Q-300 aircraft with a mass of 38,000 pounds and a go-around speed of 96 knots, the State of Charge (SoC) of a 200Ah battery should be at least 23% for a successful go-around manoeuvre. Using appropriate parameters, the presented model framework assists in identifying such constraints and delineating flight procedural changes for future regional aircraft. The study highlights areas for model enhancement, including better thermal management system models for the fuel cell stack and battery, and improved motor-propeller models. This research contributes to sustainable aviation, guiding the integration of HEPS into flight operations for enhanced efficiency and eco-friendly air travel.

Nomenclature

BSE = Battery Specific Energy

DC = Direct Current

*M.Sc. Student, Faculty of Aerospace Engineering and AIAA Student Member.

FC	=	Fuel Cell	HEPS	=	Hydrogen-Electric Propulsion System
HF	=	Hybridization Factor	HFC	=	Hydrogen Fuel Cell
Li-ion	=	Lithium Ion	MTOM	=	Maximum Take-Off Mass
PEMFC	=	Proton Exchange Membrane Fuel Cell	PMAD	=	Power Management and Distribution
PMSM	=	Permanent Magnet Synchronous Motor	SHP	=	Shaft Horse Power
SoC	=	State of Charge	TMS	=	Thermal Management System

Subscripts

amb	=	ambient	bat	=	battery
comp	=	compressor	conv	=	converter
fc	=	fuel cell	GA	=	go-around
lim	=	limit	max	=	maximum
mot	=	motor	nom	=	nominal
prop	=	propeller	ref	=	reference
req	=	required	st	=	fuel cell stack
tank	=	hydrogen storage tank	trq	=	torque

I. Introduction

The aviation industry faces challenges with the growing climate impact. Recognising this, global entities like the European Union have committed to introducing environmentally sustainable aircraft options for regional transport by 2035 [1]. Amid the array of available alternatives—ranging from sustainable aviation fuel to battery-powered solutions—liquid hydrogen-based options have garnered attention since the 1990s due to their notably low emissions and eco-friendly attributes [2]. However, a comprehensive study by Hagling et al. [3] in 2006, shed light on an important aspect: although hydrogen combustion could eradicate CO2 emissions, it still engendered water vapour and nitrogen oxides (NOx), potentially contributing to the greenhouse effect. Considering aviation applications, Friedrich et al. [4] and Kadyk et al. [5] underscored that fuel cells present myriad advantages over liquid hydrogen combustion. These benefits encompass durability, reliability, silent operations, zero emissions, and heightened efficiency, ultimately curtailing fuel necessities.

In recent years, researchers such as Zamboni et al. [6] and Palladino et al. [7] have delved into hybrid-electric propulsion systems. Their work delineated a conceptual design involving the hybridisation of gas turbines with batteries or fuel cells, offering a framework adaptable to systems incorporating fuel cells. In 2023, Pontika et al. [8] compared the mission performance of a fully-electric Fuel Cell (FC) regional aircraft with traditional and hydrogen gas turbine models. They highlighted the FC aircraft's increased weight due to a complex balance of plant, necessitating greater

thrust, impacting efficiency across different power settings. Consequently, the study recommended a hybrid system for future research: optimising the FC for heightened efficiency during cruise while strategically integrating batteries to handle peak demands during take-off and climb. This Hydrogen-Electric Propulsion System (HEPS) garnered attention from various researchers.

Marciello et al. [9] conducted a thorough investigation into the HEPS design, focusing on an energy architecture scenario where a fuel cell system serves as the primary power source with batteries acting as a backup. The study underscored that identifying the optimal point for maximum fuel savings hinges upon the strategy employed for battery usage during the flight mission. Their findings highlighted that employing battery-supported fuel cell configurations for aircraft akin to the ATR, engineered for a 600-nautical-mile range, could potentially reduce fuel consumption by over 85% for a typical 200-nautical-mile mission. Similarly, Gao et al. [10] studied a multiple-propeller, fixed-wing aircraft integrating an FC/lithium battery hybrid power system. Their research found that FC regional aircraft with a 1,000-kilometre range could potentially reduce energy consumption while significantly mitigating climate impact with a higher Maximum Takeoff Mass (MTOM) than conventional aircraft.

In order to investigate the complexities of HEPS and streamline the design process of hydrogen-electric regional aircraft, researchers have dedicated efforts in modelling the HEPS powertrain, estimating its size, and scrutinising its operational characteristics. Vietze and Weiland [11] conducted an exhaustive modelling study on a hydrogen-electric aircraft powertrain, highlighting critical factors influencing the DAHER TBM850 hybrid propulsion system's behaviour and specifying necessary powertrain requirements such as maximum tank pressure and tank volume. In addition, Staggat et al. [12] focused on modelling a powertrain topology for a regional aircraft that integrates a fuel cell with battery support. Drawing from Hoelzen et al.'s work on conceptual operational strategies [13], they adopted an operational approach using the battery stack to aid the fuel cell system during peak power demands, allowing for downsizing. In addition, surplus power from the fuel cell during low-demand flight phases was used to recharge the battery for high-power manoeuvres. The paper extensively discussed powertrain components, determining sizes and the MTOM via simulations varying the hybridisation factor (HF), which was defined as the ratio of the maximum power to be provided by the fuel cell stack to the total maximum power of the engine powertrain, and assumed Battery pack's Specific Energy (BSE). Results indicated an optimised MTOM at an HF of 0.5 and a BSE of 1000 Wh/kg, closely aligned with the ATR 72-600's MTOM. The study concluded that achieving the optimal Maximum Takeoff Mass (MTOM) for the investigated aircraft necessitates a higher Battery Specific Energy (BSE), indicating the requirement for advanced battery technology.

The existing powertrain models in literature serve as a foundation for understanding size and design strategy optimisation. However, they fall short in elucidating how the introduction of a new propulsion system might reshape flight operations and standard procedures. The integration of HEPS into aircraft demands a thorough grasp of their functionality, particularly their interaction with pilots during critical phases such as the go-around. The go-around involves swift thrust transitions that significantly impact safety and aircraft performance, necessitating a thorough

examination of HEPS performance during these pivotal moments. Regrettably, literature lacks a consolidated model capable of scrutinising and guiding flight operational procedural changes.

The main contribution of this work is to fill this gap by developing an HEPS powertrain model specifically designed to provide information to the pilot and can be used in assessing the human interaction modifications and flight procedures during the go-around phase. Following a top-down modelling approach, the representative model is intended to be sufficiently elaborate to provide the pilot with the necessary data for evaluating flight performance. while maintaining simplicity. Anticipating potential adaptations in future aircraft operations with advancements in fuel-cell-based energy sources, this tailored model aims to pave the way for a comprehensive understanding of HEPS impact on aviation operations. The study is part of the "Hydrogen Aircraft Powertrain and Storage System (HAPSS)" project under the Dutch Government's "Luchtvaart in Transitie" program. This collaborative initiative with the aviation sector aims to achieve climate-neutral flying by accelerating the adoption of zero-emission hydrogen-powered aviation through retrofitting large regional turboprop aircraft already in service [14].

This paper is outlined as follows: In section II, the necessary information required to create the model is introduced, including details on the aircraft, mission profile, and powertrain architecture. section III outlines the steps undertaken to develop the model, covering the creation of individual component models and the assembly of the complete model. Following this, section IV provides details on the simulation setup for the complete model and the methodology for conducting operational envelope exploration. The results of the simulation and operational envelope exploration are presented in section V, with a brief discussion accompanying them. section VI delves into the implications of the results, offering insights into the performance and behaviour of the model under different conditions. Finally, section VII provides a conclusion to the paper, summarising the key findings and implications of the study.

II. Background

In this study, modelling the HEPS powertrain necessitates an extensive array of information encompassing aircraft details, operational conditions, and the powertrain architecture. This section will comprehensively present these components.

A. Aircraft Information

The chosen aircraft for this modelling study is the Dash 8-Q300, which presently utilises two Pratt & Whitney Canada PW123 turboprop engines. These engines are slated for replacement by retrofitting the Hydrogen-Electric Propulsion (HEP) system into the current engine setup ensuring that the original aerodynamic performance remains unaltered. It is important to note that each of these engines drives a Hamilton Sundstrand 14SF-23 four-bladed propeller, with a diameter of 3.96 meters, through the engine gearbox.

Critical aerodynamic and operating parameters have been considered to ensure a comprehensive understanding

Table 1 Aircraft Characteristics

Property	Symbol	Value		Property	Symbol	Value	
Wing Span	b	90	[ft]	Wing Area	S	605	[sq. ft]
Aerodynamic Chord	$\bar{c}$	7.125	[ft]	Airframe Length	L	84.25	[ft]
Maximum Take-off Weight	$MTOM$	43,000	[lb]	Maximum Landing Weight	MLW	41,000	[lb]
Operating Empty Weight	OEW	26,000	[lb]	Wing Dihedral Angle	λ	2.5	[deg]
Maximum Operating Altitude	$H_{\max}$	25,000	[ft]	Maximum Cruising Speed	$V_{cr,max}$	285	[kts]
Range	R_A	1,558	[km]	Maximum Take-off Power	$MTOP$	2,500	[SHP]
Lift Coefficient	C_L	$0.5082^{\#}$	-	Drag Coefficient	C_D	$0.0228^{\#}$	-
Angle of Attack	α	$0.59^{\#}$	[deg]				

$^{\#}$Refer to the appendix

of the aircraft's operational characteristics, as detailed in Table 1. The parameters include aircraft geometry, limits and engine specifications. These precise details have been sourced from the Dash 8-Q300 aircraft operating manual and airport planning manual. They form the cornerstone of data for the subsequent phases involving modelling and simulation in this research.

B. Mission Profile

Examining potential changes in flight procedures during a go-around when using HEPS is important as performing a go-around requires thrust similar to take-off conditions, which impacts safety and aircraft performance.

For this study, representative mission conditions for Dutch airspace are chosen – go-around scenario at Amsterdam's Schiphol Airport. The mission entails executing a go-around manoeuvre during a normal Instrument Landing System (ILS) approach to Schiphol Airport Runway 06. The runway sits at an elevation of -11 feet with a heading angle of 56 degrees. As per the Jeppesen Chart for this approach [15], the Obstacle clearance altitude (OCA) at the missed approach point (MAPt) prompting the go-around call is set at 410 feet. Subsequently, in the event of a missed approach, the aircraft must climb to an altitude of 2000 feet while maintaining the same heading. The environmental conditions comply with the International Standard Atmosphere (ISA), and for this scenario, there is an assumption that wind effects are not present. The aircraft's weight was chosen as M = 38000 pounds, slightly below the maximum allowed landing weight. As outlined in the Dash Q300 Aircraft Manual, the approach speed/go-around speed, denoted as V_{GA}, is specified at 96 knots. Given the landing configuration of the aircraft, the flaps are set at 15 degrees.

For this mission, the flight path angle (γ) of the aircraft is set at 8 degrees to achieve an approximate climb rate of 1500 feet per minute, adjusting as the aircraft approaches the 2000-foot altitude mark. Throughout the climb, the

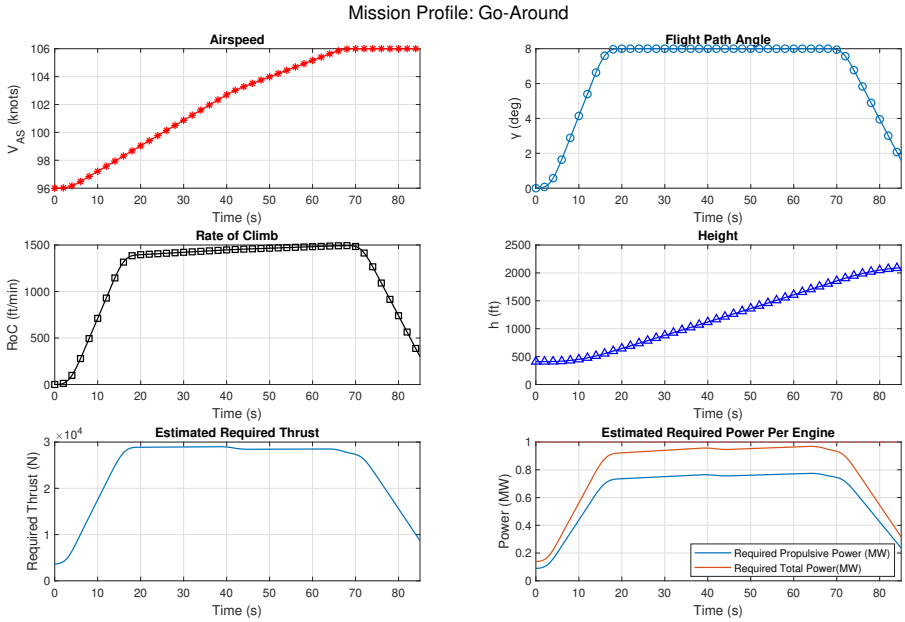

Fig. 1 Mission Profile

aircraft's speed gradually increases to 106 knots, as depicted in Figure 1. Based on rough estimates derived from the mission profile using a point-mass aircraft model, it is projected that the aircraft will require approximately 1.9 MW of power at its peak demand. This translates to 0.95 MW per engine, assuming both engines are operational throughout the mission. These estimates factor in power losses through the powertrain during the mission.

Hence, it is imperative that the powertrain to be designed possesses the capability to deliver at least 1 MW of output power per engine for this mission. This specification is to ensure that the powertrain can effectively provide the necessary propulsion and electrical power to support various flight phases and operational scenarios while upholding operational efficiency and reliability. Also, the HAPSS project opted for a 1MW powertrain to accommodate electrical cabling requirements.

The hybridization factor (HF) is commonly defined as the ratio of auxiliary power to the total powertrain requirement. Thus in this context, the HF represents the ratio of battery power to the total powertrain requirement. Following the observation by Staggat et al. [12], the powertrain is designed to have half of the required power supplied by the fuel cell stack (primary supply) for optimal HEPS system performance. Hence, the HF in this study is set to 0.5.

C. Components of HEPS Powertrain

Within the domain of a HEP system, akin to a traditional internal combustion engine, the powerplant relies on several ancillary subsystems to sustain an optimal operational state and guarantee system-wide reliability. The architecture of the powertrain holds utmost significance in modelling the HEPS. As previously mentioned, the powertrain configuration

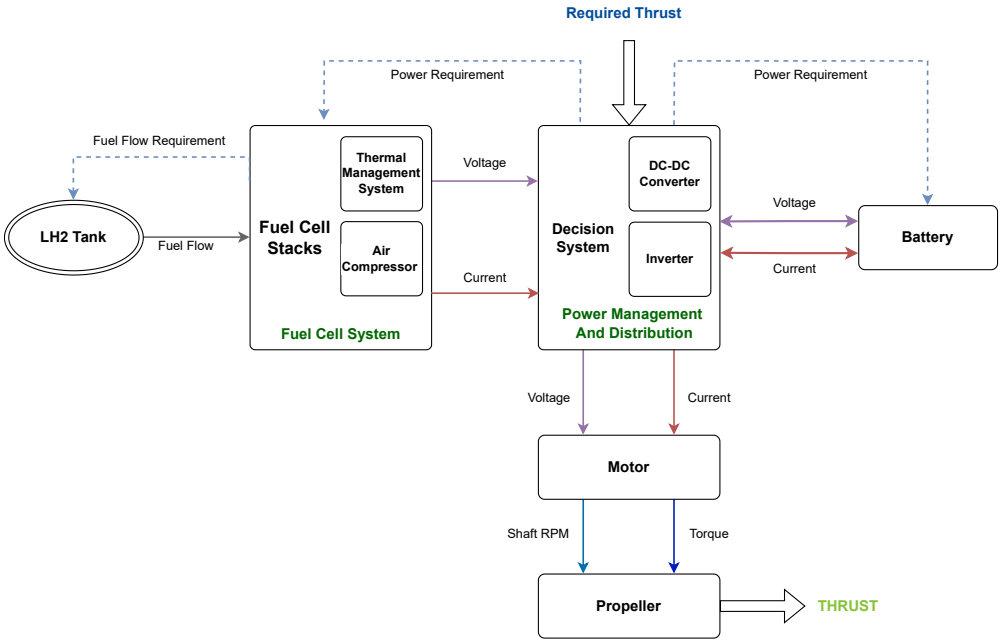

Fig. 2 Powertrain Architecture

for the HEP system will integrate FC stacks as the primary energy source, complemented by auxiliary power from batteries. The overall system architecture is visually depicted in Figure 2.

1. Liquid Hydrogen Storage

Storing hydrogen on board poses a significant challenge for hydrogen-based powertrains. Even with a superior weight energy density, hydrogen has a disadvantage in terms of volumetric energy density in comparison to conventional hydrocarbon fuels, making it difficult to store [16]. One prominent storage method in hydrogen-powered aircraft applications is the utilisation of cryo-compression tanks. Verstraete et al. [17] extensively discussed the design of twin LH2 tanks tailored for regional aircraft. These tanks are characterised by approximately 12 to 13 cm of insulation, operating at low pressures ranging from 1.7 to 3 bar, and maintaining cryogenic temperatures around 20.3 K. The hydrogen boil-off from the tank is elevated to operating temperatures before being supplied to the FC stack. Similarly, Winnefeld et al. [18] presented a tool for designing cryogenic hydrogen tanks intended for future applications in aircraft with fuel cell power supplies. In their discussion on the mechanical design of the tank, they also accounted for thermal effects including, convection and internal pressure changes.

2. Fuel Cell System

The basic fuel cell system within this powertrain is made up of key components that work together to ensure its functionality. These critical elements include the FC stack, which produces electrical energy, the Thermal Management System (TMS), which regulates optimal temperatures, and an air compressor, which supplies air to enable efficient fuel

Table 2 PEMFC Fuel Operating Conditions

Property	Symbol	Value		Property	Symbol	Value	
Operating Temperature	$T_{\text{fc},0}$	65	[°C]	H_2 Operating Pressure	$pH_{2,fc}$	1.7	[bar]
Dynamic Time Constant [21]	τ_{fc}	0.1	[s]	O2 Operating Pressure	$pO_{2,fc}$	1.1	[bar]

cell reactions. The electric power generated by the combination of these subsystems is utilised to propel the aircraft.

Among various fuel cell types, the Proton Exchange Membrane Fuel Cell (PEMFC) stands out due to its notably high power density, rapid start-up and shut-down capabilities, and its ability to function at relatively low temperatures, typically below 90°C [16, 19]. These attributes render it suitable for diverse applications, potentially replacing combustion-based propulsion systems. The chosen operating conditions for this study are presented in Table 2.

A single PEM Fuel Cell typically yields only 0.8 to 1.0 volts [16]. To achieve higher voltage output, multiple fuel cells are often connected in series, forming what's termed a FC stack. To meet the voltage requirements for powering regional aircraft, multiple stack configurations are employed to enhance power output [20]. The selection of fuel cell configurations and architecture significantly impacts system weight and power loss in the event of failure. For a 1MW powertrain (per engine), this study explores the implementation of one stack delivering 500kW to fulfil the necessary power requirements per engine.

Within an optimal operating condition at approximately 80°C, an ideal PEMFC exhibits a conversion rate where roughly 80% of the chemical energy translates into electricity, with the rest is dissipated as waste heat [16]. For larger PEMFC systems, active cooling mechanisms and robust Thermal Management Systems (TMSs) become essential to regulate temperature fluctuations within the stack. This emphasis on maintaining consistent operating temperatures is vital, as variations can significantly impact the efficiency of the fuel cell system. Consequently, the model integrates a simplified perfect TMS, ensuring the steady maintenance of the operating temperature while also estimating the heat dissipation requirements necessary to uphold the desired temperature level.

Filtered ambient air serves as the fuel cell's oxygen source, posing hurdles at higher altitudes due to reduced oxygen availability, which affects its performance. To tackle this, compressors are added to increase air pressure within the fuel cell. However, this addition increases weight and power demands, impacting aircraft efficiency [16]. Despite these implications, air compression remains an appealing choice for Hydrogen Fuel Cell (HFC) aircraft applications. This study assumes an adiabatic compressor with 85% efficiency [22].

3. Power Management and Distribution

Power Management and Distribution (PMAD) is an important subsystem that is primarily responsible for efficiently managing and distributing electric power. This system, which consists of cables, protection switches, inverters, and

converters, focuses on monitoring and controlling functions in order to safely and efficiently distribute electric power from various sources such as the hydrogen FC stack and the battery to various electrical loads throughout the aircraft. Propulsion systems, avionics, lighting, and other critical electrical components are among the loads. In this study, the power management system will include a decision system, a DC-DC converter and an inverter.

4. Battery

Batteries function as electrochemical storage units, supplying direct current (DC) in a hydrogen-electric powertrain. In this context, batteries act as supplementary power sources, typically composed of multiple lithium-ion cell-based battery packs. They play a vital role during take-off and climb phases, providing additional power when required, and are recharged during other flight phases by harnessing surplus power generated by the fuel cell.

This study will simulate the current discharge rate and State of Charge (SoC) of a battery capable of providing a maximum of 500kW of power, which is the supplementary power source of the 1MW engine power train. The battery will supply power as directed through the PMAD system. Both the SoC and discharge models are indispensable to generate the necessary output power from the battery. This becomes particularly significant in the realm of hybrid-electric aircraft, designed with operational strategies aimed at managing peak loads [23]. To ensure battery protection, a 20% SoC margin will be maintained [12, 24].

5. Motor and Propeller

The electric motors play a pivotal role in the conversion of electric power into shaft power, which is responsible for turning the aircraft's propellers. Permanent Magnet Synchronous Motors (PMSM) are widely considered the most appropriate motor for electric aircraft applications [25, 26] due to their favourable static and dynamic properties such as high efficiency, high torque to inertia ratio, high power density, low maintenance requirement and reliability [27].

Subsequently, the propellers act as the final link in the chain, responsible for the transformation of the shaft power generated by the electric motors into thrust. This thrust serves as the driving force for propelling the aircraft forward. Here, the propeller characteristics are derived from the propellers of the Dash 8-Q300: Hamilton Sundstrand 14SF-23. The propeller is presumed to function at 1200 RPM at takeoff, 1050 RPM during climb, and 900 RPM throughout level flight, descent, and the landing [28]. The key characteristics of the propeller are provided in Table 3.

Table 3 HS 14SF-23 Propeller Characteristics

Property	**Symbol**	**Value**		**Property**	**Symbol**	**Value**	
Blades	B_{prop}	4	-	Diameter	D_{prop}	13	[ft]
Max Rotations	RPM_{max}	1212	[rpm]	Efficiency	η_{prop}	0.85	-
Gear Box Factor	K	8	-	Moment of Inertia	MoI_{prop}	100	[kg m^2]

III. Methodology

The choice of modelling software plays a pivotal role in accurately simulating the powertrain. For this project, MATLAB® and Simulink® are selected due to their versatile interface and extensive library of components, making them well-suited for HEPS modelling. Furthermore, the SimScape™ toolboxes are used to enhance modelling capabilities, particularly in replicating physical signals within intricate powertrain components such as FC stacks.

The modelling approach for the HEPS follows a top-down methodology. This choice is motivated by the fact that the HEPS components are still in the design phase, resulting in a lack of concrete specifications and physical characteristics. As the system design remains the subject of ongoing research, creating a comprehensive physical model is presently unfeasible. The top-down approach offers the advantage of flexibility in model development, allowing for the expansion of model details as they become finalised in the design process. This approach enables gradual refinement of the model's complexity and accuracy as more detailed specifications and physical characteristics become available. Additionally, it allows for valuable insights into system behaviour, performance, and interactions, even in the absence of complete design specifications. In this scenario, employing a top-down methodology streamlines the development of a comprehensive HEPS powertrain model. This method entails breaking down the system into its constituent sub-components and identifying the key components. These sub-components are modelled with an appropriate level of fidelity to sufficiently represent their behaviour and provide the necessary outputs for evaluating flight performance. This approach ensures that the model remains both simple and manageable.

Initiating this methodological trajectory, the initial phase focuses on identifying the fundamental inputs and outputs important for simulating pilot interactions within the designed HEPS system. The selected inputs and outputs for this modelled HEPS system are delineated in Table 4. The model receives thrust requirement and propeller RPM requirement as representatives of the Power and Condition Lever settings, respectively. Aircraft states such as airspeed and altitude determine the operating and ambient conditions, serving as inputs to the model. The outputs provided represent information from the HEPS that pilots may need to monitor during different flight phases.

Following this, the process entails identifying and selecting critical components within the broader powertrain framework for subsequent modelling. The listing of major HEPS powertrain components is presented in Figure 3a.

Table 4 Selected Inputs and Outputs for HEPS Model

Inputs	Outputs	
1. Thrust Requirement (Power Lever)	1. Generated Thrust	2. Propeller RPM
2. Propeller RPM Requirement (Condition Lever)	3. Fuel Left in Tank	4. Fuel Cell Output Power
3. Aircraft Airspeed	5. Fuel Cell Temperature	6. Fuel Cell Efficiency
4. Aircraft Altitude	7. Battery Output Power	8. Battery Temperture
	9. Battery State of Charge	10. Motor Output Power
	11. Motor Torque	

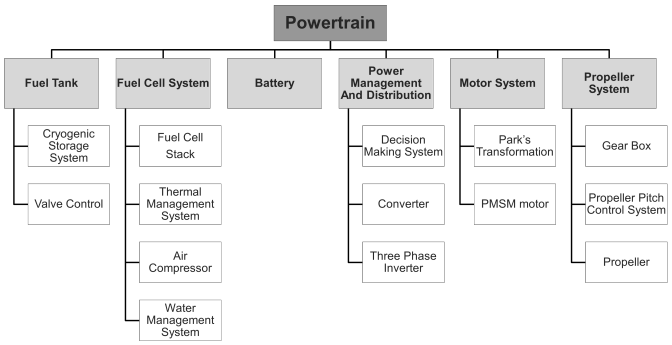

(a) Major components involved in HEPS Powertrain

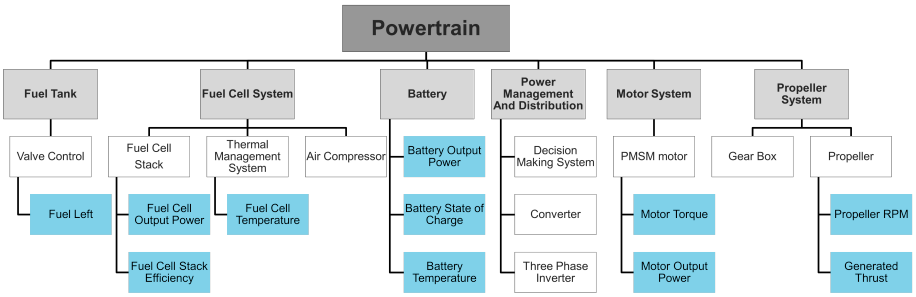

(b) Components selected for HEPS Model and their connected outputs

Fig. 3 Component Selection

A. Selection of Critical Components

The selection of critical components to be modelled is made by considering each component's significance. At the outset, it is determined that modelling the fuel tank's cryogenic storage system, while significant, is not imperative due to its intricate dynamics, such as internal pressure variations, and the need for detailed physical tank attributes [17, 18]. This study, however, primarily focuses on understanding how the behaviour of the HEPS affects flight and pilot procedures, which is not significantly impacted by pressure variations in the storage tank. Therefore, modelling the dynamics of the storage tank is deemed unnecessary, and it is assumed to maintain a constant temperature and pressure. Instead, emphasis is placed on modelling the valve for the fuel tank. For the purposes of this study, it is assumed that this valve facilitates the isobaric evaporation of liquid hydrogen and the subsequent heating of the gaseous hydrogen to achieve the desired operating temperature.

Moving on to the fuel cell system, the water management system maintains optimal water content and humidity levels within the membrane-electrode assembly (MEA) of the fuel cell. However, since usually the pilot does not need to prioritise the intricacies of water management inside the fuel cell, this system is assumed to be functioning flawlessly and is not explicitly modelled. Conversely, the TMS, responsible for regulating fuel FC temperature—an established output parameter—is deemed critical and therefore will be modelled accordingly. In addition, the HFC stack and air

compressor are integral components of the HEPS powertrain and ought to be included in the model. The HFC stack is the primary power source, and the air compressor ensures a consistent supply of oxygen to the HFC stack for optimal power generation at the constant operating pressure, despite significant variation in ambient air pressure during flight.

Subsequently, the battery will be modelled as it serves as the supplementary power source within the system. Furthermore, the decision-making system embedded within the PMAD holds significant importance and will be modelled to orchestrate the power allocation from the fuel cell system and battery, implementing the peak shaving strategy effectively. Additionally, the inclusion of the DC-DC converter in the modelling process is imperative to stabilise the voltage outputs of the power sources, maintaining a constant bus voltage of 1,500V.

Upon observation, it has been noted that although the utilisation of an inverter holds significance in real-world PMAD applications, its relevance within the specific modelling context is diminished. This is attributed to its singular function of supplying AC power solely to the PMSM motor, which, via Park transformation, internally reconverts it to DC [27]. As a result, both the inverter and the motor's internal Park transformation are considered non-essential components and will be represented solely as a gain associated with the inverter's efficiency in electrical power transfer. The dynamics of the motor itself, however, will be modelled since the motor's power delivery and shaft torque are critical system outputs that pilots may need to monitor.

Concluding the component selection process, the gear box within the propeller system will be modelled to regulate the RPM. Conversely, the propeller pitch system is excluded from modelling, as the variation in thrust resulting from pitch adjustments can be sufficiently simplified and integrated into the broader dynamics of the propeller system. Thus, the reduced component list which is considered for modelling can be seen in Figure 3b.

B. Liquid Hydrogen Tank Model

As previously discussed, the model for the hydrogen tank relies on thermodynamic equations. The liquid hydrogen is presumed to be stored at 20K and 1.7 bar [17] in an ideal cryogenic storage. The process of isobaric evaporation of liquid hydrogen and its subsequent heating to the ambient temperature occurs at the ideal valve. The following isobaric heat transfer equation [29] and ideal gas equations are utilised to model this process at the valve,

$$\Delta h_{\text{liq},T_{\text{tank}}\rightarrow\text{gas},T_{\text{fc}}} = C_{p,H_2\text{liq}}(T_{\text{BP}_{H_2},1.7\text{bar}} - T_{\text{tank}}) + \Delta h_{H_2,\text{evap}} + C_{p,H_2\text{gas}}(T_{\text{fc}} - T_{\text{BP}_{H_2},1.7\text{bar}}) \tag{1}$$

$$\Delta Q = \dot{m}\Delta h \tag{2}$$

$$\dot{m} = \rho\dot{v} = \frac{p}{R_{\text{gas}}T}\dot{v} \tag{3}$$

Here, ΔQ represents the input heat flow rate at the valve (in J/s), Δh denotes the change in specific enthalpy (in J/kg), C_p signifies the specific heat capacity of hydrogen at constant pressure (in J/kg·K), $\dot{m}$ and $\dot{v}$ stand for the mass flow (in kg/s) and volumetric flow (m^3/s) of hydrogen, respectively. Also, R_{gas} represents the specific gas constant (in

Table 5 Liquid Hydrogen and Tank Characteristics

Property	Symbol	Value		Property	Symbol	Value	
H_2 Storage Temperature [17]	T_{tank}	20	[K]	H_2 Storage Pressure [17]	$pH_{2,\text{tank}}$	1.7	[bar]
H_2 Boiling Point at P_{H_2} [30]	$T_{\text{BP}_{H_2,1.7\text{bar}}}$	22	[K]	H_2 Specific Heat of Evaporation [31]	$\Delta h_{H_2,\text{evap}}$	446.1	[kJ/kg]
RMS Specific Heat Capacity (LH2) [32]	$C_{p,H_2\text{liq}}$	10.2254#	[kJ/kg·K]	Hydrogen Gas Constant [33]	R_{H_2}	4124.18	[J/kg·K]
RMS Specific Heat Capacity (Gas)[34, 35]	$C_{p,H_2\text{gas}}$	13.395#	[kJ/kg·K]	Initial Fuel Stored (LH2)	M_{0,H_2}	100	[kg]
Hydrogen Tank Time Constant	τ_{tank}	0.005	[s]				#Refer to the appendix

Nm/kg·K), p represents the pressure (in Pa), and T denotes the temperature (in K). The values of these parameters utilised in the modelling process are displayed in Table 5.

The model accepts the reference value of fuel flow from the fuel cell as input, generating outputs such as the fuel (H_2) supply pressure, fuel flow rate, and the remaining fuel quantity in the tank. Additionally, it provides the heat flow rate to the hydrogen tank necessary for the evaporation process. The actual fuel flow rate is derived from the demanded fuel flow rate (in lpm) by filtering it through a first-order filter with a time constant of $\tau_{\text{tank}} = 0.005$ s, implying highly ideal tank and valve dynamics.

To calculate the fuel remaining in the tank, the principle of mass conservation is applied. It is assumed that although the volumetric flow of gaseous hydrogen at boiling point (T_{BP}) in the storage may differ from that at T_{fc} due to density variations, the mass flow remains constant from liquid hydrogen in the tank at 20K to gaseous hydrogen at T_{fc}. Therefore, leveraging the ideal gas law [29]:

$$\dot{m}_{\text{liq},20K} = \dot{m}_{\text{liq},BP} = \dot{m}_{\text{gas},BP} \tag{4}$$

$$= \frac{pH_{2,\text{tank}}}{R_{H_2} T_{\text{BP}}} \dot{v}_{H_2,\text{BP}} = \frac{pH_{2,\text{tank}}}{R_{H_2} T_{\text{fc}}} \dot{v}_{H_2,\text{fc}} \tag{5}$$

The mass flow rate is integrated and then subtracted from the initial fuel mass stored in the tank, M_{0,H_2}, to determine the remaining fuel quantity in the tank at any given moment. The Simulink model, which incorporates the aforementioned equations for the hydrogen tank, is illustrated in Figure 4.

C. Air Compressor Model

The design of the air compressor is integral to the system, as it is responsible for compressing atmospheric air to the required operating pressure, $pO_{2,fc} = 1.1$ bar, for air supply to the fuel cell. The compression process is modelled using adiabatic compression equations, assuming ideal gas behaviour. The specific enthalpy difference due to adiabatic

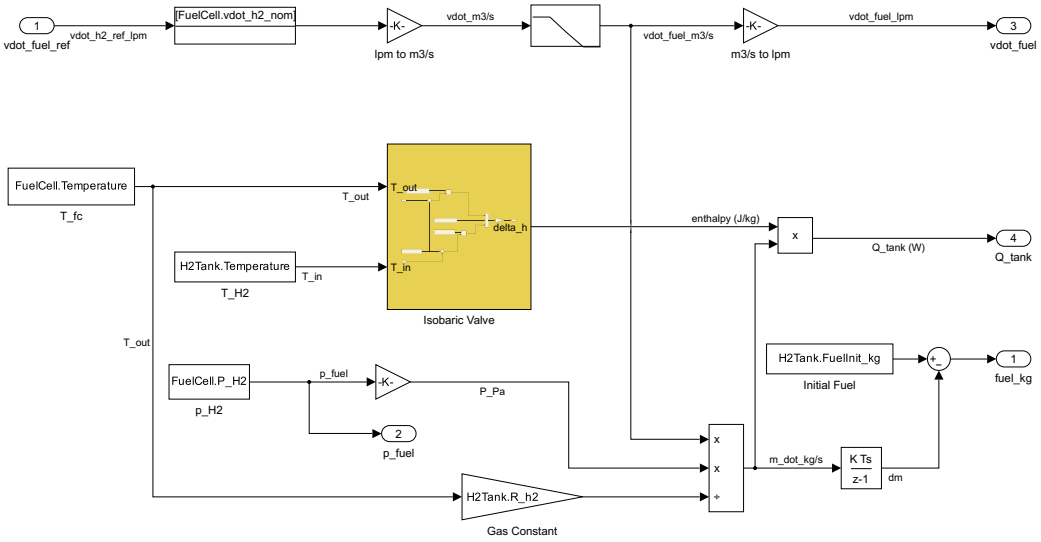

Fig. 4 Simulink Model of Liquid Hydrogen Storage Tank

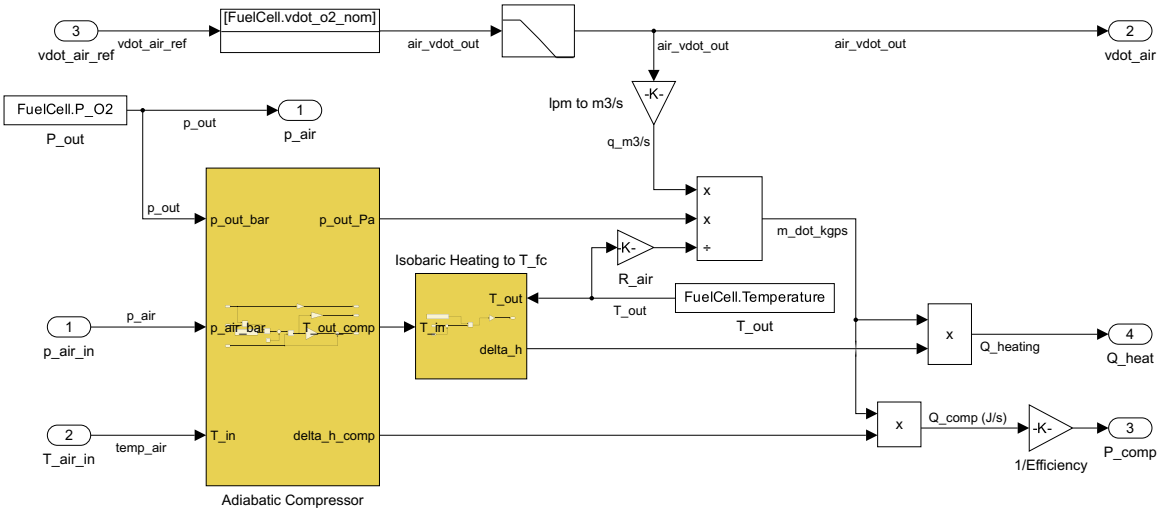

(a) Air Compressor

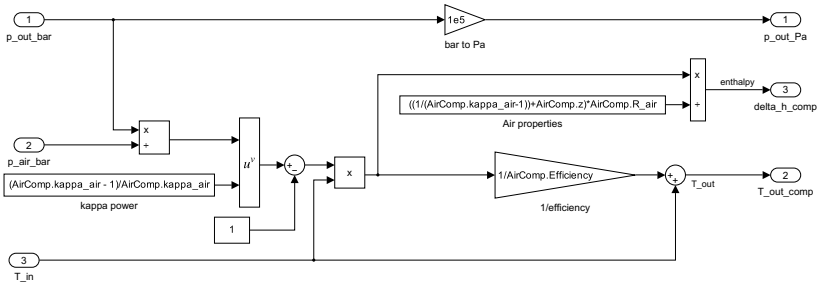

(b) Expanded model of Adiabatic Compressor

Fig. 5 Simulink Model of Air Compressor

compression and the outlet temperature are calculated as follows [36]:

$$\Delta h_{\text{comp}} = \left(\frac{1}{\kappa - 1} + z\right) R_{\text{air}} T_{\text{in,air}} \left[\left(\frac{p_{\text{out}}}{p_{\text{in}}}\right)^{\frac{\kappa-1}{\kappa}} - 1\right] \tag{6}$$

$$T_{\text{out,comp}} = \frac{1}{\eta_{\text{comp}}} T_{\text{in,air}} \left[\left(\frac{p_{\text{out}}}{p_{\text{in}}}\right)^{\frac{\kappa-1}{\kappa}} - 1\right] + T_{\text{in,air}} \tag{7}$$

Here, Δh_{comp} denotes the change in specific enthalpy for adiabatic compression (in J/kg), R_{air} represents the specific gas constant of air (in J/kg·K), κ is the isentropic exponent (or specific heat ratio) of air, z is the real gas factor, and η_{comp} is the adiabatic efficiency of the air compressor.

Similar to the hydrogen tank, the compressed air output from the compressor is heated to the fuel cell operating temperature T_{fc} via isobaric heating [29], which results in heat enthalpy change (Δh_{heat}):

$$\Delta h_{\text{heat,air}} = C_{p,\text{air}}(T_{\text{fc}} - T_{\text{out,comp}}) \tag{8}$$

Finally, the expressions for determining the heat power required for isobaric heating of air, denoted as $Q_{\text{heat,air}}$, and the power required by the air compressor [36], represented as P_{comp}, are as follows:

$$P_{\text{comp}} = \frac{\dot{m}_{\text{air}} \Delta h_{\text{comp}}}{\eta_{\text{comp}}} \tag{9}$$

$$Q_{\text{heat,air}} = \dot{m}_{\text{air}} \Delta h_{\text{heat}} \tag{10}$$

The model accepts the reference value of air flow from the fuel cell as input, alongside the ambient air pressure and temperature. Outputs comprise the air supply pressure, air flow rate, and the heat flow rate of the compressor. The actual air supply rate is determined from the demanded air supply rate (in lpm) via a first-order filter with a time constant of $\tau_{\text{comp}} = 0.001$ s, signifying ideal dynamics and assuming instantaneous availability of the required air supply, with air inlet dynamics neglected. The values of the compressor parameters used in the modelling process are provided in Table 6, while the Simulink Model is depicted in Figure 5a, with Figure 5b showing the adiabatic compressor system.

Table 6 Air Compressor Characteristics

Property	Symbol	Value		Property	Symbol	Value	
Air Gas Gas Constant [33]	R_{air}	287.058	[J/kg·K]	Air Specific Heat Capacity	$C_{p,\text{air}}$	1.008	[kJ/kg·K]
H_2 Isentropic Exponent	κ_{air}	1.401	-	Real Gas Factor of Air	z_{air}	1	-
Air Compressor Time Constant	τ_{comp}	0.001	[s]	Adiabatic Efficiency[22]	η_{comp}	0.85	-

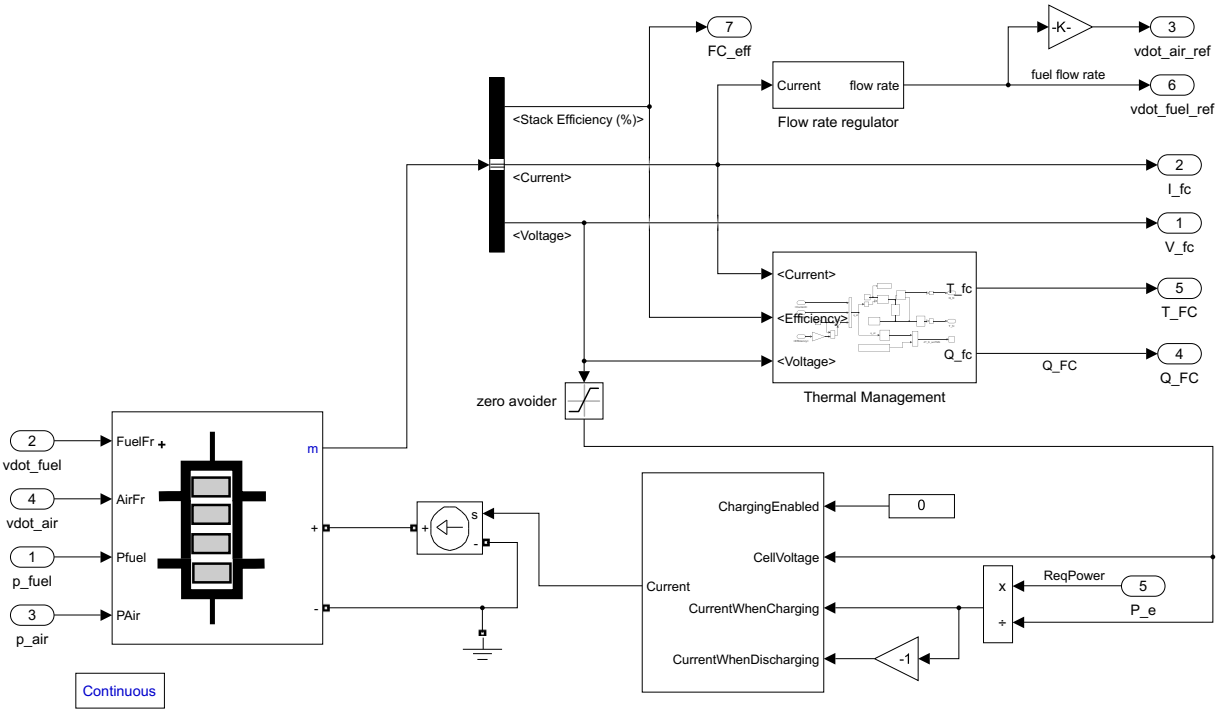

Fig. 6 Simulink Model of Fuel Cell System

D. Fuel Cell Stack Model

To model the FC stack, inputs are supplied from the LH2 tank (including the fuel flow rate $\dot{v}_{H_2}$ and fuel supply pressure $pH_{2,fc}$), the Air Compressor (with air flow rate $\dot{v}_{\text{air}}$ and air supply pressure $pO_{2,fc}$), and the Power Management and Distribution System (PMAD) for the required FC output power. The outputs of the FC stack model include the voltage V_{st} and current I_{st} output of the stack, the temperature of the stack T_{fc}, and the heat flow rate Q_{fc} from the stack. Additionally, the required fuel flow rate $\dot{v}_{H_2,ref}$ and the required air flow rate $\dot{v}_{air,ref}$ are determined and provided as output.

As depicted in the Simulink model of the fuel cell system shown in Figure 6, the modelling of the FC stack utilises a SimScape Electrical block named "Fuel Cell Stack." This block is founded on the PEM Fuel Cell mathematical model introduced by Souleman et al. [37], incorporating assumptions of ideal thermal management and water management systems, along with negligible pressure drops and constant internal resistance. However, since the preset models provided by Simscape have lower output power compared to the requirement of 500 kW for this regional aircraft powertrain, the block is tuned with parameters outlined in Table 2 and Table 7 to simulate a FC stack capable of providing 500 kW of power. The parameters used in this modelling study are based on assumptions, as actual datasheets or specifications for a 500 kW 1500 Vdc FC stack were unavailable. These parameters have been extrapolated to align with the requirements of the task, under the assumption that such a state-of-the-art FC stack will be developed in the future, as a result of ongoing research in fuel cell technology.

Table 7 500kW 1500Vdc Fuel Cell Stack Characteristics

Property	Symbol	Value		Property	Symbol	Value	
Number of Cells	N_{fc}	800	-	Open Circuit Voltage	E_{oc}	1550	[V]
Voltage at 1A	V_1	1549.5	[V]	Nominal Operating Point	$I_{\text{nom}}, V_{\text{nom}}$	335, 1500	[A], [V]
Maximal Operating Point	$I_{\text{end}}, V_{\text{end}}$	350, 1499	[A], [V]	Nominal Stack Efficiency	$\eta_{\text{st,nom}}$	55	[%]
Nominal Air Flow Rate	$\dot{v}_{\text{air,nom}}$	7200	[lpm]	Concentration of H_2 in Fuel	x_{H_2}	99.95	[%]
Fuel Cell Time Constant	τ_{fc}	0.1	[s]	Concentration of O_2 in Air	x_{O_2}	21	[%]

The tuning of the SimScape block provides cell parameters such as the Nernst voltage of one cell E_n, fuel cell resistance R_{fc}, exchange current i_0, and nominal utilisation of hydrogen and oxygen. These parameters are saved for future use in calculation of required fuel flow rate. The SimScape block with these characteristics is employed, with signal variation for fuel flow rate, air flow rate, fuel supply pressure, and air supply pressure. The VI characteristics of the FC stack are shown in Figure 7.

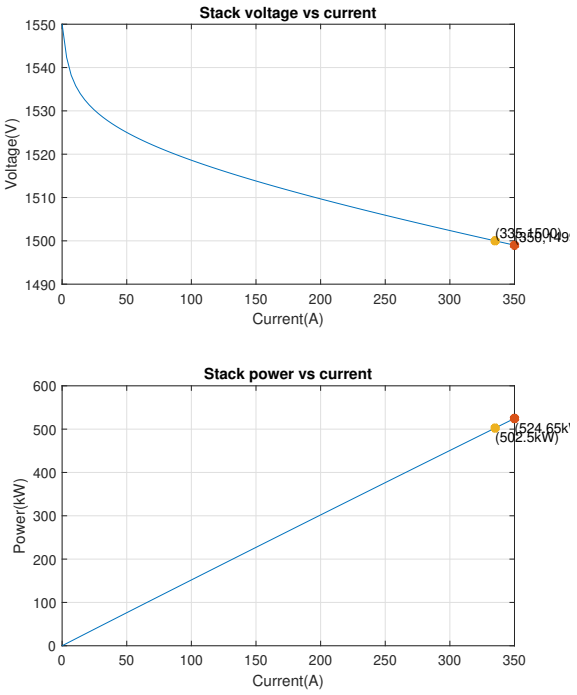

Fig. 7 Fuel Cell Stack VI Characteristics

To control the output of the stack, a "Battery CC-CV" Simulink block is used, which serves as a battery management system for constant voltage output. This controller is fed with the stack voltage V_{st} and required current as per the power requirement received from PMAD. The output of this block is utilized to drive an ideal current source across the terminals of the FC stack, ensuring that the desired current I_{st} flows from the stack. The outputs of the FC stack, such as the current, voltage, and stack efficiency, are selected from the output bus.

The reference fuel flow rate and air flow rate are calculated as follows [37]:

$$\dot{v}_{H_2,\text{ref}} = \frac{60000 R T_{\text{fc}} N_{\text{fc}} I_{\text{st}}}{2F(pH_{2,fc} * 101325)(0.01 U_{f,H_2})(0.01 x_{H2})} \tag{11}$$

$$\dot{v}_{air,\text{ref}} = \dot{v}_{H_2,\text{ref}} \frac{U_{f,O_2}}{U_{f,H_2}} \tag{12}$$

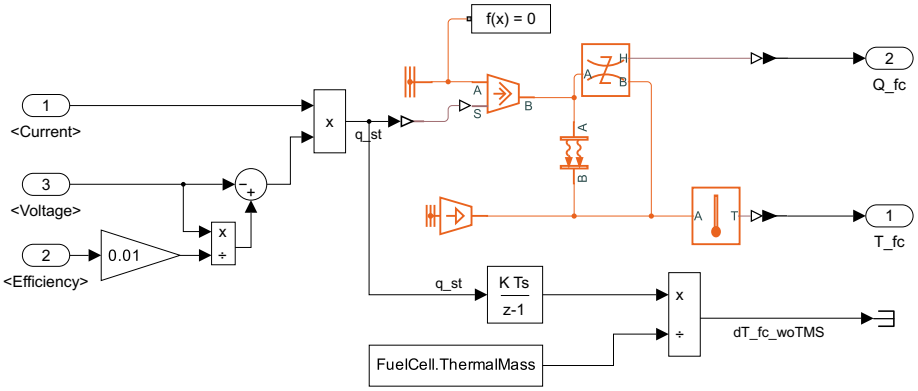

Fig. 8 Expanded view of TMS in Fuel Cell System

Here, U_{f,H_2} and U_{f,O_2} represent the nominal percentage utilization of the fuel (H_2) and oxidant (O_2) respectively with R = 8.3145 J/mol·K (Universal Gas Constant) and F = 96485 A·s/mol (Faraday's Constant).

Regarding the thermal management of the FC stack, assuming an ideal TMS within the stack implies no change in the system temperature T_{fc}. However, it is important to evaluate the amount of heat power that needs to be dissipated from the FC stack. It is estimated using the following equation [38, 39]:

$$q_{\text{st}} = Q_{\text{heat,fc}} = (V_{\text{st,ideal}} - V_{\text{st}})I_{\text{st}} \tag{13}$$

$$= \left(\frac{1}{\eta_{\text{st}}} - 1\right) V_{\text{st}} I_{\text{st}} \tag{14}$$

$$\frac{dT_{\text{fc}}}{dt} = \frac{q_{\text{st}}}{C_{th}} \tag{15}$$

Here, q_{st} represents the total heat inside the FC stack (in J/s), also denoted as $Q_{\text{heat,fc}}$. $\frac{dT_{\text{fc}}}{dt}$ represents the temperature change rate that could result if the heat is not dissipated (in K/s), and C_{th} denotes the thermal mass of the stack in (J/K). This thermal system is modelled simply using the "Convective Heat Transfer" SimScape block. The expanded view of the thermal management model is presented in Figure 8.

E. Battery Model

The battery model is designed to supplement power during peak demand periods such as take-off and climb phases. In addition, if surplus power is available from the fuel cell, the battery can be charged when its state of Charge (SoC) falls below a certain threshold. Inputs to the battery from the PMAD include the required battery output power and the battery charge signal. Outputs encompass the battery output voltage V_{bat}, current I_{bat}, state of Charge SOC_{bat}, and the heat power generated by the battery Q_{bat}.

As illustrated in the Simulink model in Figure 9, the battery is modelled using SimScape Electrical's "Battery" model. This block represents the battery as a series resistor and a charge-dependent voltage source, given by,

$$V_{\text{bat}} = V_{\text{nom}} \left[\frac{SOC}{1 - \beta(1 - SOC)} \right] \tag{16}$$

Here, SOC denotes the current state-of-charge of the battery, V_{nom} is the voltage when the battery is fully charged at no load (nominal voltage), and β is a constant internally calculated using the block parameters $V1$ and $AH1$. $AH1$ represents the charge (in C) when the no-load voltage is $V1$ ($V1 < V_{\text{nom}}$).

In a parallel manner to the FC stack scenario, no specific battery specifications are accessible to meet the requirements of providing a 500 kW 1500 Vdc output for the powertrain. The parameters for this anticipated battery system, as outlined in Table 8, have been extrapolated from EVESCO's 500 kW Energy Storage System ES-500500-EU datasheet [40]. It is assumed that advancements in battery technology will lead to the availability of such systems in the future. Constants related to charge dynamics are assumed, with the battery temperature set at 298.16 K (25°C). Thermal mass of the battery, along with temperature dependence constants, are also assumed.

The battery output control is executed similarly to the fuel cell system, employing a "Battery CC-CV" controller to drive an ideal current source across the battery terminals. The determination of the state of Charge (SoC) is based on

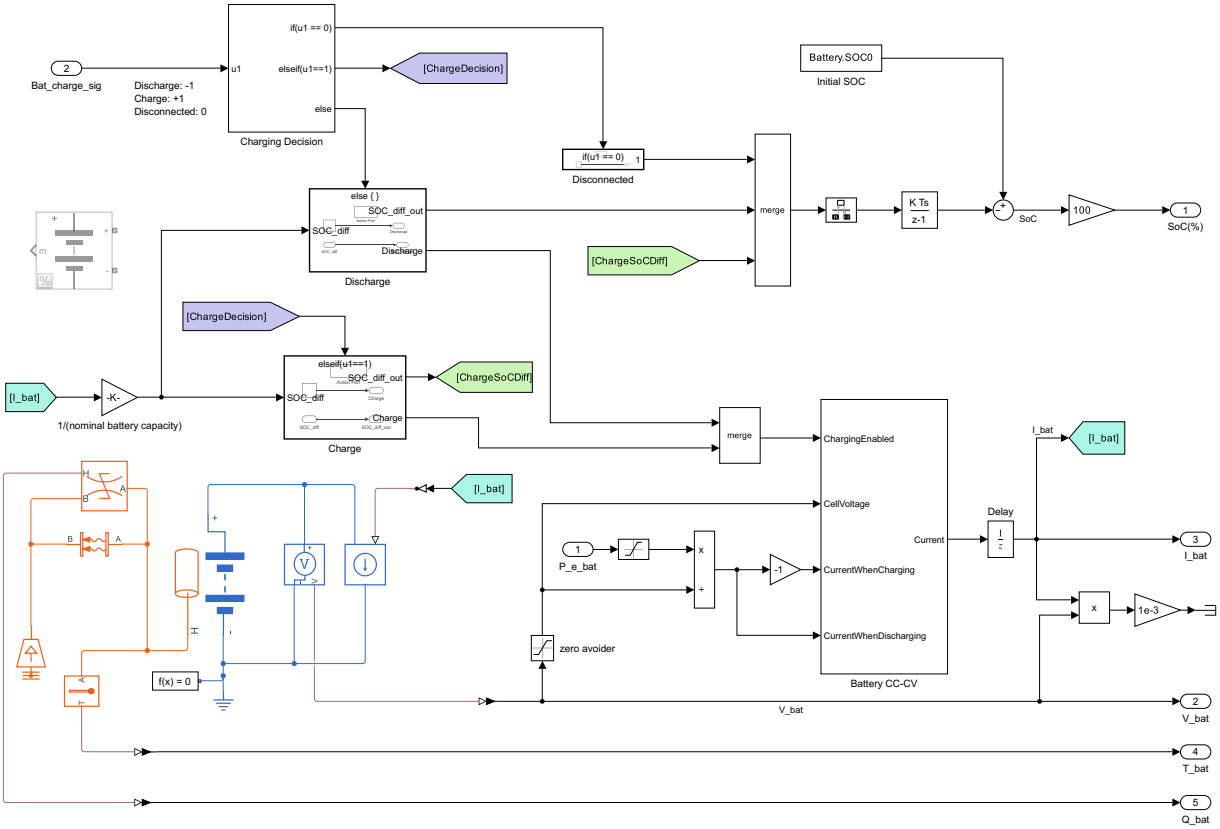

Fig. 9 Simulink Model of Battery System

Table 8 500kW 1500Vdc 200Ah Battery Characteristics

Property	Symbol	Value		Property	Symbol	Value	
Nominal Voltage	$V_{\text{bat,nom}}$	1497.6	[V]	Internal Resistance	R_{bat}	0.2	[Ω]
Nominal Battery Capacity	$C_{\text{nom,bat}}$	200	[Ah]	No-load Operating Point	$V1, AH1$	1482, 0.7	[V], [C]
Battery First Time Constant	$\tau_{1,\text{bat}}$	10	[s]	First Polarisation Resistance	$R_{\text{pol1,bat}}$	0.005	[Ω]
Battery Second Time Constant	$\tau_{2,\text{bat}}$	30	[s]	Second Polarisation Resistance	$R_{\text{pol2,bat}}$	1e-4	[Ω]
Initial SoC	SOC_0	50	[%]	Battery Operating Temperature	$T_{\text{bat,0}}$	298.16	[K]

the battery charge signal u, and is calculated as follows [41]:

$$u = \begin{cases} 1, & \text{if charging} \\ \text{-1}, & \text{if discharging} \\ 0, & \text{if disconnected} \end{cases} \Rightarrow I_{\text{bat}} = \begin{cases} <0, & \text{if u = 1} \\ >0, & \text{if u = -1} \\ 0, & \text{if u = 0} \end{cases} \tag{17}$$

$$SOC_{\text{bat}} = SOC_0 - \int \frac{I_{\text{bat}}}{C_{\text{nom,bat}}} dt, \tag{18}$$

Additionally, an ideal TMS of the battery is modelled using the SimScape block "Convective Heat Transfer." The heat power dissipated $Q_{\text{heat,bat}}$ is measured using the "Heat Flow rate Sensor" and connected to an output port, along with the battery temperature sensed using the "Temperature Sensor" block, as depicted in Figure 9.

F. Propeller Model

The propeller system in this model was modelled simply using the propulsive efficiency equation for a symmetric flight, given as [42]:

$$\eta_{\text{prop}} = \frac{P_{\text{prop}}}{P_{\text{mot}}} \tag{19}$$

$$P_{\text{prop}} = F_T V_a \tag{20}$$

$$P_{\text{mot}} = \omega_{\text{mot}} T_{\text{mot}} = \omega_{\text{prop}} T_{\text{prop}} \tag{21}$$

Here, P_{prop} represents the power delivered by the propeller, while P_{mot} denotes the shaft power delivered by the motor. The thrust generated by the propeller is given by F_T (in N), where V_a is the airspeed (in m/s), ω_{mot} represents the angular velocity of the motor shaft (in rad/s), and T_{mot} denotes the mechanical torque of the motor shaft (in N·m).

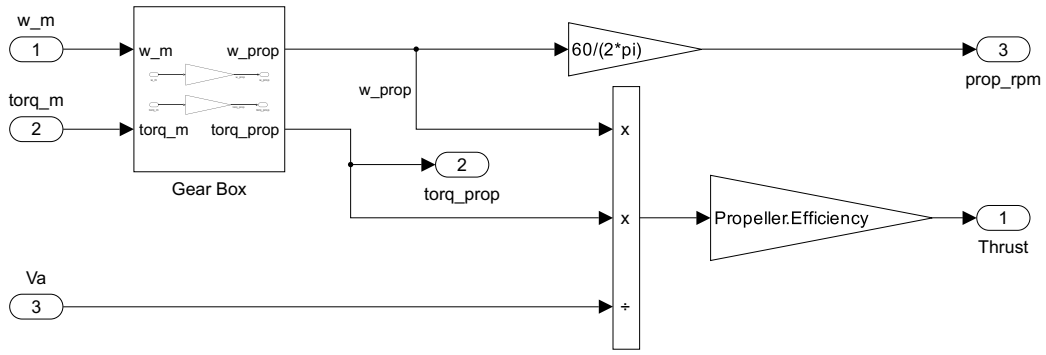

Fig. 10 Simulink Model of Propeller

In addition to the propulsive efficiency equation, a gear box is modelled to adjust the angular velocity for the propeller shaft. Specifically, $\omega_{\text{prop}} = \omega_{\text{mot}}/K$ and $T_{\text{prop}} = KT_{\text{mot}}$, where the Gear Box Factor is denoted by K. It is assumed that the propeller efficiency remains constant throughout the go-around mission profile. The thrust F_T and propeller RPM are calculated from using Equation 19 to Equation 21:

$$F_T = \eta_{\text{prop}} \frac{\omega_{\text{prop}} T_{\text{prop}}}{V_a} \tag{22}$$

$$RPM_{\text{prop}} = \frac{60}{2\pi} \omega_{\text{prop}} \tag{23}$$

These equations, integrated with the gear box model, are implemented in the Simulink model as depicted in Figure 10.

G. Motor Model

PMSM motors employed in aircraft applications possess non-linear dynamics [27], typically necessitating control methodologies like Field-Oriented Control which employs vector-controlled Pulse Width Modulation (PWM) [43, 44] or Predictive Torque Control [44] to drive the motor. However, modelling such control intricacies exceeds the scope of this study, which aims to develop a representative system. Consequently, the motor is simplified and modelled as a first-order dynamic model of shaft angular velocity and shaft torque. The dynamic time constants for the motor dynamics are detailed in Table 9.

Table 9 Motor Characteristics

Property	Symbol	Value		Property	Symbol	Value	
Motor Efficiency	η_{mot}	0.98	-	Time Constant for Torque	$\tau_{mot,trq}$	0.5	[s]
Time Constant for Angular Velocity	$\tau_{mot,\omega}$	0.01	[s]				

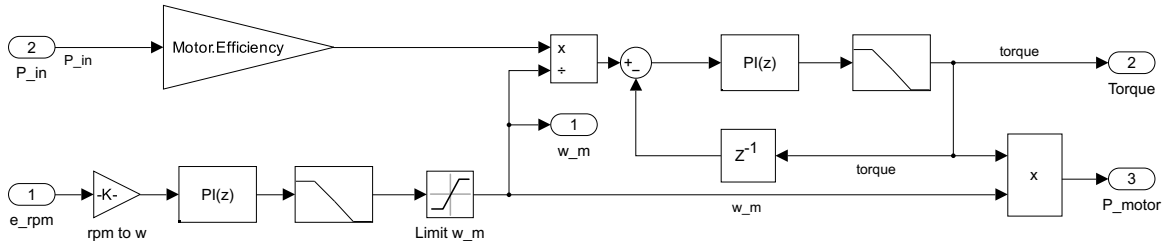

Fig. 11 Simulink Model of Motor

The PMAD provides inputs including the input power $P_{\text{in,mot}}$ and the error in propeller RPM e_{RPM}. The input e_{RPM} undergoes processing by a PI controller followed by first-order dynamics with time constant $\tau_{\text{mot},\omega}$ to yield the motor shaft angular velocity ω_{mot} (in rad/s). This value is then transmitted to the propeller, which calculates RPM_{prop} and relays it back to the PMAD, forming a closed loop.

Additionally, the motor shaft angular velocity ω_{mot} (in rad/s) is used to compute the reference motor shaft torque using the equation:

$$P_{\text{mot,ref}} = \omega_{\text{mot}} T_{\text{mot,ref}} = \eta_{\text{mot}} P_{\text{in,mot}} \tag{24}$$

This reference torque serves as input for a control loop regulating motor shaft torque T_{mot}, utilizing a PI controller and first-order torque dynamics with time constant $\tau_{\text{mot,trq}}$. Thus, the motor system is implemented as illustrated in Figure 11.

H. Power Management and Distribution (PMAD) Model

The final component addressed in the modelling of the HEPS is the Power Management and Distribution System (PMAD). It functions as a crucial element in overseeing and distributing power within the HEPS. This study focuses on modelling three principal subsystems within the PMAD: the Power Decision System, DC-DC Converters, and Motor Control Outputs. Each of these subsystems assumes a significant role in regulating the flow of power within the HEPS, thereby enhancing the overall efficiency and performance of the aircraft. The Simulink model representing the PMAD, illustrated in Figure 12, integrates these subsystems to effectively manage and allocate power within the HEPS. Also, the parameters governing the decisions are set as shown in Table 10.

Table 10 PMAD Operational Settings

Property	Symbol	Value		Property	Symbol	Value	
Maximum Engine Power	$P_{\text{max,eng}}$	1000	[kW]	Hybridisation Factor	HF	0.5	-
Load Power Requirement	P_{load}	30	[kW]	Power Margin	ΔP	50	[kW]
SoC Charge Limit	$SOC_{\text{lim,charge}}$	45	[%]	SoC Discharge Limit	$SOC_{\text{lim,discharge}}$	20	[%]

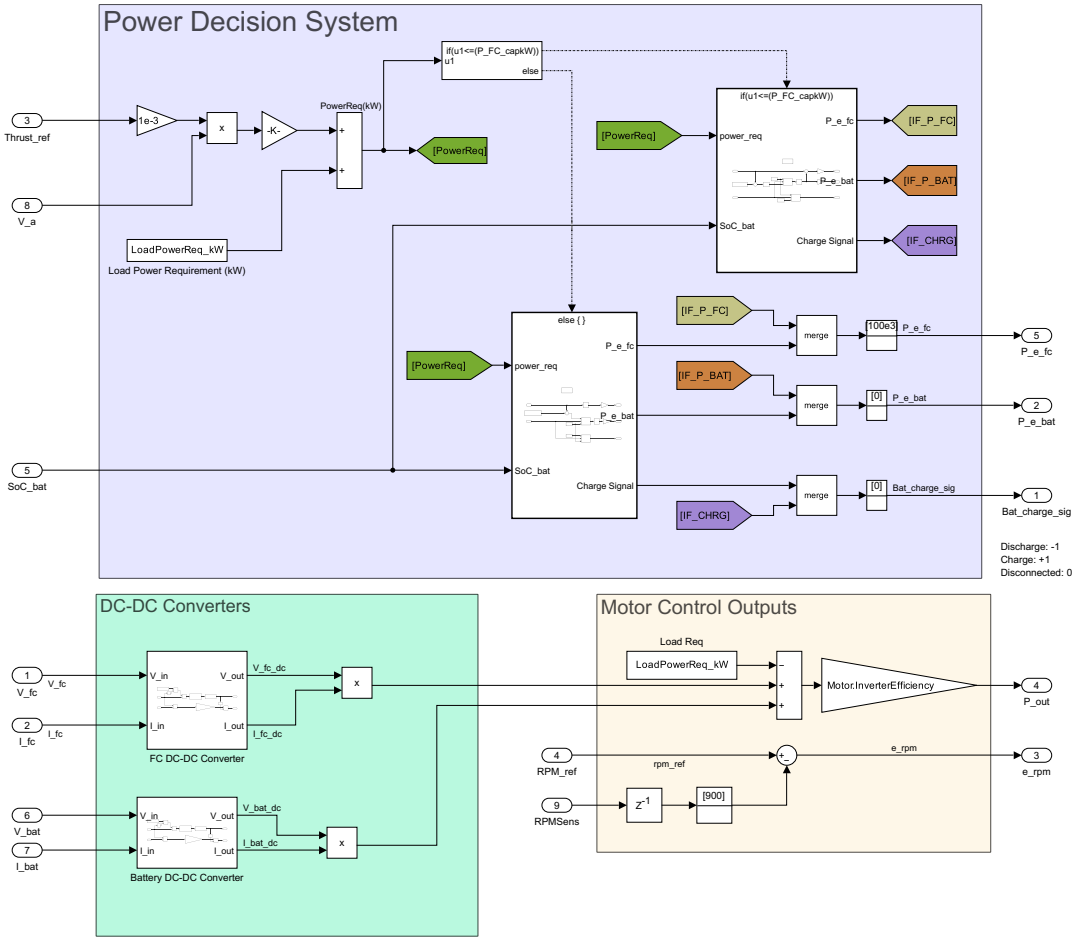

Fig. 12 Simulink Model of the Power Management and Distribution System

1. Power Decision System

This subsystem assumes the responsibility of decision-making concerning power distribution, predicated on various inputs such as the reference thrust $F_{T,\text{ref}}$ (expressed in Newtons), airspeed V_a (measured in meters per second), and battery state of charge SOC_{bat}. It determines the requisite power from both the FC stack and the battery to fulfil the operational demands of the aircraft.

The power required to drive the propeller and motor to generate the desired thrust is computed using $F_{T,\text{ref}}$ and V_a through the formula:

$$P_{\text{req}} = \frac{F_{T,\text{ref}} V_a}{\eta_{\text{mot}} \eta_{\text{prop}}} \tag{25}$$

Nevertheless, within the aircraft, additional electrical loads such as the air compressor, pressurising system, cockpit power, lighting, and air conditioning may necessitate power from this powertrain. Let us postulate that this extra power required by the aircraft systems remains constant throughout the go-around phase, denoted as P_{load}. Thus, the total power required from the power sources is given by: $P_{\text{total}} = P_{\text{req}} + P_{\text{load}}$.

Algorithm 1 Power Distribution: Peak Shaving Algorithm [13]

$P_{\text{fc,cap}} \leftarrow P_{\text{max,eng}} \cdot (1 - HF)$
$\Delta P \leftarrow$ Power Margin
if $P_{\text{total}} \leq P_{\text{fc,cap}}$ **then** ▷ If required power is less than available stack power
  if $SOC_{\text{bat}} < SOC_{\text{lim,charge}}$ **then** ▷ If Battery SoC is below certain charge limit
    $P_{\text{fc,req}} \leftarrow P_{\text{fc,cap}} - \Delta P$ ▷ FC Stack to charge the Battery
    $u \leftarrow 1$ ▷ Battery Charge
  else
    $P_{\text{fc,req}} \leftarrow P_{\text{total}}$
    $u \leftarrow 0$ ▷ Battery Disconnected
  end if
  $P_{\text{bat,req}} \leftarrow u(P_{\text{fc,cap}} - \Delta P - P_{\text{total}})$
else if $P_{\text{total}} > P_{\text{fc,cap}}$ **then** ▷ If required power is more than available stack power
  $P_{\text{fc,req}} \leftarrow P_{\text{fc,cap}}$ ▷ FC Stack working at full power
  if $SOC_{\text{bat}} < SOC_{\text{lim,discharge}}$ **then** ▷ If Battery SoC is below certain discharge limit
    $u \leftarrow 0$ ▷ Battery Disconnected
    $P_{\text{bat,req}} \leftarrow 0$
  else
    $u \leftarrow -1$ ▷ Battery Discharge
    $P_{\text{bat,req}} = P_{\text{total}} - P_{\text{fc,cap}}$ ▷ Extra power provided by battery
  end if
end if

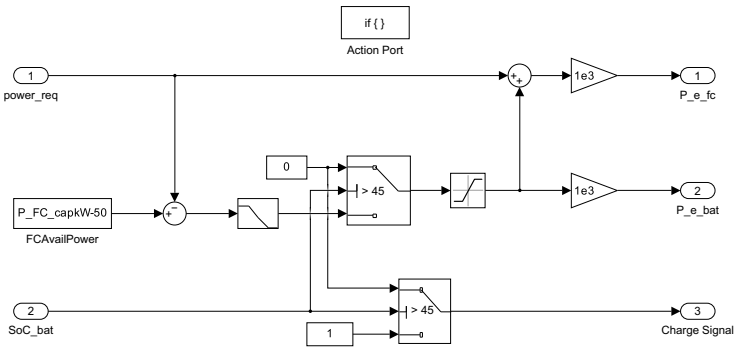

(a) Power Required ≤ Available Stack Power

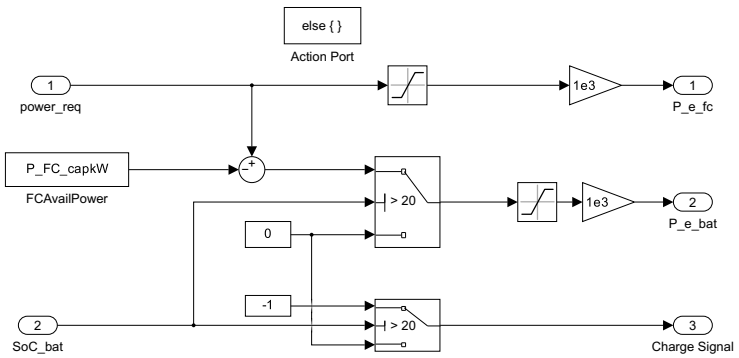

(b) Power Required > Available Stack Power

Fig. 13 Model of PMAD Decision System Peak Shaving Implementation

Subsequently, based on the hybridisation factor (HF), again defined as the ratio of the maximum power to be provided by the battery to the total maximum power of the engine powertrain, a peak-shaving strategy inspired by the work of Hoelzen et al. [13] is implemented. According to this strategy, the fuel cell and battery collaborate to supply power during peak power requirement phases, such as take-off and climb. In contrast, during phases with lower power requirements, such as cruise and landing, only the fuel cell provides power. Additionally, the fuel cell can charge the battery if necessary during these phases. This operational approach adheres to the algorithm outlined in Algorithm 1, the implementation of which is depicted in Figure 13. It is noteworthy that the battery undergoes charging only when its SoC is below the charging limit $SOC_{\text{lim,charge}}$, and it ceases to provide power (discharge) if its SoC falls below the discharging limit $SOC_{\text{lim,discharge}}$. Currently, existing aircraft do not employ this charge-discharge strategy during flight. However, it is assumed that this control logic will be implemented in future aircraft designs.

For this study, $SOC_{\text{lim,charge}}$ was set at 45% to assess the model's implementation of the charge-discharge algorithm across a wider range of SoC values; however, in real-world scenarios, this limit could be different. The $SOC_{\text{lim,discharge}}$ is set at 20% for battery protection, as discussed earlier. Additionally, a power margin ΔP is used to prevent instantaneous switching of battery from discharge to charge phase when P_{total} drops below $P_{\text{fc,cap}}$.

2. DC/DC Converter

The DC/DC converters serve the purpose of maintaining a constant voltage output from both the fuel cell V_{fc} and the battery V_{bat}, ensuring they align with the bus voltage V_{bus} = 1500 V. These converters are pivotal in stabilising the voltage output from the fuel cell and the battery, thereby ensuring compatibility with the bus voltage. By regulating voltage levels, these converters optimise power transfer efficiency and enhance system stability. In this model, two DC/DC converters are employed, one for the FC stack output and another for the battery output.

Mathematically, the DC/DC converters are modelled according to the equation given by Luo et al.[45] as depicted in Figure 14:

$$G_{\text{conv}}(s) = \frac{1}{1 + s\tau_{\text{conv}} + s^2\tau_{\text{conv}}\tau_{\text{d,conv}}} \tag{26}$$

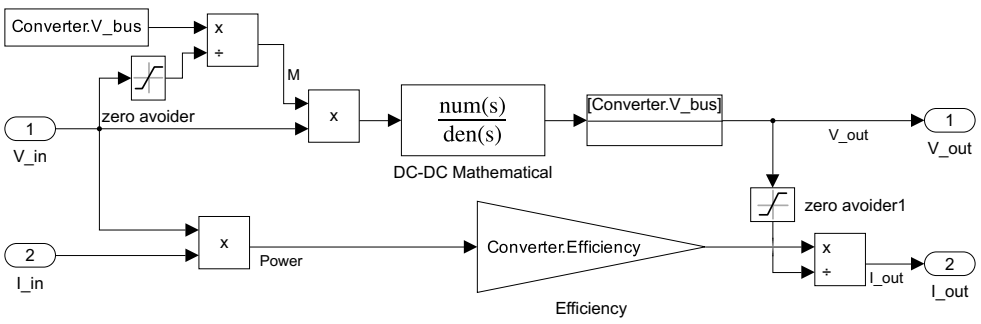

Fig. 14 Simulink Model of DC/DC Converter

Table 11 DC/DC Converter Characteristics

Property	Symbol	Value		Property	Symbol	Value	
Converter Efficiency [13]	η_{conv}	0.98	-	Converter Dynamic Time Constant	τ_{conv}	0.2	[s]
Converter Damping Time Constant	$\tau_{\text{d,conv}}$	0.06	[s]	Bus Voltage	V_{bus}	1500	[V]

Here, τ_{conv} and $\tau_{\text{d,conv}}$ represent the dynamic time constant and damping time constant of a DC/DC converter, respectively. The input voltage $V_{\text{in,conv}}$ undergoes transformation through a feedforward voltage gain $K_{\text{conv}} = \frac{V_{\text{bus}}}{V_{\text{in,conv}}}$ before being applied to the mathematical model to generate the DC/DC converter's output voltage $V_{\text{out,conv}}$. The resulting current $I_{\text{out,conv}}$ is computed as in the following equation. The parameters of the DC/DC Converter, with their assumed values, are presented in Table 11.

$$I_{\text{out,conv}} = \eta_{\text{conv}} \frac{V_{\text{in,conv}} I_{\text{in,conv}}}{V_{\text{out,conv}}} \tag{27}$$

3. Motor Control Outputs

This subsystem primarily involves straightforward calculations. It involves subtracting P_{load} from the sum of the power outputs generated by the two DC/DC converters and passing it through the inverter efficiency ($\eta_{\text{inv}} = 0.98$ [13]) gain to simulate a simple inverter. The output of the inverter is then transmitted as power output to the motor. Moreover, it determines the error between the simulated RPM and the reference RPM signal supplied to the model, as outlined in subsection III.G, and forwards it to the motor.

I. Consolidated Model

The consolidated HEPS Powertrain model is constructed by integrating all the component models – with varying fidelity – according to the architecture depicted in Figure 2. This model encompasses four inputs: reference thrust, reference RPM, altitude, and airspeed, as mentioned in Table 4. Correspondingly, the Simulink Model yields eleven outputs specified in the table, along with four additional outputs which are the heat power generated by the stack and battery, and the heat power required for heating hydrogen and air to $T_{\text{fc,0}}$. The model is represented in Figure 15.

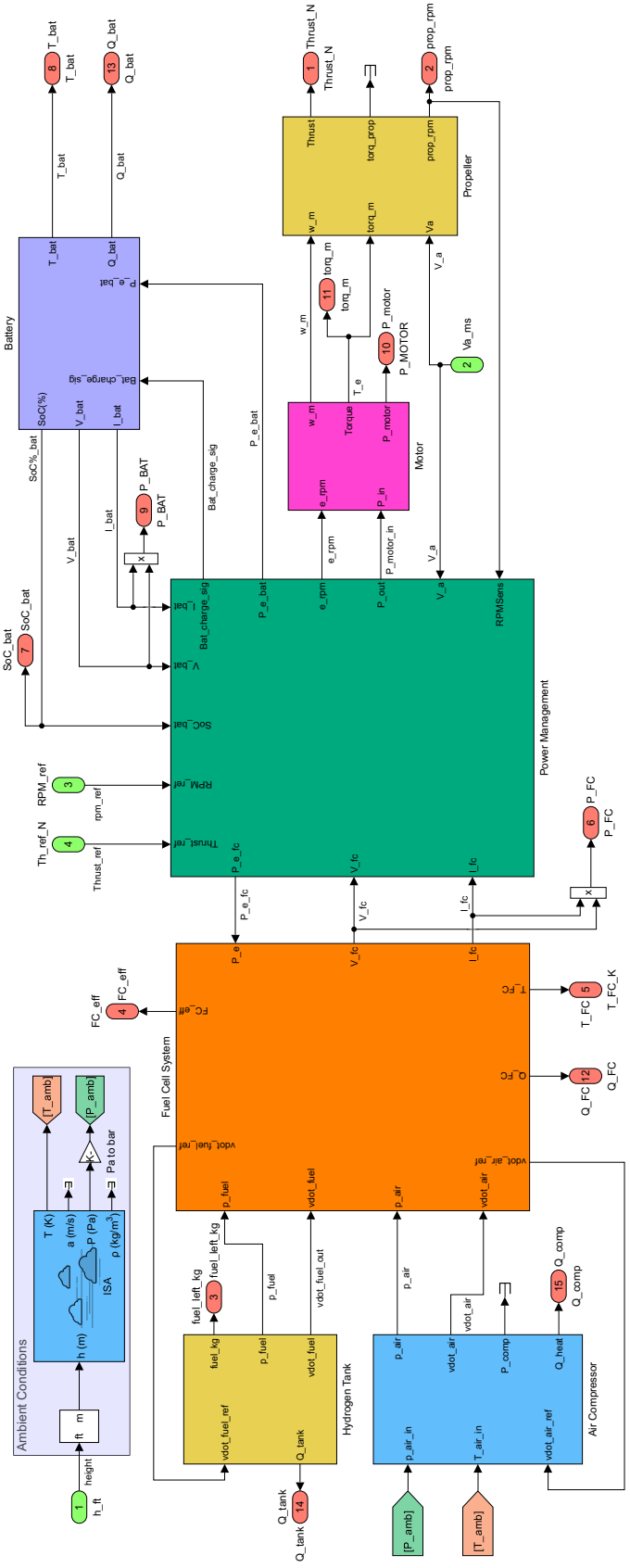

Fig. 15 Full Simulink Model for 1MW Engine HEPS Powertrain

IV. Model Simulation and Operational Envelope Exploration Setup

To simulate the HEPS powertrain model effectively for this mission, continuous input of the true airspeed (V_a) in meters per second, flight path angle (γ) in radians, and the reference propeller RPM ($RPM_{\text{prop,ref}}$) for a go-around scenario is essential throughout the simulation duration. Initially, the desired flight path angle (γ) and airspeed (V_a) are employed to determine the required thrust and altitude of the aircraft. This is accomplished by employing aircraft performance equations [42] based on the point-mass aircraft symmetric flight free-body diagram (Figure 16). This preliminary step lays the groundwork for subsequent simulation endeavours.

$$h = h_0 + \int V_a \sin(\gamma) dt \tag{28}$$

$$F_{\text{T,ref}} = F_D \cos\alpha - F_L \sin\alpha + M[g \sin(\gamma + \alpha) + \dot{V}_a \cos\alpha] \tag{29}$$

$$= \frac{1}{2} C_D \rho V_a^2 S \cos\alpha - \frac{1}{2} C_L \rho V_a^2 S \sin\alpha + M \left[g \sin(\gamma + \alpha) + \dot{V}_a \cos\alpha\right] \tag{30}$$

Here, h_0 represents the initial altitude (in m), F_D denotes the drag force (in N), F_L denotes the lift force (in N), α denotes the angle of attack (in rad), M signifies the mass of the aircraft (in kg), V_a denotes the true airspeed of the aircraft (in m/s), $\dot{V}_a$ stands for the aircraft acceleration (in m/s^2), g represents the acceleration due to gravity in (in m/s^2), C_D indicates the drag coefficient of the aircraft, C_L indicates the lift coefficient of the aircraft, ρ represents the air density (in kg/m^3), and S denotes the wing area (in m^2). Through these computations, all four inputs - V_a, $F_{\text{T,ref}}$, h, and $RPM_{\text{prop,ref}}$ - are integrated into the Simulink model to facilitate the simulation process.

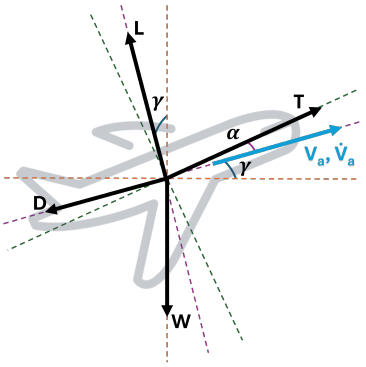

Fig. 16 Point-mass aircraft FBD

In this simulation, airspeed and flight path angle are established based on the mission profile shown in Figure 1 with aircraft mass M = 38000 lbs and $V_{GA} = V_{a_0}$ = 96 kts. It is important to note that unlike conventional carbon-based propulsion systems, the HEPS boasts high fuel efficiency. Therefore, the variation in aircraft mass due to fuel burn during short missions is relatively small, and neglected here. Consequently, the aircraft mass is assumed to remain constant throughout the simulation. Beginning with an initial altitude of 410 feet (h_0 = 410 ft), the aircraft ascends and stabilises at an altitude of 2000 feet, meeting the Schiphol go-around requirement. This milestone is reached approximately 85 seconds into the simulation. Therefore, the simulation duration is set to T_{sim} = 85 at a frequency of 1000 Hz to accommodate the higher rate required for simulating the fuel cell system model effectively. A dedicated model is developed within Simulink to execute this simulation, thereby enhancing the facilitation of the entire process. The model, depicted in Figure 17, provides a structured framework for seamlessly running the simulation, ensuring efficiency and accuracy in the analysis of the HEPS powertrain.

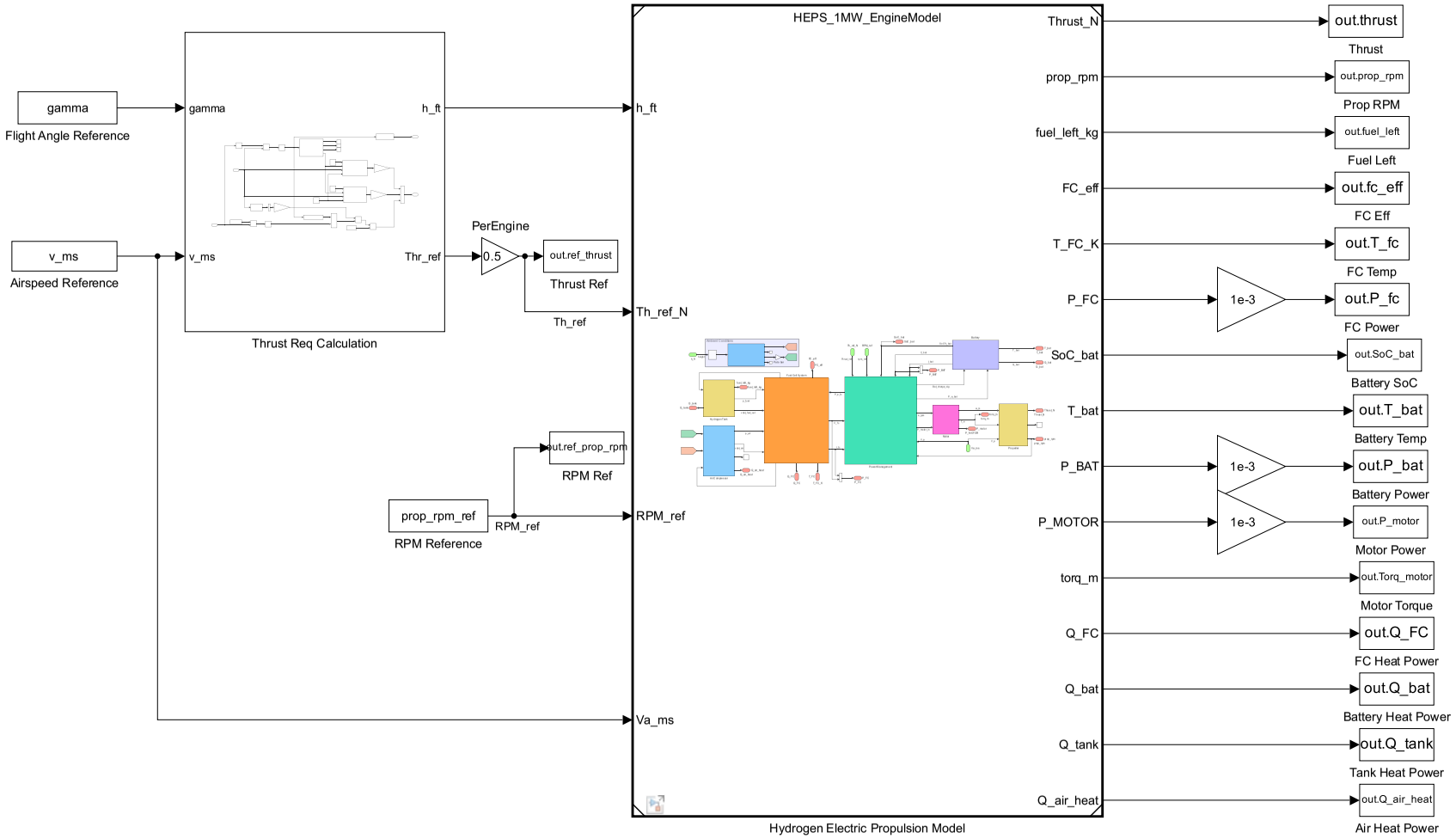

Fig. 17 Simulink Model to run the HEPS Powertrain with given mission profile

A. Unit Tests

Prior to initiating tests on the entire model, a thorough examination of its sub-units is vital. This step aids in the isolation and prompt identification of any faults, leading to fewer complications during the consolidated model simulation. In this context, three main power units within the comprehensive system undergo evaluation: two units responsible for providing power and one unit consuming power. These unit models are visually represented in Figure 18.

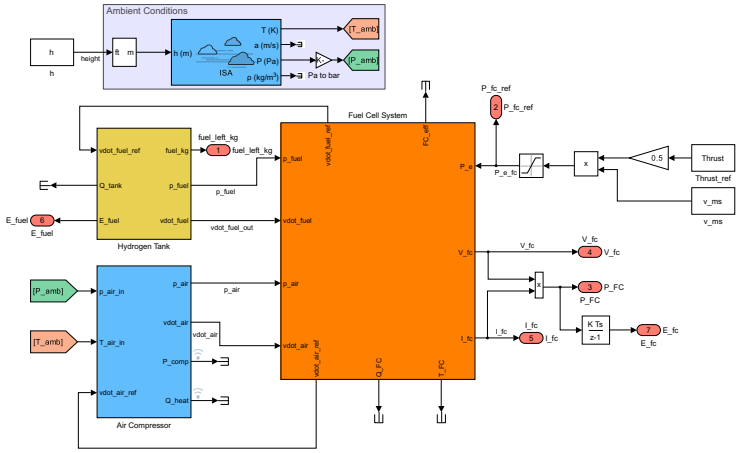

(a) Fuel Cell Power Unit

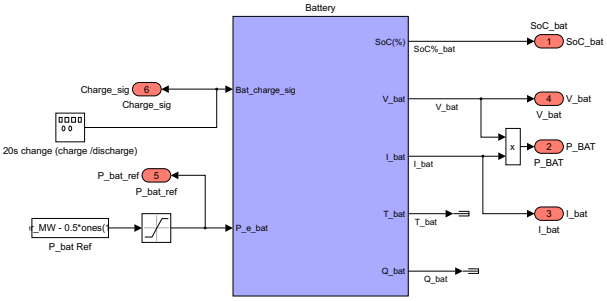

(b) Battery Power Unit

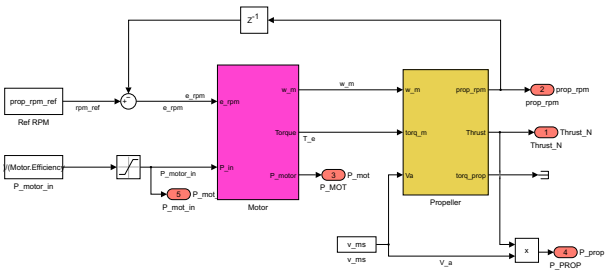

(c) Propulsion Power Unit

Fig. 18 Power Units present in the Model

The Fuel Cell Power Unit, serving as the primary power source for the HEPS powertrain, is the first unit scrutinised. This unit encompasses the fuel cell system, hydrogen tank, and air compressor, collectively contributing to the generation of electrical power. Next, the Battery Power Unit, acting as an auxiliary power source, undergoes assessment. This unit comprises the battery, playing a vital role in storing and supplying electrical energy as required. Lastly, the Propulsion Power Unit, responsible for consuming power to propel the aircraft forward, is examined. This unit includes the motor and the propeller, essential components for generating thrust and facilitating aircraft movement.

To evaluate their functionality, these units are subjected to mock inputs, simulating various operating condition.

B. Operational Envelope Exploration

Exploring the operational envelope of the HEPS Powertrain Simulink model is critical because it allows for the identification of key factors influencing system behaviour. This exploration aids in determining the most suitable operating conditions for the mission profile. Furthermore, it helps to evaluate the model's reliability by checking for consistent performance across various conditions by systematically adjusting input parameters and observing corresponding output responses.This exploration serves a dual purpose as a sensitivity analysis of the model, suggesting areas for model refinement and facilitating targeted optimisation efforts to enhance model fidelity for real-world applications.

During a go-around, a pilot's primary concern is ensuring that the aircraft can deliver adequate power for take-off thrust and climb thrust under the prevailing conditions. Therefore, it is important to monitor the model's outputs, including power outputs, thermal conditions, thrust generation, battery SoC, and fuel remaining in the tank, across various scenarios and parameters such as:

1) **Battery Initial State of Charge** SOC_0:

   The initial state of charge of the battery affects the amount of stored energy available for propulsion during the go-around maneuver. A higher SoC ensures a greater reserve of electrical energy, allowing for continuous power delivery during critical flight phases.

   For the exploration, the battery's initial SoC ranges from 15% to 85% at the same $C_{\text{nom,bat}}$ of 200Ah.

2) **Battery Nominal Capacity** $C_{\text{nom,bat}}$:

   The capacity of the battery determines its energy storage capability and the rate of drop in the SoC. A higher battery capacity translates to a greater amount of available energy, which is essential for providing the required power during the go-around phase

   The nominal capacity of the battery is varied between 20 Ah and 500 Ah, with the bus voltage of 1500V.

3) **Aircraft Mass** M:

   The weight of the aircraft directly influences its performance during the go-around manoeuvre. Heavier aircraft require more propulsion power to achieve the desired climb rate and altitude, so weight is an important factor in determining energy requirements and overall propulsion system efficiency.

   The aircraft weight is varied between 34000 lbs and 40000 lbs (MLM) during the exploration to simulate an increasing payload. This increase in payload equates to approximately 40 passengers, with an average weight of 150 lbs each, being accommodated in the aircraft.

4) **Velocity at Go-around** V_{GA}:

   The velocity at go-around has a significant impact on the aerodynamic forces acting on the aircraft, as well as the power needed for propulsion. Higher velocities may require more propulsion power to maintain safe flight parameters during the go-around phase.

Go-around Velocity is increased from 96 kts to 104 kts.

5) **Propeller Efficiency** η_{prop}:

Propeller efficiency directly impacts thrust generation and, consequently, the aircraft's climb rate and manoeuvrability during go-around manoeuvres. High propeller efficiency leads to more effective propulsion, lower energy losses, and improved overall system effectiveness and responsiveness.

For the exploration, the propeller efficiency is varied between 0.7 and 1.

To facilitate the exploration, a dedicated MATLAB script was developed to streamline the iterative simulation process of the model depicted in Figure 17. This script operates systematically by adjusting parameters of interest and executing the Simulink model for each distinct parameter set. It collects and stores the resultant simulation output data to enable further analysis. Subsequently, the script leverages this accumulated data to generate graphical representations of the simulation outputs. These visualisations offer a comparative view across different values of the varied parameter, thereby aiding in the discernment of how variations in specific parameters impact the overall system behaviour.

V. Results

A. Individual Unit Tests

As discussed in the previous section, test runs of the individual units were conducted to check and correct the model. The final simulation results for these power unit runs are presented in Figure 19.

Upon examining the simulation results of the fuel cell power unit (in Figure 19a), it becomes evident that the fuel cell power unit effectively fulfils its role in providing the required power. This assertion is supported by the close alignment observed between the plots of the reference power $P_{\text{ref,fc}}$ and the actual power delivered by the FC Stack P_{fc}. Moreover, an interesting observation emerges regarding the consumption of hydrogen, which closely mirrors the output power dynamics. Specifically, when the power provided by the stack is low, the drop in the liquid hydrogen mass M_{H_2} in the tank occurs at a slower rate. Conversely, when the fuel cell operates at its maximum power output, the depletion of hydrogen accelerates accordingly. The stack voltage V_{st} and current I_{st} graph exhibit an initial surplus voltage when the stack provides less power than its nominal rating. Subsequently, the voltage gradually stabilises, reaching its nominal value of 1500V. Correspondingly, the current increases in line with the power demand. The observed variation in stack output voltage underscores the critical role of the DC/DC converter in maintaining a constant bus voltage, ensuring consistent and reliable power distribution throughout the system. Finally, it is worth noting that the energy supplied by the FC stack consistently accounts for approximately 50-60% of the energy stored in the hydrogen fuel consumed with gravimetric energy density being about 120 MJ/kg [46]. This aligns with the nominal efficiency defined for the FC stack.

In the simulation of the battery power unit (refer to Figure 19b), the input charge signal u determines whether the battery is being charged or discharged, toggling between these modes via a square wave. The power plot of the battery

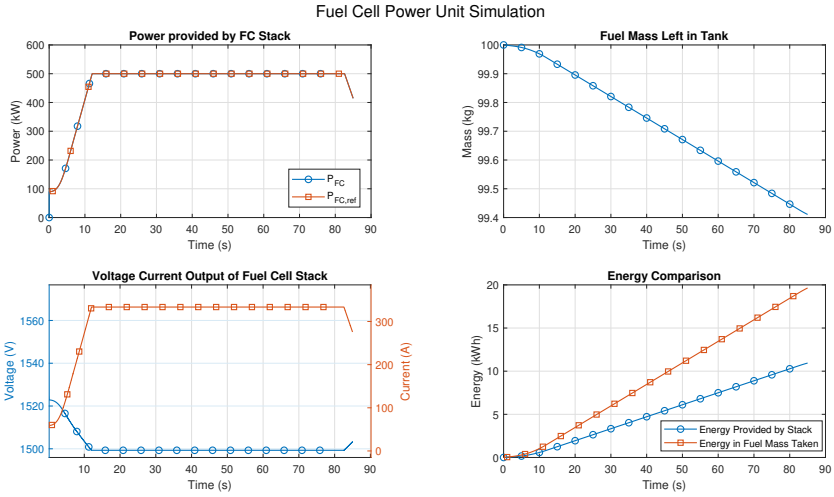

(a) Simulation Results for Fuel Cell Power Unit

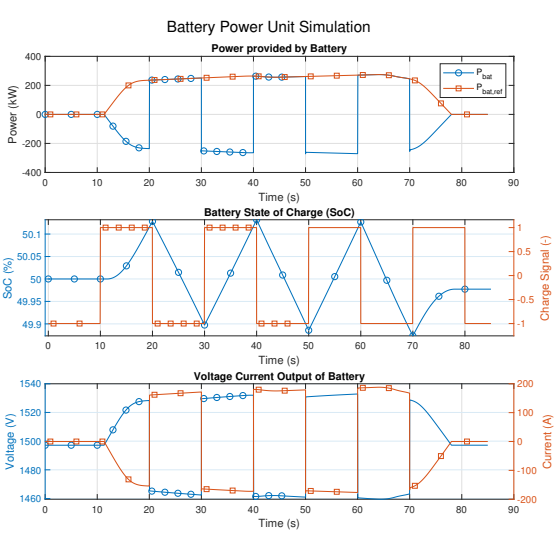

(b) Simulation Results for Battery Power Unit

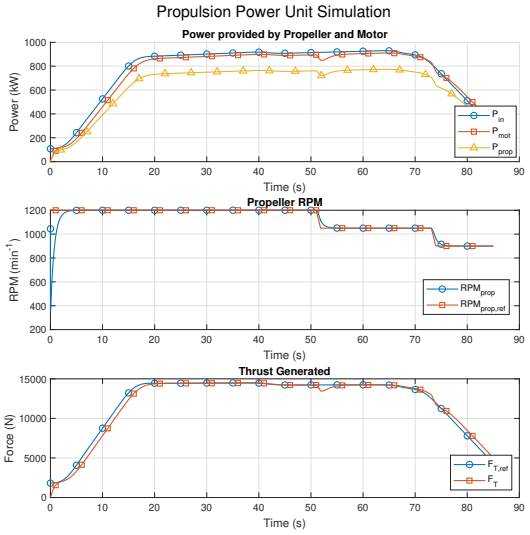

(c) Simulation Results for Propulsion Power Unit

Fig. 19 Simulation Results for Power Units

illustrates that it provides or consumes power in accordance with this charge signal, denoted by $P_{\text{bat}} = uP_{\text{bat,ref}}$. This charge and discharge behaviour is also reflected in the SOC_{bat} graph, where the state of charge increases for $u = 1$ and decreases for $u = -1$. Moreover, the battery voltage V_{bat} exhibits an increase during charging and drops slightly below 1500V during discharge. The battery current I_{bat} follows the power demands accordingly. Thus, a DC/DC converter is also required for the battery to maintain a constant bus voltage.

Lastly, the simulation of the propulsion power unit (depicted in Figure 19c) illustrates the reduction in the power delivered by both the motor, P_{mot}, and the propeller, P_{prop}, compared to the input power provided to the motor, P_{in}, due

to their respective efficiency factors. The propeller RPM, RPM_{prop}, closely tracks the reference RPM, $RPM_{\text{prop,ref}}$, with a slight lag attributed to the motor's dynamics. The initial few seconds of these plots are disregarded, as the initial conditions of the system may differ in a real-world scenario. Finally, the thrust generated, F_{T}, by this unit closely follows the reference thrust, $F_{\text{T,ref}}$, albeit with a slight lag, again attributable to system dynamics.

B. Complete Model Simulation

With all the individual units functioning as desired, the full model undergoes simulation. The expected outputs identified earlier can be categorised into four groups based on their common characteristics. These categories are as follows:

- Power-related outputs: P_{fc}, P_{bat}, and P_{mot}.
- Thermal outputs: T_{fc}, T_{bat}, $Q_{\text{heat,fc}}$, $Q_{\text{heat,bat}}$, $Q_{\text{heat,tank}}$, and $Q_{\text{heat,air}}$.
- Battery or Fuel Cell-related outputs: η_{st}, SOC_{bat}, and M_{H_2}.
- Propulsion-related outputs: T_{mot}, RPM_{prop}, and F_T.

The simulation results of the complete HEPS Engine Powertrain model system under the specified conditions and mission profile are presented in the aforementioned categories in Figure 20.

From the analysis of Figure 20a, it becomes evident that during the initial phase, such as when the aircraft is preparing for take-off or executing a go-around thrust, the power is solely provided by the FC stack. However, as the demand for power escalates significantly during the climb, the battery supplements the FC stack by supplying additional power. This support from the battery is discontinued only when the aircraft begins to stabilise, following the predefined mission profile. It is noteworthy that the power delivered by the motor to the propeller closely mirrors the total power supplied by both the stack and battery. This dynamic power distribution between the FC stack and the battery during different flight phases, particularly during go-around manoeuvres, underscores the versatility and adaptability of the HEPS powertrain. The smooth transition from fuel cell power to combined fuel cell and battery power underscores the system's capability to meet sudden increases in power demand effectively, ensuring uninterrupted and reliable propulsion.

Moving on to the thermal analysis depicted in Figure 20b, it is observed that, as anticipated due to the assumption of an "ideal" TMS, the temperatures of both the FC stack and the battery remain constant. To sustain this stability, the heat generated by the FC stack ($Q_{\text{heat,fc}}$) and the battery ($Q_{\text{heat,bat}}$) must be dissipated entirely. The substantial waste heat, as high as 400kW, generated by the FC stack indicated in the graphs emphasises the necessity of a highly efficient TMS onboard the aircraft for both the FC stack and the battery. Particularly during go-around manoeuvres when power demands are at their peak, maintaining thermal stability of these components becomes crucial to prevent overheating and ensure optimal performance. The significant heat power generated underscores the need for implementing advanced thermal management strategies to dissipate excess heat effectively and maintain system integrity. Furthermore, the

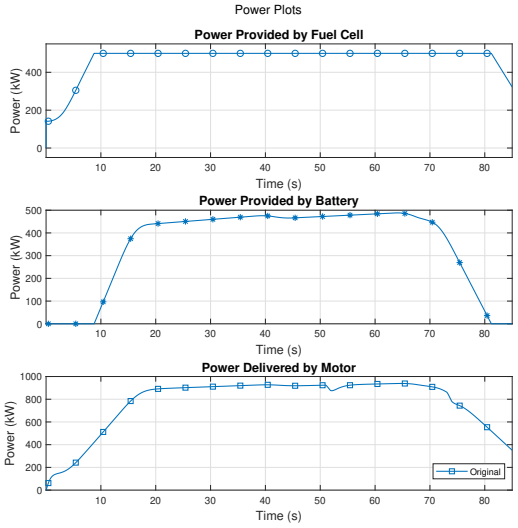

(a) Simulation Results for Power Related outputs

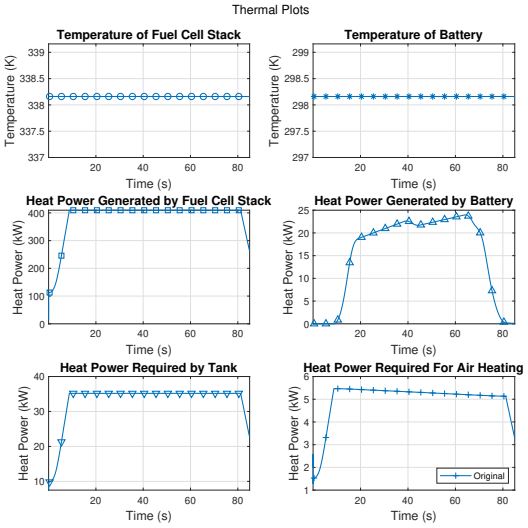

(b) Simulation Results for Thermal outputs

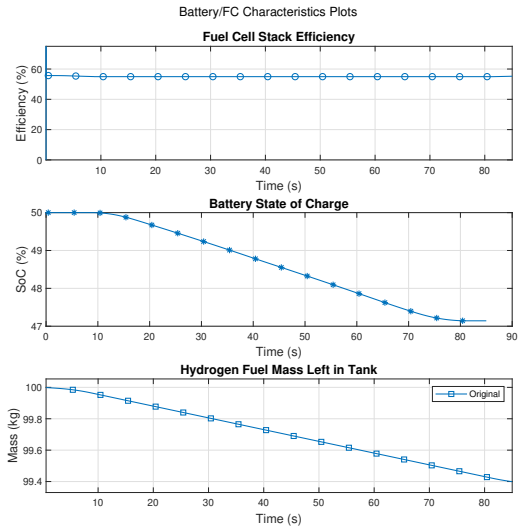

(c) Simulation Results for Battery/FC related outputs

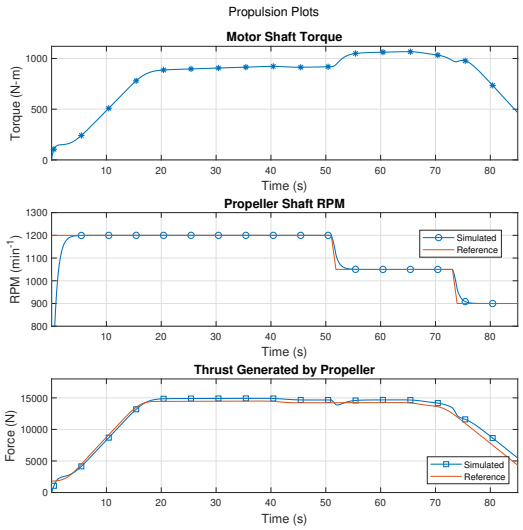

(d) Simulation Results for Propulsion related outputs

Fig. 20 Simulation Results of the HEPS Powertrain Engine

heat demand graphs for H_2 evaporation and heating in the tank as well as air heating show a combined heat power requirement of around 40 kW. This observation suggests that the heat extracted from the battery and FC Stack could be used to heat the air and hydrogen via the TMS to improve thermal flow through the system. Nonetheless, it is important to note that there is an extensive surplus of heat that must be dissipated in order to ensure optimal operation of FC stack.

Regarding the battery and fuel cell characteristics analysis presented in Figure 20c, the fuel stack efficiency remains relatively constant throughout the mission, hovering around the nominal efficiency of $\eta_{\text{st,nom}} = 55\%$. This consistent fuel

stack efficiency throughout the mission period indicates the steady performance of the fuel cell system, which is critical for sustaining propulsion during critical flight phases like go-around. The Battery SoC experiences a decline during the climb phase, wherein the battery provides peak shaving power, before stabilising once the battery is disconnected. It is observed that the SoC drops by approximately 3% by the end of the given mission, which aids in determining the lowest SoC% required for the go-around to be completed safely. In this case, it would be the 23% taking the SoC margin of 20% into account. In the graph depicting fuel left in the tank, the gradual decrease in fuel mass corresponds to hydrogen consumption by the fuel cell throughout the mission. The consumption of hydrogen mass is very low (~0.6 kg), even during the peak power requirement flight phase of a single go-around. It stores approximately 20 kWh of energy, underscoring the fuel efficiency of liquid hydrogen propulsion. When accounting for inefficiencies in the modelled powertrain, this produces approximately 8.5kWh of propulsive energy. This analysis aids in determining the lowest levels of fuel required in the tank for successfully completing power-intensive manoeuvres such as the go-around.

Finally, as depicted in Figure 20d, the propeller RPM closely tracks the reference signal, as does the thrust generated by the propeller. The motor shaft torque gradually increases to adjust the propeller shaft torque accordingly, matching the thrust requirement while maintaining a constant propeller RPM. The close tracking of propeller RPM and thrust with the reference signals during go-around signifies the responsiveness of this HEPS system representative model.

C. Operational Envelope Exploration

The results of the operational envelope exploration for the HEPS engine powertrain model are presented and analysed in the section that follows. This analysis seeks to provide insights into the system's behaviour under various conditions by systematically varying multiple parameters, with the goal of not only contributing to informed decision-making for real-world applications by examining the operational limits of the HEPS powertrain in given conditions but also suggest potential improvements in the model.

1. Sensitivity to Battery Initial State-of-Charge

As previously discussed, the Initial State of Charge (SoC) of the battery holds significant importance for the successful execution of a go-around manoeuvre, as it directly influences the battery's ability to deliver the required power during the manoeuvre. Consequently, the parameter SOC_0 is systematically varied within the range of 85% charge to 15%, representing a typical battery operating range, with a constant battery capacity $C_{\text{nom,bat}} = 200$ Ah. The simulation results for varying values of SOC_0 are depicted in Figure 21.

In Figure 21a, it is observed that altering the initial SoC has no discernible impact on the stack efficiency, which aligns with expectations. The next graph in the figure illustrates the battery's SoC throughout the mission. While a decline in SoC is evident across most model simulations, a more detailed view of cases with $SOC_0 \leq 0.4$ 2 reveals an initial increase in SOC_{bat}, attributed to the battery's charging with surplus power drawn from the FC stack, as dictated

by the PMAD algorithm. Subsequently, the SoC decreases due to discharge during the climb phase, with additional charging occurring at the end if the SoC remains below the charging threshold. Furthermore, when $SoC_0 \leq 0.2$, the battery discharge is disconnected by the PMAD, resulting in the SoC remaining unchanged. The effect of battery charging is further evidenced in the stack power graph (Figure 21b), wherein higher power is drawn from the stack during initial and final stages for $SOC_0 \leq 0.4$ compared to other SOC_0 values. The charging process is also evident in the P_{bat} graph, with negative power denoting charging power consumed by the battery for $SOC_0 \geq 0.4$. Moreover, for

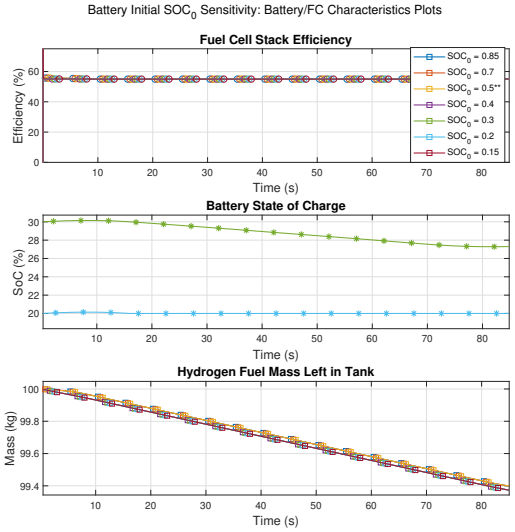

(a) Simulation Results for Battery/FC related outputs: Expanded View of SoC

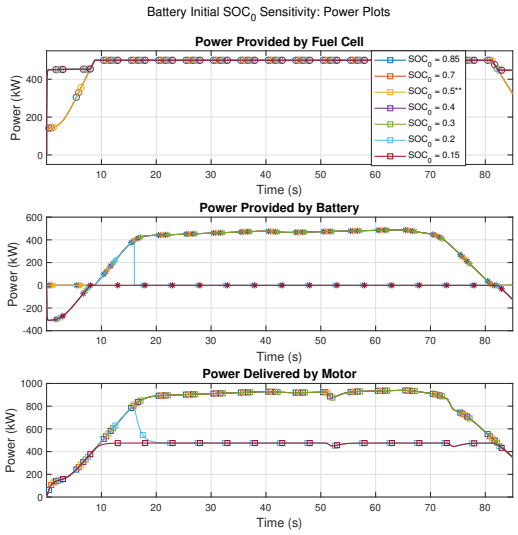

(b) Simulation Results for Power Related outputs

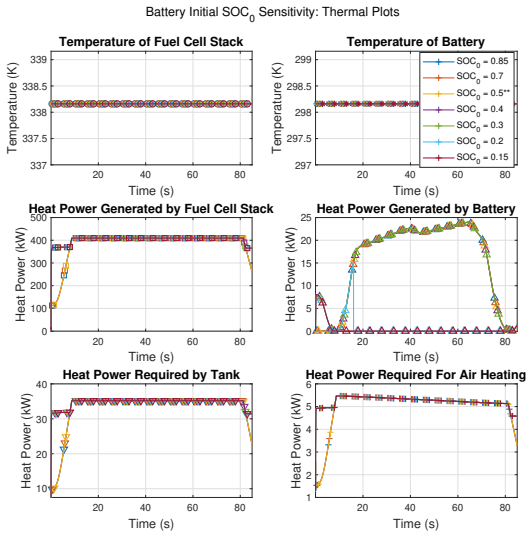

(c) Simulation Results for Thermal outputs

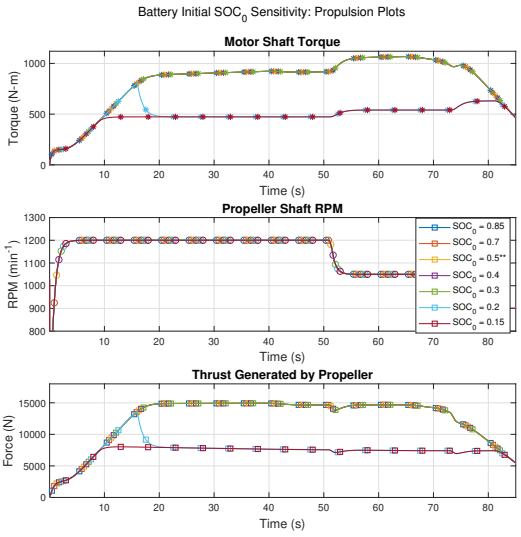

(d) Simulation Results for Propulsion Related outputs

Fig. 21 SOC_0 Sensitivity Analysis Graphs

$SOC_0 \leq 0.2$, as the battery becomes disconnected to ensure battery protection, the power graph drops to zero.

The charging activity impacts the heat power generated by both the stack (due to additional power provision) and the battery (during charging), as well as the increased power required for hydrogen and air heating (Figure 21c), stemming from heightened consumption during the stack's supplementary power output. Consequently, the slightly diminished fuel mass left in the liquid hydrogen tank for $SOC_0 \leq 0.4$, shown in Figure 21a, is attributable to this increased consumption. Under the assumption of an ideal TMS, there is no observable effect of SOC_0 variation on the stack and battery temperatures.

As depicted in Figure 21b and Figure 21d, disconnecting the battery for $SOC_0 \leq 0.2$ leads to a notable decrease in power supplied to the motor, resulting in inadequate motor torque and hence diminished thrust generation. This highlights the unsuitability of this range of initial SoC for completing a go-around maneuver with battery protection, underscoring the necessity of a minimum initial battery SoC of 23% for a nominal battery capacity $C_{\text{nom,bat}}$ of 200 Ah. Intriguingly, these adjustments do not affect the propeller RPM, even with reduced power.

2. Sensitivity to Battery Nominal Capacity

In addition to SOC_0, the nominal capacity of the battery ($C_{\text{bat,nom}}$) is another vital parameter that reflects the energy storage capacity of the battery unit. Variations in this parameter are essential for evaluating the performance of the powertrain during the go-around phase. The simulation results for different values of $C_{\text{bat,nom}}$ are presented in Figure 22.

In this context, modifying this parameter of the battery unit does not influence the fuel stack efficiency, remaining fuel in the tank, or the overall power delivered to the motor. Consequently, this lack of impact extends to the power

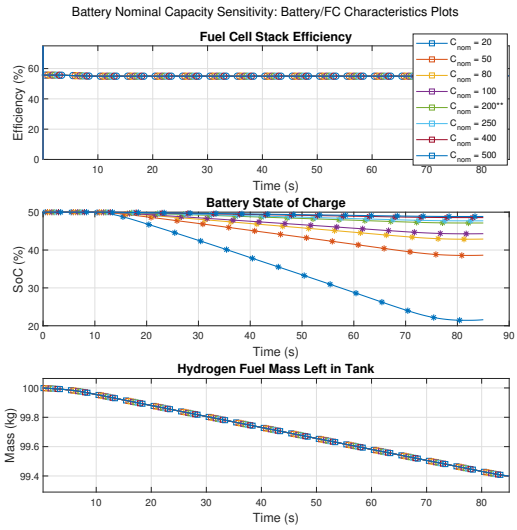

(a) Simulation Results for Battery/FC related outputs

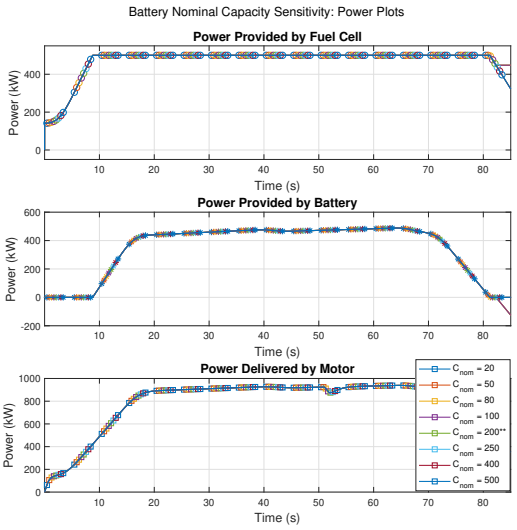

(b) Simulation Results for Power Related outputs

Fig. 22 $C_{\text{bat,nom}}$ Sensitivity Analysis Graphs

output of the motor, motor torque, propeller RPM, and the thrust generated by the propeller. Primarily, it affects three key outputs of our model: the battery State of Charge (SoC), the power supplied by the fuel cell, and the power supplied by the battery under mission conditions.

As the nominal capacity decreases, the charge stored in the battery diminishes accordingly, resulting in a rapid decline in the battery SoC. This phenomenon is illustrated in the simulation results depicted in Figure 22a, wherein the SoC experiences a substantial drop to around 20% for $C_{\text{nom,bat}} = 20$ Ah. Such a significant decrease implies that if a need arises for a second go-around, an aircraft equipped with a 20 Ah battery would need to wait until the battery is sufficiently charged before the pilot can attempt another go-around. Conversely, an aircraft with a nominal capacity of 50 Ah sees its SoC drop only to around 40%, providing ample margin to attempt another go-around without delay.

The power plots indicate that with an initial SoC of 50%, there is no immediate need to charge the battery at the outset. However, once the battery's power support to the stack is exhausted, the SoC drops below the charging threshold for cases where $C_{\text{nom,bat}} \leq 100$ Ah, prompting recharging with the stack power. Similar implications to that of SoC analysis emerge for heat power generation/requirements due to charging in the final stages,for simulations where $C_{\text{nom,bat}} \leq 100$ Ah. No change in the temperature of either the battery or the FC stack are observed for this analysis, due to the ideal TMS.

3. Sensitivity to Aircraft Mass

The weight of an aircraft plays a crucial role in determining the energy demands of its powertrain system, especially during high-power phases like the go-around, where maintaining consistent airspeed and rate of climb is paramount. To assess its impact, the aircraft weight is varied within the range of 34,000 lbs to 40,000 lbs, which corresponds to the maximum landing mass of the Dash 8-Q300 aircraft. The simulation outcomes corresponding to these weight variations are depicted in Figure 23.

Variations in aircraft mass prompt corresponding adjustments in thrust requirements to maintain consistent airspeed throughout the mission profile. Specifically, an increase in mass necessitates higher thrust requirements, while a decrease in mass diminishes these demands. Consequently, the power demand fluctuates accordingly, with heavier aircraft requiring more power and lighter aircraft necessitating less, as evidenced in the power characteristics depicted in Figure 23a. While alterations in aircraft mass did not significantly affect power derived from the stack, as it consistently provides 500 kW power for almost the entire duration of the mission, heavier aircraft experience this power demand over a longer duration. However, an increase in power derived from the battery is observed as aircraft mass increases. For aircraft masses of 39,000 and 40,000 lbs, the battery even operates at maximum power for a duration, underscoring its critical role in heavier aircraft configurations.

The amplified power demand from the battery implies increased heat generation by the battery, as depicted in Figure 23b. Although other heat power characteristics also experience some alterations with changes in aircraft mass,

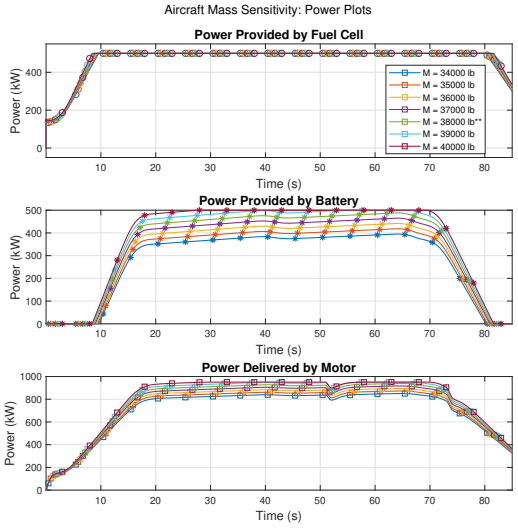

(a) Simulation Results for Power Related outputs

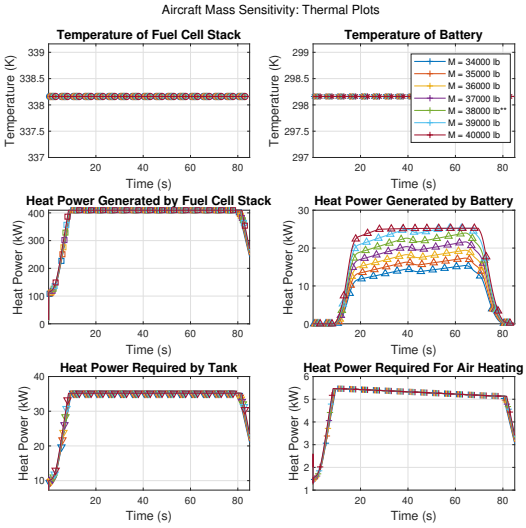

(b) Simulation Results for Thermal outputs

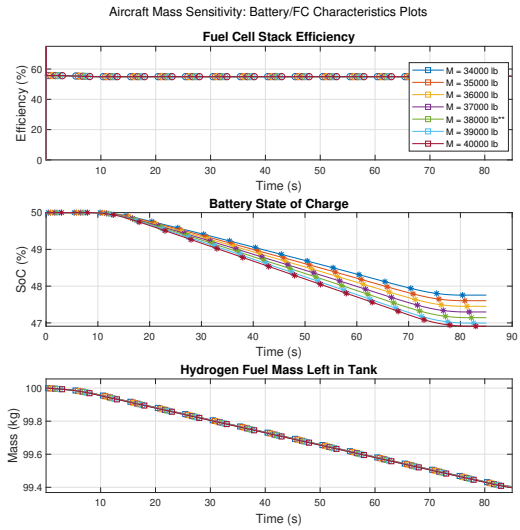

(c) Simulation Results for Battery/FC related outputs

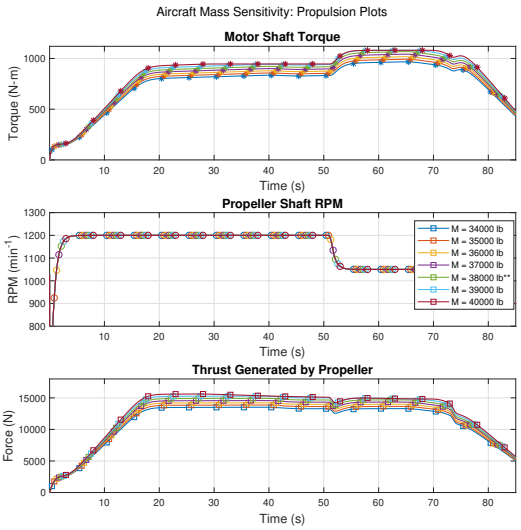

(d) Simulation Results for Propulsion related outputs

Fig. 23 Aircraft Mass Sensitivity Analysis Graphs

these changes are not as substantial as the increased power demand from the battery. The battery power increase also results in a more rapid decline in State of Charge (SoC) for heavier aircraft. However, the difference in final SoC between the heaviest and lightest aircraft is only 1%, as shown in Figure 23c which means that even heavier aircraft can complete the go-around successfully with the help of battery power under current mission conditions. The slight increase in stack power results in only a negligible decrease in the hydrogen mass left in the tank for heavier aircraft configurations. In addition, the variation in aircraft mass has minimal impact on stack efficiency.

Due to the elevated thrust requirements arising from heavier aircraft, the combined power provided by the FC stack and battery results in increased motor torque and consequently higher thrust for the mission. Remarkably, changes in aircraft mass do not influence propeller RPM. However, it is important to note that due to the limit on the maximum power supplied from the battery-FC combination, the thrust generated for heavier aircraft (39,000 lbs and 40,000 lbs) is slightly lower than the required thrust for those aircraft masses. As a result, these aircraft may take a little longer than expected to complete the mission.

4. Sensitivity to Velocity at Go-Around

The go-around speed (V_{GA}) stands as one of the main parameters governing thrust requirements during a go-around manoeuvre, thus influencing the energy demands of the powertrain. Consequently, a sensitivity analysis was conducted to assess the system's response to variations in V_{GA}. The range of V_{GA} was systematically explored, spanning from 96 knots to 104 knots. The selection of 96 knots as the baseline choice is deliberate, stemming from its designation as the prescribed go-around speed for the chosen aircraft mass, as delineated in the aircraft manual. The simulation results are depicted in Figure 24.

The analysis of the powertrain's response to changes in V_{GA} unveiled subtle but noticeable shifts across various parameters. Notably, as go-around speeds increased, both the stack and the battery generated slightly greater electrical power, as illustrated in Figure 24a. This increased power demand had a significant impact on the battery's heat generation, which increased considerably. This contrasted with the relatively minor effects observed on other heat-related characteristics within the system. As depicted in Figure 24c, the variation of go-around speed had no discernible

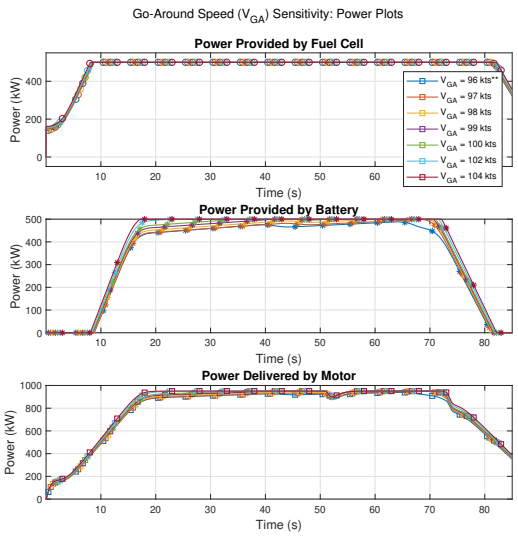

(a) Simulation Results for Power Related outputs

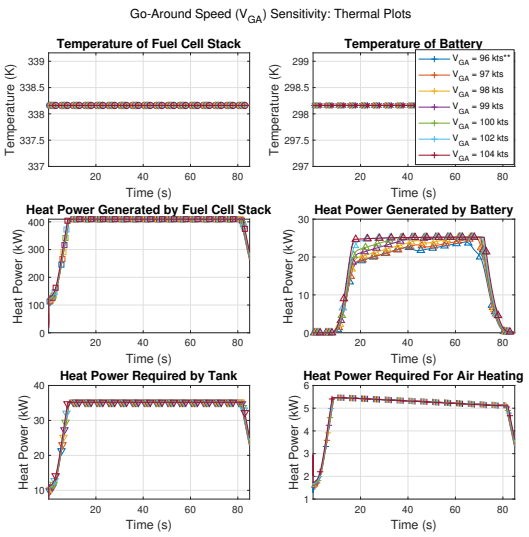

(b) Simulation Results for Thermal outputs

Fig. 24 V_{GA} Sensitivity Analysis Graphs

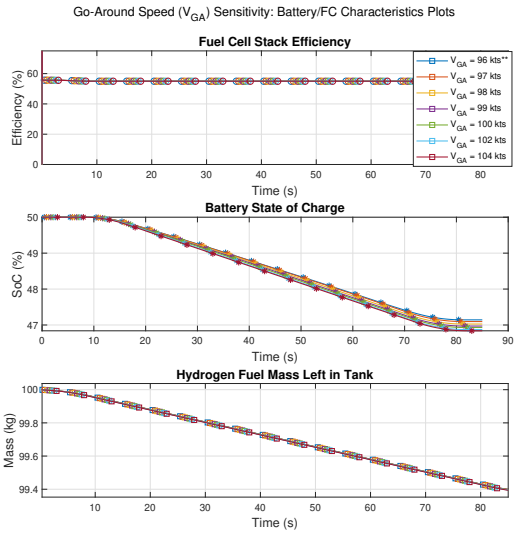

(c) Simulation Results for Battery/FC related outputs

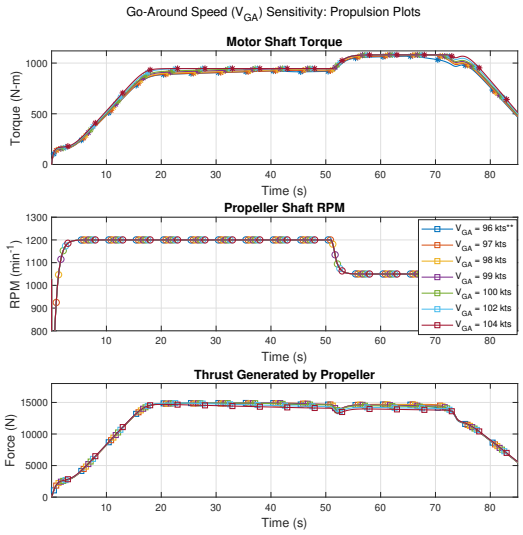

(d) Simulation Results for Propulsion related outputs

Fig. 24 V_{GA} Sensitivity Analysis Graphs

effect on stack efficiency or the remaining hydrogen in the tank. However, a slight decrease in battery State of Charge (SoC) was observed for higher speeds, corresponding to the elevated power demand imposed on the battery. Moreover, Figure 24a and Figure 24d showcase a slight increase in motor power, accompanied by an elevation in motor torque. The propeller RPM, however, remained unaffected by changes in V_{GA}. Consequently, these observed variations in motor performance led to slight variation in thrust, consistent with the expected effects of changes in go-around speed.

5. Sensitivity to Propeller Efficiency

The analysis of propeller efficiency serves as a critical evaluation of the thrust generation capabilities within the HEPS powertrain. Variations in propeller efficiency, ranging from 0.7 to 1, are systematically examined to assess their impact on system performance, as depicted in Figure 25.

As anticipated, a decrease in propeller efficiency necessitates higher electrical power generation from both the fuel cell and the battery to maintain the same thrust requirements. In Figure 25a, it is evident that for propeller efficiencies $\eta_{\text{prop}} \leq 0.8$, the battery power reaches its maximum for almost the entire duration of the climb. This heightened power demand from the battery is channelled to the motor, translating into increased motor torque. However, due to the 1 MW power constraint of the powertrain, the combined power output from the fuel cell and the battery proves insufficient to meet the demands of lower efficiency propellers. Conversely, higher propeller efficiencies result in significantly lower power derivation from the battery.

The consequential increase in power generation leads to a notable rise in battery heat generation, surpassing other heat characteristics, as illustrated in Figure 25b. Meanwhile, Figure 25c demonstrates that variations in propeller

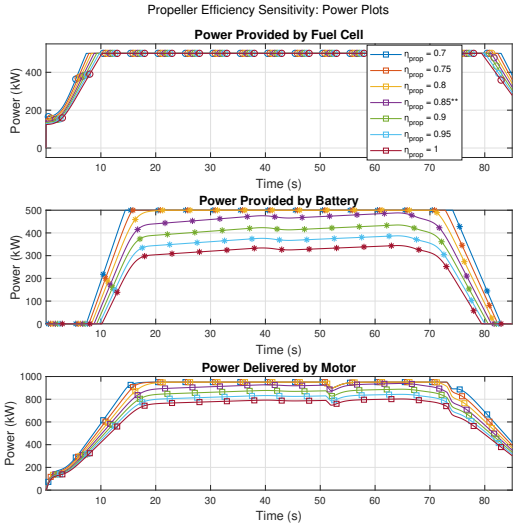

(a) Simulation Results for Power Related outputs

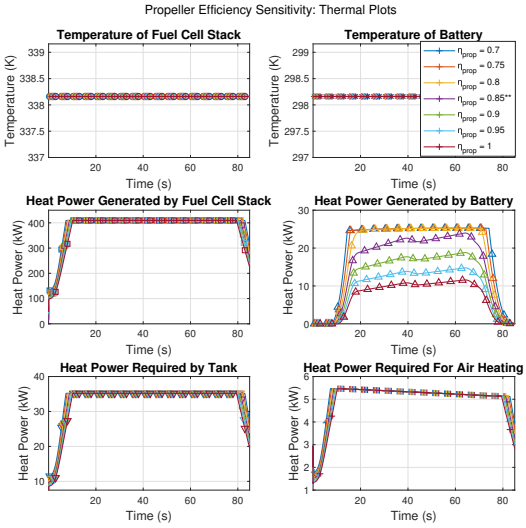

(b) Simulation Results for Thermal outputs

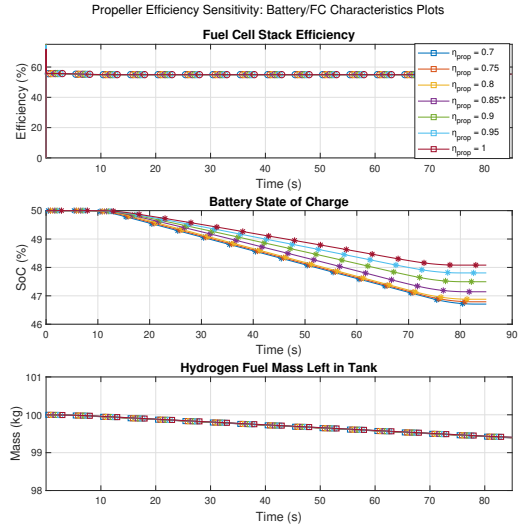

(c) Simulation Results for Battery/FC related outputs

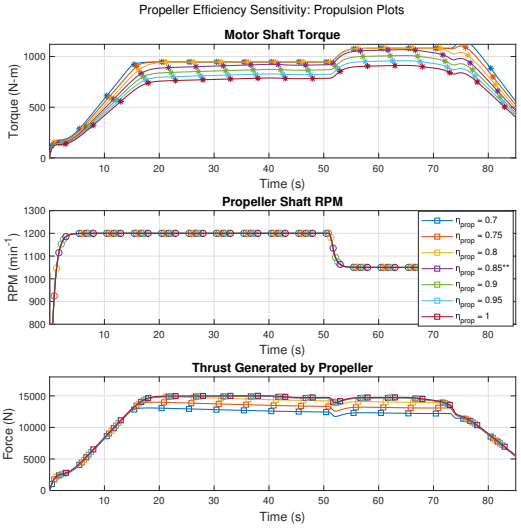

(d) Simulation Results for Propulsion related outputs

Fig. 25 η_{prop} Sensitivity Analysis Graphs

efficiency cause negligible fluctuations in the remaining hydrogen mass in the tank, while stack efficiency remains constant. The battery SoC exhibits a steeper decline in response to the utilisation of battery power for lower efficiency simulations. The graphs presented in Figure 25d illustrates that, while the propeller RPM remains constant, variations in efficiency have a notable impact on thrust generation. Simulations with propeller efficiencies of $\eta_{prop} \geq 0.85$ demonstrate sufficient thrust, contrasting with those exhibiting lower efficiency. Hence, for optimal performance of this specific HEPS powertrain within the prescribed mission profile, a propeller efficiency of 0.85 or higher is recommended.

VI. Discussion

In the context of the provided mission profile, the HEPS Engine Powertrain model operates as anticipated, delivering power and generating thrust as needed, facilitated by the implementation of the peak-shaving algorithm. This enables a comprehensive assessment of the powertrain under different conditions, achieved through sensitivity analysis.

The model demonstrates sensitivity to both the initial state-of-charge and nominal battery capacity, affecting battery power and SoC dynamics. However, these parameters primarily impact stack output during battery charging and do not directly influence thrust output unless the battery SoC drops below the discharge limit, ceasing to provide electrical power. This behaviour aligns with real-world expectations for HEPS powertrain systems, as directed by the peak-shaving algorithm. Moreover, variations in aircraft mass primarily impact the battery's peak shaving power during climb phases, leading to heightened heat generation, especially since the fuel stack operates at full power throughout the mission. This emphasises the critical need for an optimal TMS and highlights a limitation of modelling only a 1MW powertrain, which may result in sub-optimal thrust for heavier aircraft. Conversely, the model exhibits relative robustness to minor variations in go-around speed, with only slight deviations in output compared to the baseline model. This includes minimal changes in thrust generation and decreases in battery SoC. However, the powertrain model exhibits high sensitivity to propeller efficiency, leading to power demands frequently exceeding the powertrain's capacity. This results in significantly reduced thrust generation for the majority of the climb phase of the mission, causing delays in completion. This limitation renders the current powertrain configuration unsuitable for propellers with lower efficiency.

The model facilitates the assessment of various flight procedures and operational scenarios, enabling the identification of optimal procedures tailored to specific mission profiles. For the go-around mission profile analysed, it is essential to ensure that the aircraft's battery has a SoC of at least 23% with a capacity of 200Ah or 40% SoC with a capacity of 20Ah to prevent a loss of thrust during climb. This underscores the importance of verifying appropriate battery levels before go-around execution. In addition, if battery charging is necessary, pilots should allot sufficient time for charging before executing the go-around, potentially requiring earlier go-around checks. The analysis also suggests that, for effective completion of the mission within the simulation duration, the aircraft weight should not exceed 38,000 pounds, as heavier weight results in reduced thrust. However, this restriction does not imply an absolute constraint on aircraft weight, but rather emphasises the trade-off between weight and thrust generation. Regarding go-around speed, while there is no significant restriction, lower speeds (baseline at 96 knots) are preferable for effective go-around energy management. Moreover, while propeller efficiency may not directly impact flight procedural changes, it signals a longer duration required to complete the go-around. This may necessitate procedures for calculating duration and informing air traffic control (ATC) about the extended climb after the go-around manoeuvre.

The current 1MW powertrain model has been designed with adaptability in mind, offering flexibility to accommodate higher power requirements for both the powertrain and FC stack through tweaking of the model parameters. However, such adjustments would necessitate careful re-tuning of the FC stack and battery model, which are sensitive in nature.

This is currently challenging due to the lack of reliable state-of-the-art specifications capable of higher power output. Nevertheless, as more details about such systems become available, these adjustments could become more feasible.

During the operational envelope exploration, it was observed that despite the high heat generation throughout the mission due to ideal TMS assumptions, stack and battery temperatures remain unaffected by parameter changes. To enhance the realism of the HEPS powertrain model, future improvements could focus on implementing more realistic TMS for the FC stack and battery systems. the consistent tracking of the RPM reference signal by the propeller RPM, even under conditions of low input power and component model failures, reveals a flaw in the model: the RPM control loop in the motor model operates independently with a first-order filter and error in RPM, separate from the rest of the powertrain model. This highlights the need to address the simplicity and isolation of motor dynamics within the powertrain model. To improve model fidelity, future versions could incorporate more intricate and interconnected motor-propeller models, thereby eliminating component isolation.

Additionally, the current simulation of the HEPS powertrain relied on mathematically calculated inputs, resulting in the aircraft's velocity and altitude remaining constant in accordance with the predefined mission profile, regardless of the thrust generated by the powertrain. However, future research could integrate this model into a broader aircraft model, supplanting the engine model. This integration would enable real-time testing and simulation based on the aircraft's dynamics, potentially allowing for the utilisation of this model in flight simulators. Such integration could facilitate the simulation of aircraft equipped with HEPS powertrains using parameters tailored to the specific powertrain and aircraft configuration. In the long term, an enhanced iteration of the model developed in this study can serve as a valuable training tool for pilots, allowing them to acquaint themselves with the operation of HEPS powertrain systems and practice various flight procedures in a simulated environment.

Lastly, this model serves as a versatile tool capable of simulating various HEPS configurations, operating conditions, and mission requirements by adjusting modelling parameters and providing diverse inputs for different missions. This approach enables comprehensive evaluations of HEPS powertrain responses through a relatively simplified model. The model's usefulness extends to analysing critical performance metrics such as power delivery, efficiency, and thermal management to optimise system design and operation. By simulating the powertrain's behaviour under different scenarios, researchers can pinpoint opportunities for design enhancement. Moreover, the model's flexibility enables the simulation of a broad range of design alternatives and scenarios to meet diverse application needs.

VII. Conclusion

The objective of this study was to develop a representative model of a Hydrogen-Electric Propulsion System (HEPS) powertrain for a retrofitted future regional aircraft and analyse its behaviour during a critical go-around mission, which necessitates careful energy management. The HEPS powertrain model was constructed by simulating various subsystems, including the FC stack, battery, hydrogen tank, air compressor, Power Management and Distribution

(PMAD) system, motor, and propeller. The designed HEPS powertrain in this study is a 1MW system with a HF of 0.5, indicating that the FC stack supplies 500kW of power as the primary source, while an additional 500kW is provided by the auxiliary battery during peak power demands. Simulation of the powertrain under specified mission conditions demonstrated the seamless implementation of this strategy.

Operational envelope analysis conducted on the model unveiled the significant impact of parameters such as initial battery state of charge, battery capacity, and propeller efficiency on various performance attributes of the designed powertrain, including power consumption, heat dissipation, and thrust generation during the go-around procedure. These insights are invaluable for optimizing battery management strategies, determining optimal battery capacities, and enhancing overall system efficiency and reliability.

The model framework demonstrated in this study is highly versatile, enabling the simulation of various Hydrogen-Electric Propulsion System (HEPS) configurations and mission scenarios by adjusting parameters. It effectively evaluates key performance metrics such as power delivery, thereby aiding in system refinement. Moreover, the developed model serves as a valuable tool for assessing the impact of Hydrogen-Electric Propulsion System (HEPS) powertrains on flight procedures tailored to diverse missions, including the go-around manoeuvre. It aids in the identification of optimal procedures by analysing the model's output and evaluating the effectiveness of different strategies, thereby fulfilling the study's objective of creating a model capable of this task.

Future enhancements may prioritise improving model accuracy by integrating more sophisticated motor-propeller models to address component isolation. Additionally, advancements could involve implementing realistic Thermal Management Systems when its specifications are known. Ultimately, an upgraded version of the model holds promise as an invaluable pilot training tool, offering a simulated environment for practising HEPS powertrain operations and flight procedures. In addition, future research efforts could also explore the development of battery charge-discharge control and the implementation of the peak-shaving strategy within the Power Management and Distribution (PMAD) systems of HEPS aircraft.

This endeavour represents a fundamental step toward integrating Hydrogen-Electric Propulsion Systems (HEPS) into practical aviation scenarios, contributing significantly to the advancement of sustainable regional aviation propulsion systems. It signifies a major milestone in transitioning toward environmentally friendly aviation solutions.

Appendix

Drag Polar Curve

The Dash-8 Q300's lift and drag coefficients were calculated using Digital DATCOM Software. Estimated aircraft geometry from the Dash-8 Q300's Aircraft Planning Manual, as well as varying mission profile conditions such as Mach number, altitude, velocity of sound, and angles of attack ranging from -6.5 to 3 degrees, were loaded into the

software. Matlab was used to extract and process the DATCOM output, which included Lift Coefficients (C_L) and Drag Coefficients (C_D) for 40 different conditions. Using Matlab's Curve Fitting routine, a drag polar equation, presented as Equation 31, was derived from the obtained coefficient data.

$$C_D = 0.03125C_L^2 - 0.005447C_L + 0.01745 \tag{31}$$

The equation defines the relationship between the drag coefficient and the lift coefficient over an altitude range of 0-2,000 feet and velocities ranging from 95 to 120 knots, providing valuable insights into the aerodynamic properties of the Dash-8 Q300 aircraft for this study.

Hydrogen Specific Heat Calculation

The specific heat capacity of hydrogen exhibits considerable variation across the wide temperature range pertinent to this study, extending from 20 K to 338 K, encompassing transitions between the liquid and gaseous phases. For the cryogenic temperature range of 14 K to 22 K, the Specific Heat Capacity (C_p) of Liquid Hydrogen was referenced from Choi's 2004 report [32], which credits the data to Roge et al. [47] and Roder et al. [48]. Additionally, the Specific Heat Capacity of gaseous hydrogen from 175 K to 375 K was extracted from an online database provided by The Engineering Toolbox [34]. The values for the intermediate temperature range were linearly interpolated. The specific heat capacity of liquid and gaseous hydrogen utilised in this study is the root mean square of the interpolated database, ranging from 20 K to 22 K for liquid hydrogen and 33 K to 365 K for gaseous hydrogen. This interpolation is illustrated graphically in Figure 26.

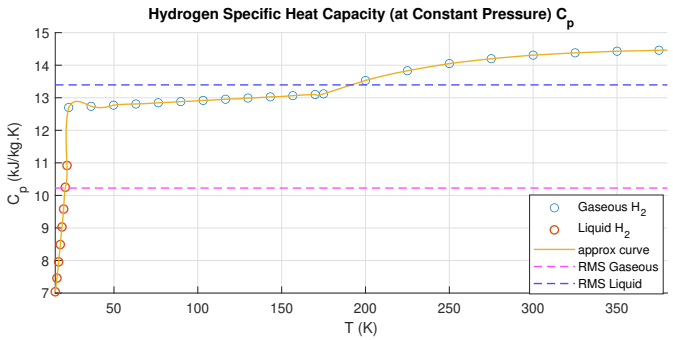

Fig. 26 Approximate Graph of Specific Heat Capacity of Hydrogen

References

[1] Directorate-General for Research and Innovation (European Commission), *Fly the Green Deal – Europe's vision for sustainable aviation*, Publications Office of the European Union, 2022. https://doi.org/doi/10.2777/732726, URL https://data.europa.eu/doi/10.2777/732726.

[2] Victor, D. G., "Liquid hydrogen aircraft and the greenhouse effect," *International Journal of Hydrogen Energy*, Vol. 15, 1990, pp. 357–367. https://doi.org/10.1016/0360-3199(90)90186-3.

[3] Haglind, F., Hasselrot, A., and Singh, R., "Potential of reducing the environmental impact of aviation by using hydrogen Part I: Background, prospects and challenges," *Aeronautical Journal*, Vol. 110, 2006, pp. 533–540. https://doi.org/10.1017/S000192400000141X.

[4] Friedrich, K. A., Kallo, J., Schirmer, J., and Schmitthals, G., "Fuel Cell Systems for Aircraft Application," *ECS Transactions*, Vol. 25, 2009, pp. 193–202. https://doi.org/10.1149/1.3210571.

[5] Kadyk, T., Winnefeld, C., Hanke-Rauschenbach, R., and Krewer, U., "Analysis and Design of Fuel Cell Systems for Aviation," *Energies*, Vol. 11, 2018, p. 375. https://doi.org/10.3390/EN11020375.

[6] Zamboni, J., Vos, R., Emeneth, M., and Schneegans, A., "A method for the conceptual design of hybrid electric aircraft," *AIAA Scitech 2019 Forum*, 2019. https://doi.org/10.2514/6.2019-1587.

[7] Palladino, V., Jordan, A., Bartoli, N., Schmollgruber, P., Pommier-Budinger, V., and Benard, E., "Preliminary studies of a regional aircraft with hydrogen-based hybrid propulsion," *AIAA Aviation and Aeronautics Forum and Exposition, AIAA AVIATION Forum 2021*, 2021. https://doi.org/10.2514/6.2021-2411.

[8] Pontika, E., Zaghari, B., Zhou, T., Enalou, H. B., and Laskaridis, P., "Integrated Mission Performance Analysis of Novel Propulsion Systems: Analysis of a Fuel Cell Regional Aircraft Retrofit," *AIAA SCITECH 2023 Forum*, 2023. https://doi.org/10.2514/6.2023-0840.

[9] Marciello, V., Stasio, M. D., Ruocco, M., Trifari, V., Nicolosi, F., Meindl, M., Lemoine, B., and Caliandro, P., "Design Exploration for Sustainable Regional Hybrid-Electric Aircraft: A Study Based on Technology Forecasts," *Aerospace*, Vol. 10, 2023. https://doi.org/10.3390/AEROSPACE10020165.

[10] Gao, Y., Jausseme, C., Huang, Z., and Yang, T., "Hydrogen-Powered Aircraft: Hydrogen-electric hybrid propulsion for aviation." *IEEE Electrification Magazine*, Vol. 10, 2022, pp. 17–26. https://doi.org/10.1109/MELE.2022.3165725.

[11] Vietze, M., and Weiland, S., "System analysis and requirements derivation of a hydrogen-electric aircraft powertrain," *International Journal of Hydrogen Energy*, Vol. 47, 2022, pp. 38793–38810. https://doi.org/10.1016/J.IJHYDENE.2022.09.052.

[12] Staggat, M., Ludowicy, J., Bahrs, V., Link, A., and Kazula, S., "Modelling of a battery supported fuel cell electric power train topology for a regional aircraft," *Journal of Physics: Conference Series*, Vol. 2526, 2023, p. 012061. https://doi.org/10.1088/1742-6596/2526/1/012061.

[13] Hoelzen, J., Liu, Y., Bensmann, B., Winnefeld, C., Elham, A., Friedrichs, J., and Hanke-Rauschenbach, R., "Conceptual Design of Operation Strategies for Hybrid Electric Aircraft," *Energies*, Vol. 11, No. 1, 2018. https://doi.org/10.3390/en11010217, URL https://www.mdpi.com/1996-1073/11/1/217.

[14] Aviation in Transition Foundation, "Hydrogen Aircraft Powertrain and Storage Systems (HAPSS) | Aviation in Transition," , 2023. URL https://luchtvaartintransitie.nl/project-item/hydrogen-aircraft-powertrain-and-storage-systems/.

[15] Luchtverkeersleiding Nederland (LVNL), "Integrated Aeronautical Information Package: AD 2.EHAM-IAC-06.1," , 2024. URL https://eaip.lvnl.nl/web/2024-03-07-AIRAC/html/index-en-GB.html.

[16] Larminie, J., and Dicks, A., *Fuel Cell Systems Explained (2nd Edition)*, John Wiley & Sons, 2003. URL https://app.knovel.com/hotlink/toc/id:kpFCSEE002/fuel-cell-systems-explained/fuel-cell-systems-explained.

[17] Verstraete, D., Hendrick, P., Pilidis, P., and Ramsden, K., "Hydrogen fuel tanks for subsonic transport aircraft," *International Journal of Hydrogen Energy*, Vol. 35, 2010, pp. 11085–11098. https://doi.org/10.1016/J.IJHYDENE.2010.06.060.

[18] Winnefeld, C., Kadyk, T., Bensmann, B., Krewer, U., and Hanke-Rauschenbach, R., "Modelling and Designing Cryogenic Hydrogen Tanks for Future Aircraft Applications," *Energies*, Vol. 11, No. 1, 2018. https://doi.org/10.3390/en11010105, URL https://www.mdpi.com/1996-1073/11/1/105.

[19] O'Hayre, R., Cha, S.-W., Colella, W., and Prinz, F. B., *Fuel Cell Fundamentals*, John Wiley & Sons Ltd., 2016. https://doi.org/10.1002/9781119191766.

[20] Zaghari, B., Zhou, T., Enalou, H. B., Pontika, E., and Laskaridis, P., "The Impact of Multi-Stack Fuel Cell Configurations on Electrical Architecture for a Zero Emission Regional Aircraft," *AIAA SCITECH 2023 Forum*, 2023. https://doi.org/10.2514/6.2023-1593.

[21] Zhou, T., Enalou, H. B., Pontika, E., Zaghari, B., and Laskaridis, P., "Minimising the effect of degradation of fuel cell stacks on an integrated propulsion architecture for an electrified aircraft," *2022 IEEE Transportation Electrification Conference and Expo, ITEC 2022*, 2022, pp. 1064–1069. https://doi.org/10.1109/ITEC53557.2022.9813899.

[22] Campbell, J., *Gas Conditioning and Processing: The Equipment Modules*, 9th ed., Campbell Petroleum Series, PetroSkills, 2014.

[23] Finger, D. F., Braun, C., and Bil, C., "Impact of Battery Performance on the Initial Sizing of Hybrid-Electric General Aviation Aircraft," *Journal of Aerospace Engineering*, Vol. 33, 2020. https://doi.org/10.1061/(ASCE)AS.1943-5525.0001113.

[24] Vratny, P. C., Kuhn, H., and Hornung, M., "Influences of voltage variations on electric power architectures for hybrid electric aircraft," *CEAS Aeronautical Journal*, Vol. 8, 2017, pp. 31–43. https://doi.org/10.1007/s13272-016-0218-z.

[25] Zhang, X., Bowman, C. L., O'Connell, T. C., and Haran, K. S., "Large electric machines for aircraft electric propulsion," *IET Electric Power Applications*, Vol. 12, 2018, pp. 767–779. https://doi.org/10.1049/iet-epa.2017.0639.

[26] Giangrande, P., Madonna, V., Sala, G., Kladas, A., Gerada, C., and Galea, M., "Design and Testing of PMSM for Aerospace EMA Applications," *IECON 2018 - 44th Annual Conference of the IEEE Industrial Electronics Society*, 2018, pp. 2038–2043. https://doi.org/10.1109/IECON.2018.8591318.

[27] Jaber, F. F., and Abdulhasan, A. F., "Mathematical Model of Permanent Magnet Synchronous Motor," *University of Thi -Qar Journal for Engineering Sciences*, Vol. 12, 2022, pp. 10–14. https://doi.org/10.31663/tqujes.12.2.444(2022), URL https://jeng.utq.edu.iq/index.php/main/article/view/483/417.

[28] Quillet, D., Boulanger, V., Rancourt, D., Freer, R., and Bertrand, P., "Parallel Hybrid-Electric Powertrain Sizing on Regional Turboprop Aircraft with Consideration for Certification Performance Requirements," , 7 2021. https://doi.org/10.2514/6.2021-2443, URL https://doi-org.tudelft.idm.oclc.org/10.2514/6.2021-2443.

[29] Knudsen, J., and Katz, D., *Fluid Dynamics and Heat Transfer*, Chemical engineering series, McGraw-Hill, 1958. URL https://books.google.nl/books?id=l80mAAAAMAAJ.

[30] The Engineering Toolbox, "Hydrogen - Density and Specific Weight vs. Temperature and Pressure," , 2018. URL https://www.engineeringtoolbox.com/hydrogen-H2-density-specific-weight-temperature-pressure-d_2044.html.

[31] Aziz, M., "Liquid Hydrogen: A Review on Liquefaction, Storage, Transportation, and Safety," *Energies 2021, Vol. 14, Page 5917*, Vol. 14, 2021, p. 5917. https://doi.org/10.3390/EN14185917, URL https://www.mdpi.com/1996-1073/14/18/5917/htmhttps://www.mdpi.com/1996-1073/14/18/5917.

[32] Choi, J., "Liquid Hydrogen Properties," Tech. rep., HANARO Utilization Technology Developement Division, 2004.

[33] The Engineering Toolbox, "Universal and Individual Gas Constants," , 2004. URL https://www.engineeringtoolbox.com/individual-universal-gas-constant-d_588.html.

[34] The Engineering Toolbox, "Hydrogen - Specific Heat," , 2005. URL https://www.engineeringtoolbox.com/hydrogen-d_976.html.

[35] H2 Tools Portal, "Hydrogen Specific Heat at different temperatures and pressures | Hydrogen Tools," , 2007. URL https://h2tools.org/hyarc/hydrogen-data/hydrogen-specific-heat-different-temperatures-and-pressures.

[36] Dominic, S., and Maier, U., "Dynamic Modeling and Simulation of Compressor Trains for an Air Separation Unit," *IFAC Proceedings Volumes*, Vol. 47, 2014, pp. 432–437. https://doi.org/10.3182/20140824-6-ZA-1003.01510.

[37] Souleman, N. M., Tremblay, O., and Dessaint, L. A., "A generic fuel cell model for the simulation of fuel cell power systems," *2009 IEEE Power and Energy Society General Meeting, PES '09*, 2009. https://doi.org/10.1109/PES.2009.5275853.

[38] Liso, V., Nielsen, M. P., Kær, S. K., and Mortensen, H. H., "Thermal modeling and temperature control of a PEM fuel cell system for forklift applications," *International Journal of Hydrogen Energy*, Vol. 39, No. 16, 2014, pp. 8410–8420. https://doi.org/https://doi.org/10.1016/j.ijhydene.2014.03.175, URL https://www.sciencedirect.com/science/article/pii/S0360319914008672.

[39] Qu, Y., Li, D., and Wang, R., "Study on integrated thermal management system of hydrogen fuel cell vehicles based on heat pump air conditioning," *Journal of Cleaner Production*, Vol. 434, 2024, p. 139951. https://doi.org/10.1016/J.JCLEPRO.2023.139951.

[40] EVESCO, "ELECTRIC VEHICLE ENERGY STORAGE - ES500500 EU," , 2022. URL https://www.power-sonic.com/wp-content/uploads/2022/02/ES-500500EU-500kW-500kWh-battery-energy-storage-system.pdf.

[41] Kumar, R. R., Bharatiraja, C., Udhayakumar, K., Devakirubakaran, S., Sekar, K. S., and Mihet-Popa, L., "Advances in batteries, battery modeling, battery management system, battery thermal management, soc, soh, and charge/discharge characteristics in ev applications," *IEEE Access*, Vol. 11, 2023, pp. 105761–105809. https://doi.org/10.1109/access.2023.3318121.

[42] Ruijgrok, G., *Elements of airplane performance*, VSSD, 2009. 2e editie onderwijsboek met 'minor adjustments'.

[43] Mahammadsoaib, M. S., and Sajid, M. P., "Vector controlled PMSM drive using SVPWM technique - A MATLAB / simulink implementation," *International Conference on Electrical, Electronics, Signals, Communication and Optimization, EESCO 2015*, 2015. https://doi.org/10.1109/EESCO.2015.7253938.

[44] Rodríguez, J., Kennel, R., Espinoza, J., Trincado, M., Silva, C., and Rojas, C. A., "High-performance control strategies for electrical drives: an experimental assessment," *IEEE Transactions on Industrial Electronics*, Vol. 59, 2012, pp. 812–820. https://doi.org/10.1109/tie.2011.2158778.

[45] Luo, F. L., and Ye, H., "Mathematical modeling of power DC/DC converters," *2004 International Conference on Power System Technology*, Vol. 1, 2004, pp. 17–22. https://doi.org/10.1109/ICPST.2004.1459959, URL http://ieeexplore.ieee.org/document/1459959/.

[46] Møller, K. T., Jensen, T. R., Akiba, E., and Li, H., "Hydrogen - a sustainable energy carrier," *Progress in Natural Science: Materials International*, Vol. 27, 2017, pp. 34–40. https://doi.org/10.1016/j.pnsc.2016.12.014.

[47] Roge, H. J., and Arnold, R. D., "Vapor Pressures of Hydrogen, Deuterium, and Hydrogen Deuteride and Dew-Point Pressures of Their Mixtures," *Journal of Research of the National Bu reau of Standards*, Vol. 47, No. 2, 1951. https://doi.org/10.6028/jres.047.009, URL https://nvlpubs.nist.gov/nistpubs/jres/47/jresv47n2p63_a1b.pdf.

[48] Roder, H. M., Childs, G. E., McCarty, R. D., and Angerhofer, P. E., "Survey of the Properties of the Hydrogen Isotopes Below Their Critical Temperatures," , 8 1973. https://doi.org/10.2172/4244810, URL https://www.osti.gov/biblio/4244810.

Part III

Appendix

A

Longer Duration Simulation Results

In the results section, the simulation focused solely on the climb phase of the go-around, with a duration limited to 85 seconds. However, the comprehensive nature of the model enables analysis beyond this initial phase, extending to subsequent flight segments such as the cruise section. This expanded analysis is depicted in Figure A.1, which illustrates an additional 15 seconds of cruising at 2000ft altitude post-climb. During this cruising phase, key flight parameters such as airspeed, flight path angle, and reference RPM are held constant to simulate steady-state conditions.

Examining the power requirements during cruising reveals a consistent demand well below the 500 kW capacity of the stack. Consequently, all power during this phase is supplied solely by the FC stack, resulting in a corresponding reduction in fuel mass within the tank and diminished heat generation by the fuel cell stack. As both fuel and air consumption decrease during cruising, the amount of heat needed to warm them up to the fuel cell operating temperature also decreases accordingly.

The battery remains inactive throughout the cruising phase, maintaining its state of charge (SoC) unchanged. However, it is worth mentioning that if the SoC were to drop below 45% (or the charging limit), surplus power would be generated by the FC stack to charge the battery, ensuring optimal energy management according to the peak-shaving algorithm.

Despite these adjustments, the propulsion system continues to function as expected during cruising, with the model consistently generating the required thrust albeit with minor delays.

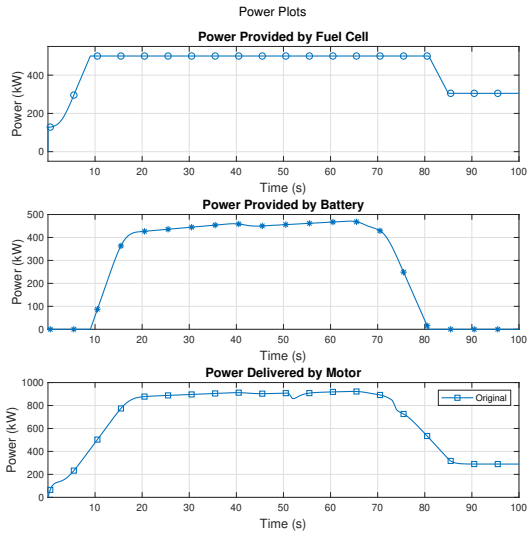

(a) Simulation Results for Power Related outputs

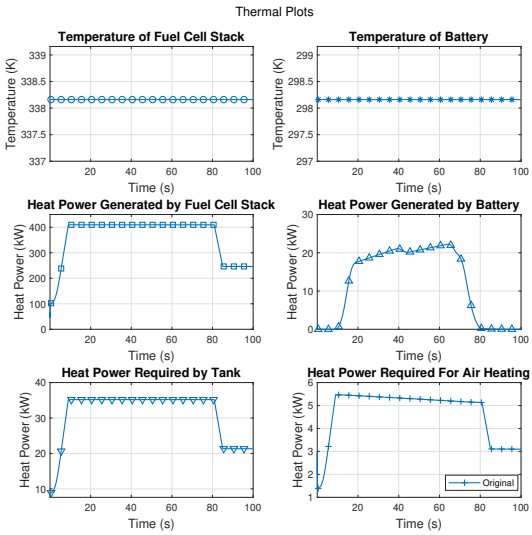

(b) Simulation Results for Thermal outputs

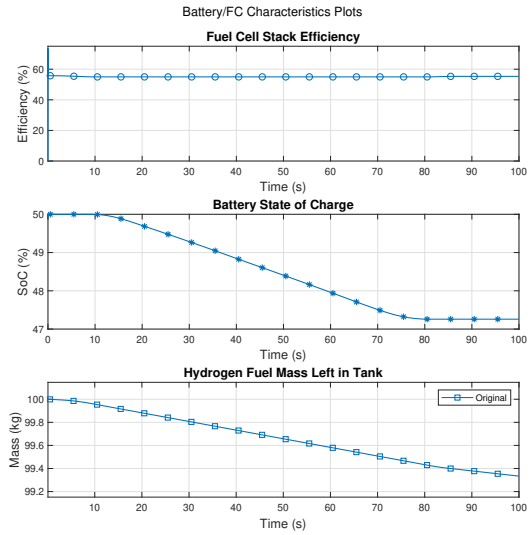

(c) Simulation Results for Battery/FC related outputs

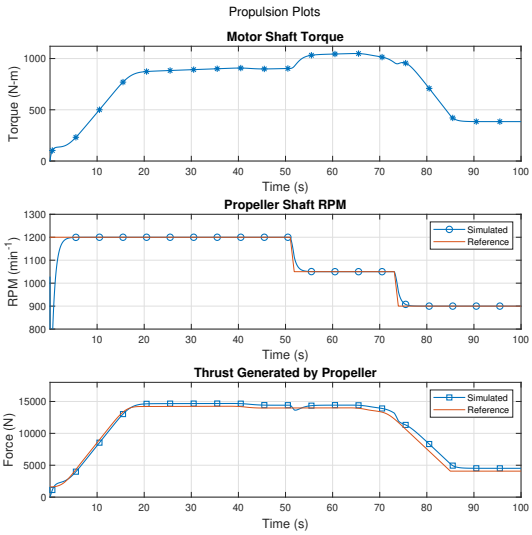

(d) Simulation Results for Propulsion related outputs

Figure A.1: Simulation Results of the HEPS Powertrain Engine: Longer Duration

B

All Graphs from Operational Analysis

In the context of operational analysis, the omission of certain graphs from the scientific paper was deliberate due to their lack of relevance in substantiating the drawn conclusions. Including them would have unnecessarily occupied space without contributing significantly to the article's discourse. As a result, this chapter encompasses all operational analysis graphs, including those related to two parameters that had minimal impact on the model's responses, making their inclusion in the scientific article unnecessary. Additionally, it covers a parameter affected by the powertrain limitation of the model.

On the subsequent pages, the analysis of the HEPS powertrain model's responses to various parameters is presented through a series of graphical representations:

- Figure B.1 provides insights into the model's reactions to different Initial Battery State of Charge (SoC) values.
- Figure B.2 showcases the model's behaviour across different Battery nominal capacities.
- Figure B.3 illustrates the model's responses to variations in aircraft masses.
- Figure B.4 displays the model's performance under different go-around speeds.
- Figure B.5 demonstrates the model's outputs under varying propeller efficiency conditions.

Furthermore, three bonus operational analyses are included:

- Figure B.6 presents the model's reactions to changes in fuel cell operating temperature.
- Figure B.7 showcases the model's responses to adjustments in the battery's thermal mass.
- Finally, Figure B.8 illustrates the model's outputs under varying hybridisation factors. This variation has significant implications for the model's operation, which will be discussed in a later section.

Each set of graphs contributes to a comprehensive understanding of the HEPS powertrain model's behaviour and performance characteristics under specific parameter variations, enriching the analysis and insights derived from the study.

Sensitivity to Hybridisation Factor

The hybridisation factor plays a pivotal role in dictating the power demands to be covered by both the battery and the fuel cell within the hydrogen-electric propulsion system (HEPS). It serves as a fundamental component of the peak shavings strategy, influencing the system's reliance on the FC stack. For the sensitivity analysis, the powertrain model is subjected to variations in the hybridisation factor (HF), ranging from 0.25 to 0.5, with the simulation results depicted in Figure B.8.

Upon examination of the power figures, it is evident that the powertrain model encounters a critical issue, as the FC stack model crashes when unable to provide more than 500-550 kW of power. This outcome is anticipated, considering that the FC stack is specifically parameterised to deliver 500 kW of power and no more. Given its role as the primary power source in the powertrain model, the crash of the FC stack precipitates the crash of the motor model downstream in the powertrain. Consequently, without power input from the FC stack and the battery, no motor torque is generated, leading to a cessation of thrust generation for HF values below 0.5.

Remarkably, the battery continues to operate effectively, as it remains disconnected from the aftermath of the fuel cell crash. However, an interesting observation emerges regarding the propeller RPM, which continues to adhere to the RPM reference signal in Figure B.8(d). This observation underscores a flaw in the model, wherein the RPM control loop operates independently between an isolated first-order filter in the motor and the error between actual RPM and reference. This disconnects the RPM control loop from the rest of the powertrain model, highlighting a potential area for refinement and optimisation in future iterations of the model.

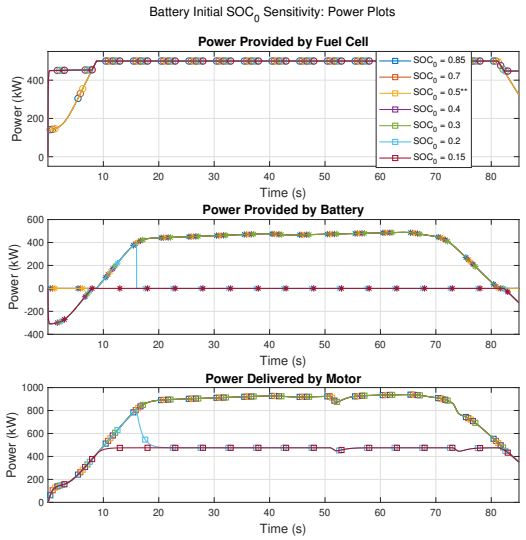

(a) Simulation Results for Power Related outputs

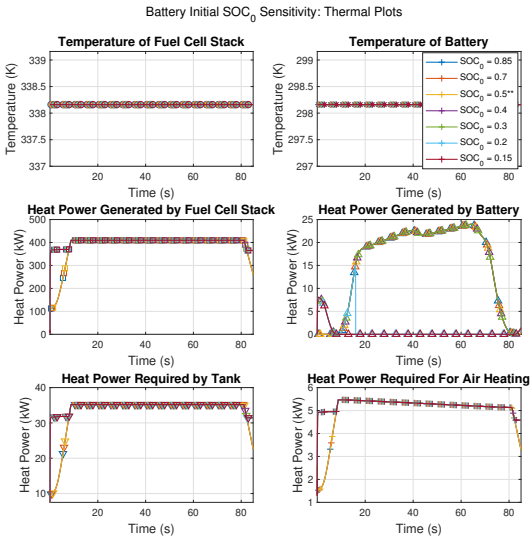

(b) Simulation Results for Thermal outputs

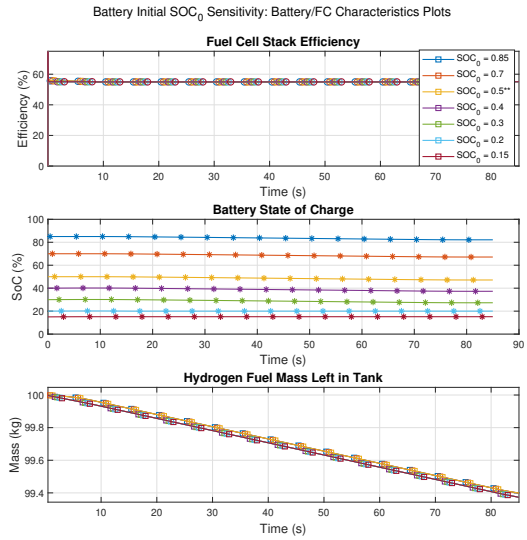

(c) Simulation Results for Battery/FC related outputs

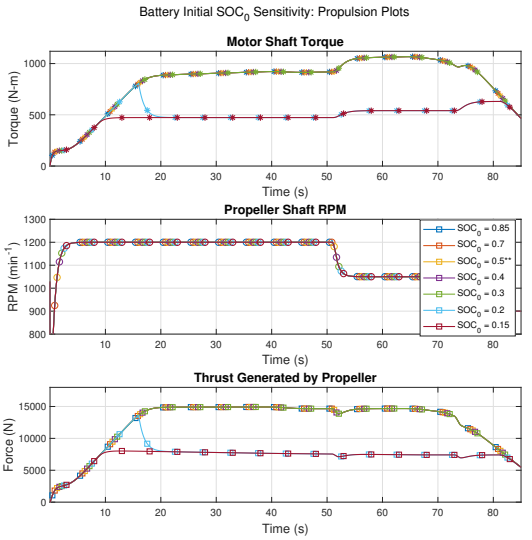

(d) Simulation Results for Propulsion related outputs

Figure B.1: Battery Initial SoC Sensitivity Analysis Graphs

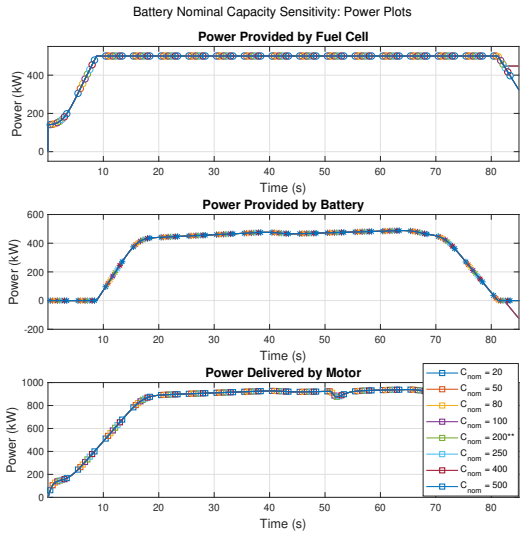

(a) Simulation Results for Power Related outputs

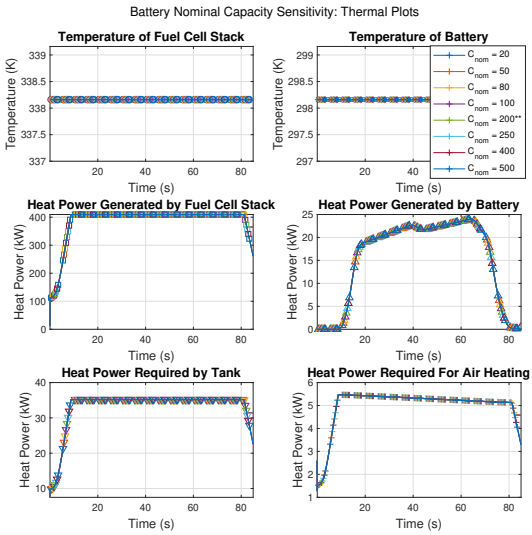

(b) Simulation Results for Thermal outputs

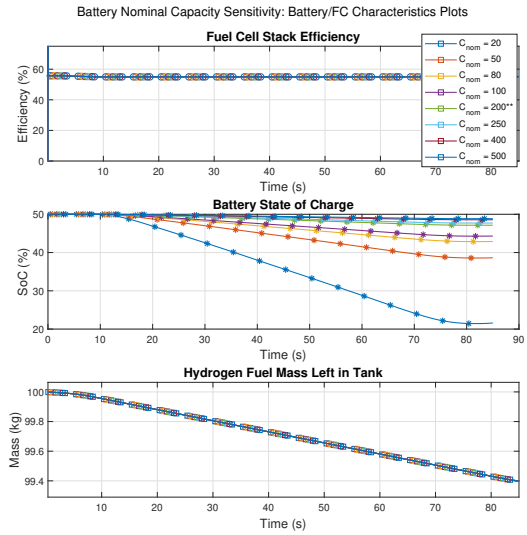

(c) Simulation Results for Battery/FC related outputs

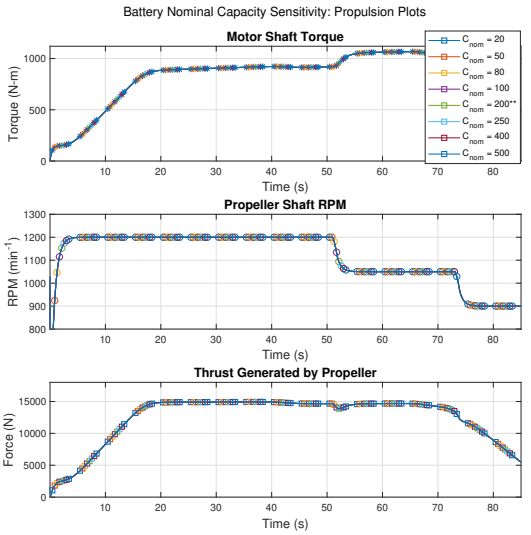

(d) Simulation Results for Propulsion related outputs

Figure B.2: Battery Nominal Capacity Sensitivity Analysis Graphs

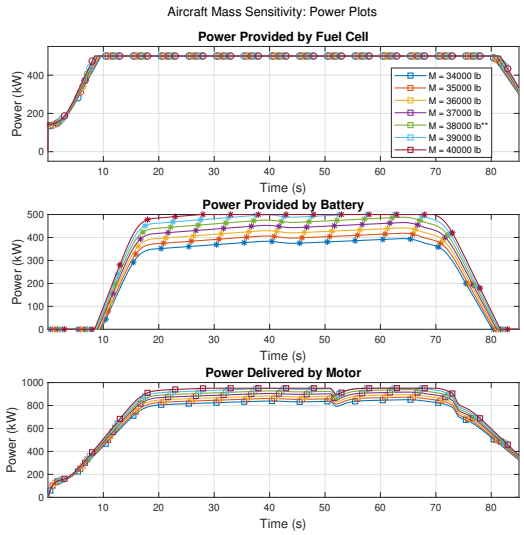

(a) Simulation Results for Power Related outputs

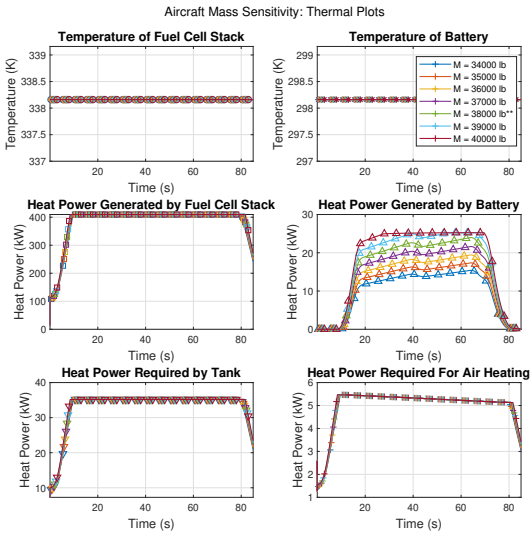

(b) Simulation Results for Thermal outputs

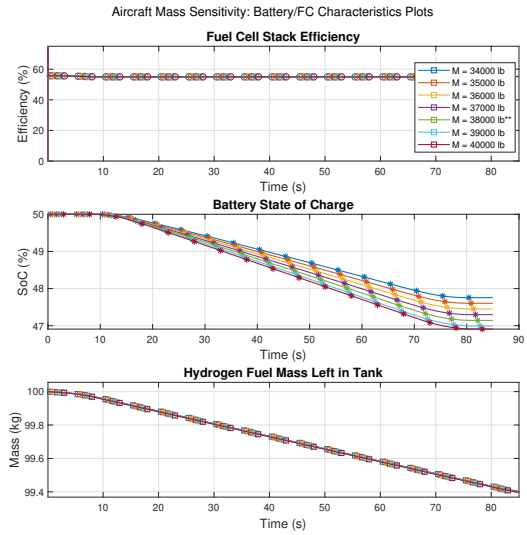

(c) Simulation Results for Battery/FC related outputs

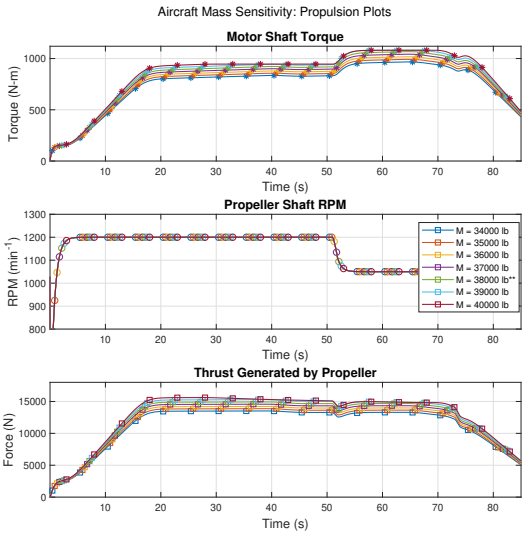

(d) Simulation Results for Propulsion related outputs

Figure B.3: Aircraft Mass Sensitivity Analysis Graphs

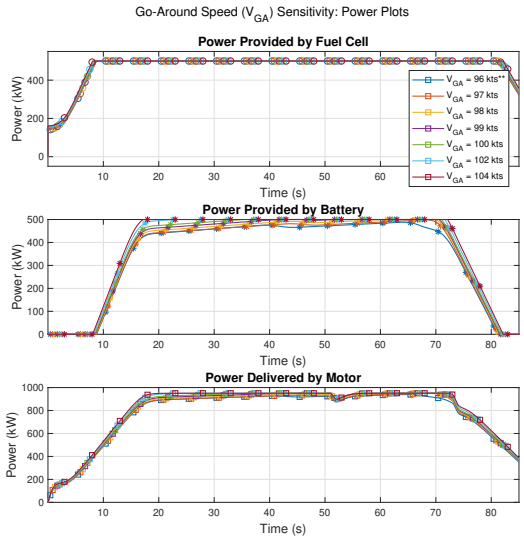

(a) Simulation Results for Power Related outputs

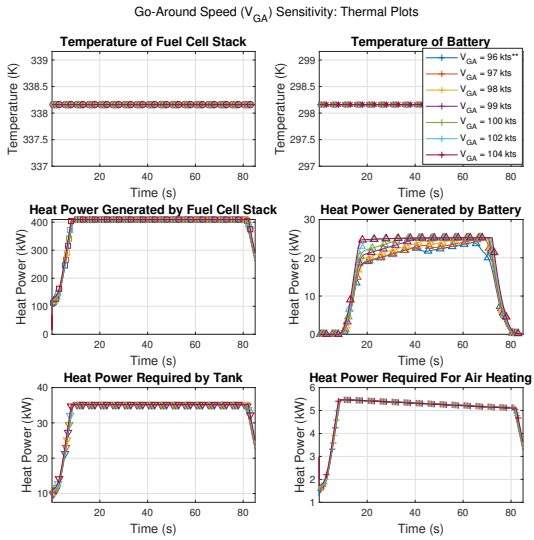

(b) Simulation Results for Thermal outputs

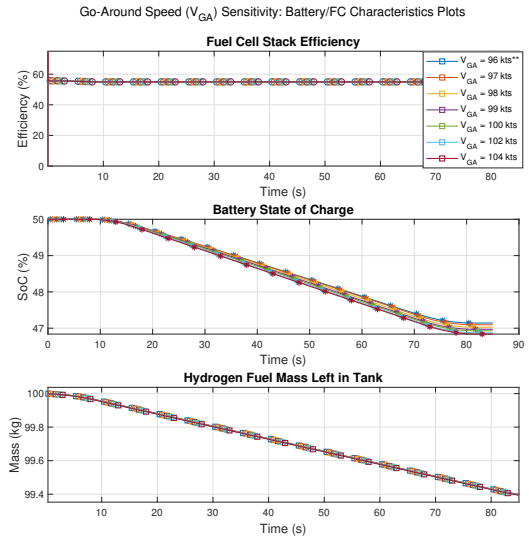

(c) Simulation Results for Battery/FC related outputs

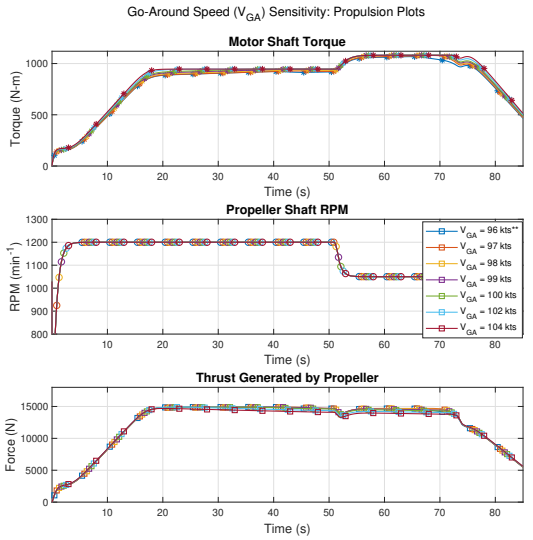

(d) Simulation Results for Propulsion related outputs

Figure B.4: Go-Around Speed Sensitivity Analysis Graphs

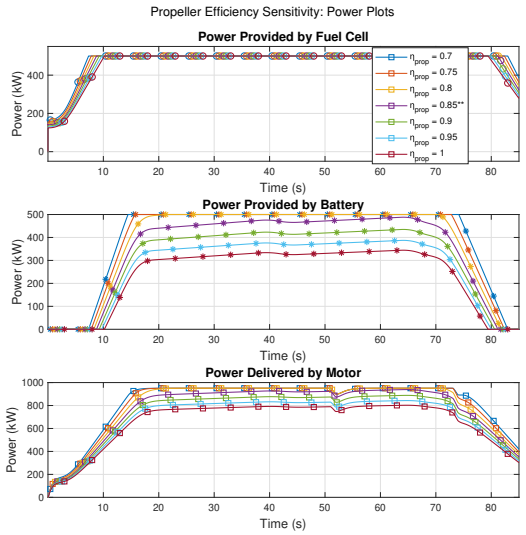

(a) Simulation Results for Power Related outputs

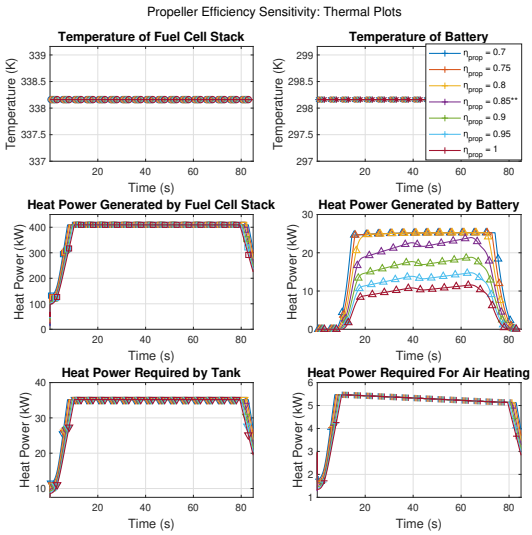

(b) Simulation Results for Thermal outputs

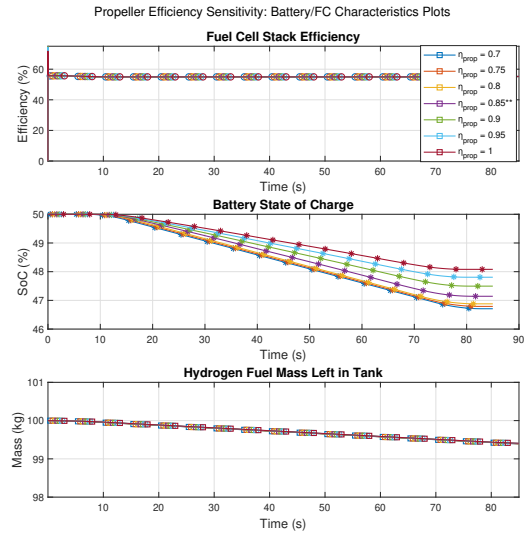

(c) Simulation Results for Battery/FC related outputs

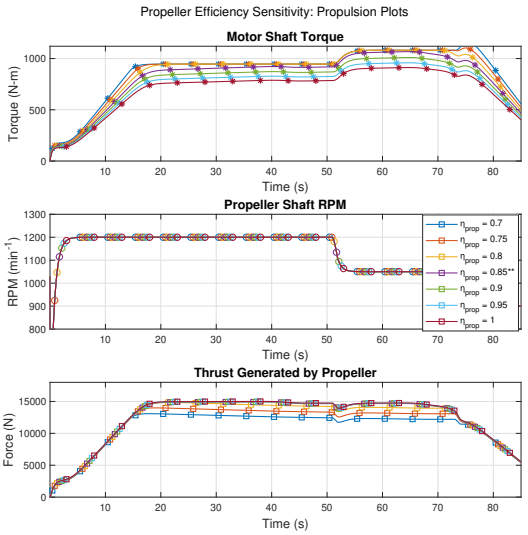

(d) Simulation Results for Propulsion related outputs

Figure B.5: Propeller Efficiency Sensitivity Analysis Graphs

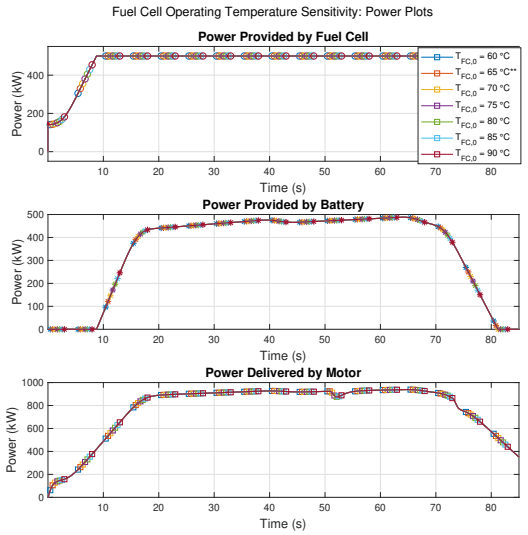

(a) Simulation Results for Power Related outputs

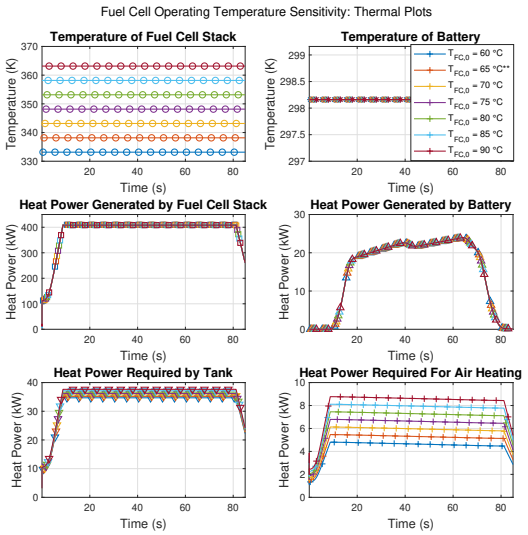

(b) Simulation Results for Thermal outputs

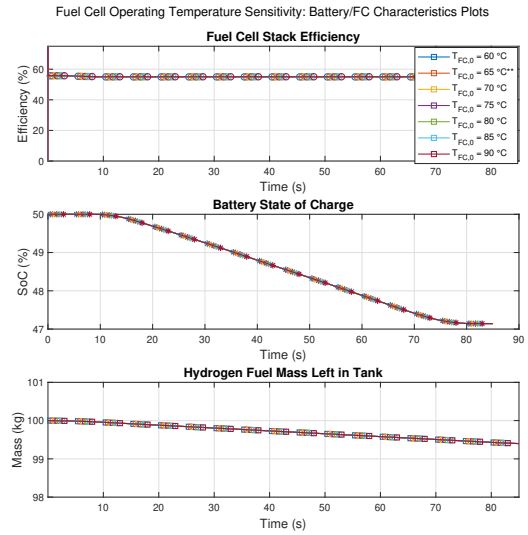

(c) Simulation Results for Battery/FC related outputs

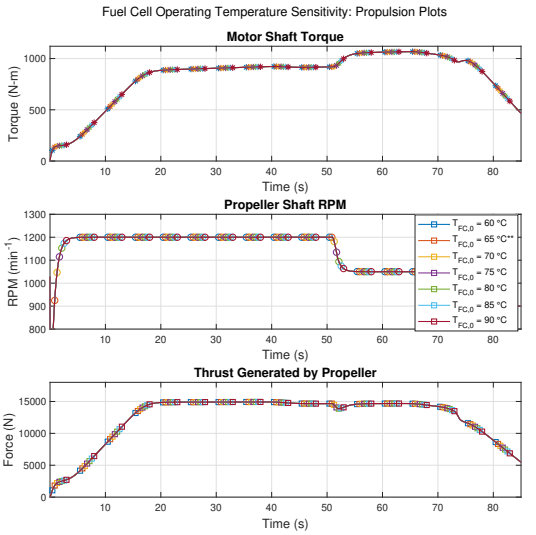

(d) Simulation Results for Propulsion related outputs

Figure B.6: Fuel Cell Operating Temperature Sensitivity Analysis Graphs

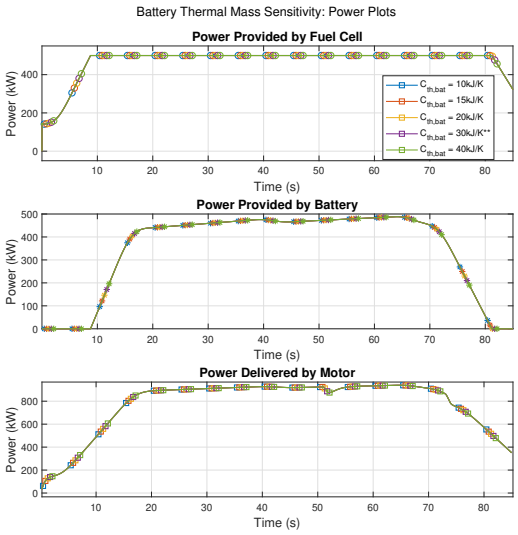

(a) Simulation Results for Power Related outputs

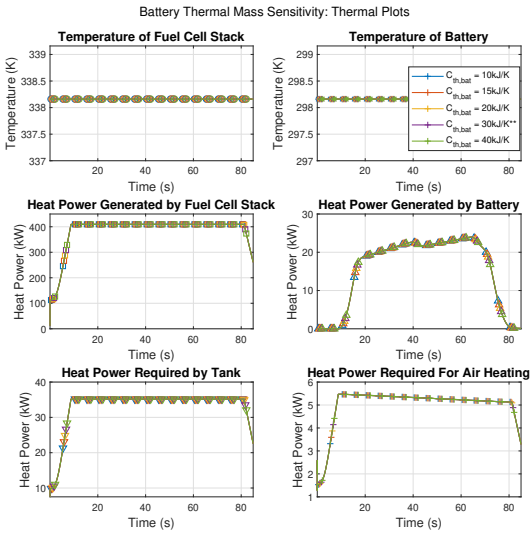

(b) Simulation Results for Thermal outputs

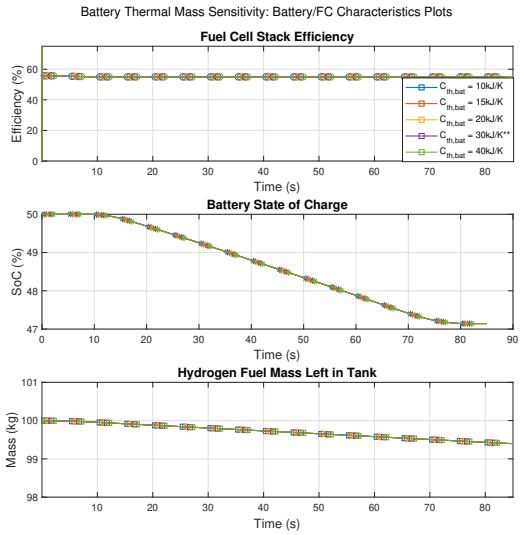

(c) Simulation Results for Battery/FC related outputs

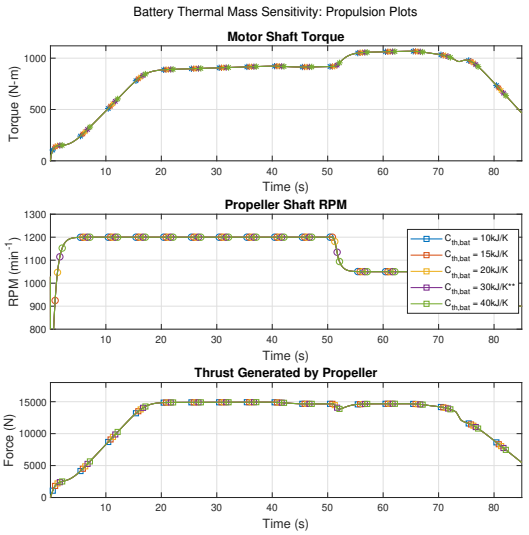

(d) Simulation Results for Propulsion related outputs

Figure B.7: Battery Thermal Mass Sensitivity Analysis Graphs

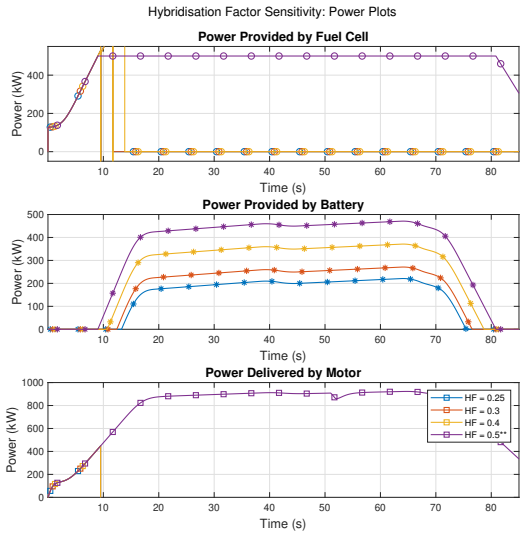

(a) Simulation Results for Power Related outputs

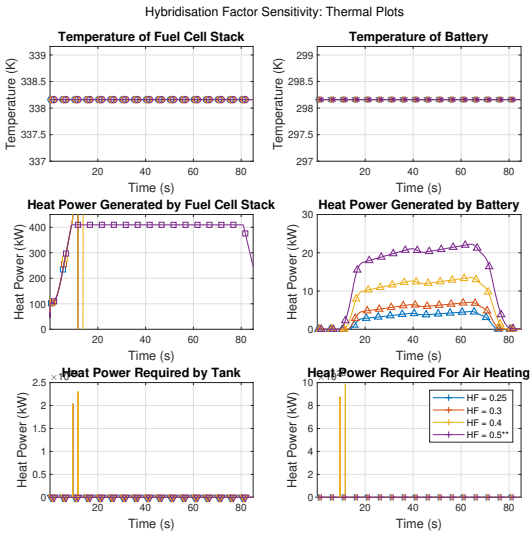

(b) Simulation Results for Thermal outputs

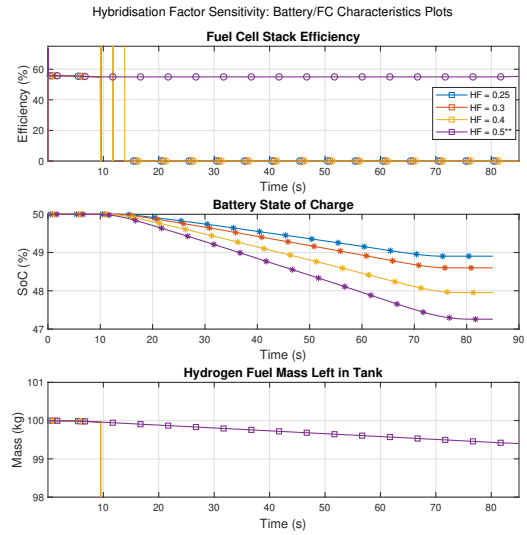

(c) Simulation Results for Battery/FC related outputs

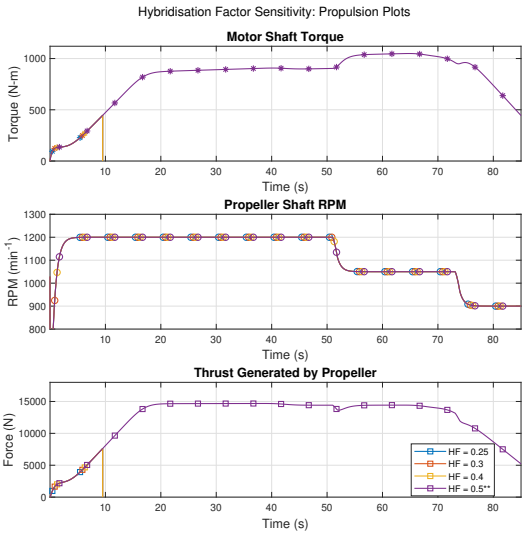

(d) Simulation Results for Propulsion related outputs

Figure B.8: Hybridization factor Sensitivity Analysis Graphs

C

Example Input to DIGITAL DATCOM

To determine the lift and drag coefficients of the Dash 8-Q300 aircraft, an input file was prepared for use with the DIGITAL DATCOM Software. Example contents of the input file is as follows :

```
$FLTCON NMACH=1.0, MACH=0.1457, VINF=1.1157E3,
NALPHA=20.0,ALSCHD=-6.0,-5.5,-5.0,-4.5,-4.0,-3.5,-3.0,-2.5,-2.0,
-1.5,-1.0,-0.5,0.0,0.5,1.0,1.5,2.0,2.5,3.0,3.5,
RNNUB=4.1005E6,NALT=1.0, ALT=188.0,
WT=38000.0, GAMMA=9.0, LOOP=1.0$
$OPTINS SREF=605.0, CBARR=7.125, BLREF=90.0$
$SYNTHS XCG=33.2, ZCG=0.0, XW=33.167, ZW=5.232, ALIW=1.71, XH=75.583,
ZH=19.393, ALIH=0.0, XV=62.75, ZV=0.0$
$BODY NX=11.0, X=0.5,5.0,10.0,11.0,50.0,55.0,60.0,70.0,75.0,78.0,78.25,
S=0.7854,25.9672,56.7450,61.1673,61.1673,53.4562,38.4845,15.9043,8.2958,
1.2272,0.0001$
NACA-W-6-66-418
$WGPLNF CHRDTP=3.9167,SSPNOP=32.08, SSPNE=40.5, SSPN=45.0, CHRDBP=8.333,
CHRDR=8.333, SAVSI=0.0, SAVSO=5.34, CHSTAT=0.25,DHDADI=2.5,TYPE=1.0$
NACA-H-4-0012
$HTPLNF CHRDTP=4.9167, SSPNE=12.5, SSPN=13.0, CHRDR=6.667, SAVSI=7.96,
DHDADI=0.0,CHSTAT=0.25, TYPE=1.0$
NACA-H-4-0015
$VTPLNF CHRDTP=9.0, SSPNE=13.625, SSPN=20.445,
CHRDR=15.0, SAVSI=36.267,CHSTAT=0.25, DHDADI=0.0, TYPE=1.0$
$PROPWR NENGSP=2.0, PHALOC=27.0, PHVLOC=9.75, PRPRAD=6.5,
NOPBPE=4.0, YP=12.916$
$SYMFLP FTYPE=1.0, NDELTA=1.0, DELTA=15.0$
CASEID DASH 8 Q300 GO AROUND SCHIPHOL
SAVE
BUILD
PLOT
NEXT CASE
```

The FLTCON section of the file specifies the testing flight conditions, including the aircraft's Mach number, speed of sound, Reynolds number, altitude, and 20 angle of attack values ranging from -6 to 3.5 degrees. Additionally, the weight and flight path angle of the aircraft are provided.

In the OPTINS section, details such as wing area, wing span, and aerodynamic chord of the aircraft are specified. The SYNTHS and BODY sections contain estimated geometric points of the aircraft, including the center of gravity point, wing height, and tail height.

"NACA-W-6-66-418" is provided as a rough reference for the wing airfoil, with additional information on wing geometry in section WGPLNF. Similarly, "NACA-H-4-0012" and section HTPLNF provide rough estimations for the horizontal stabilizer, while "NACA-H-4-0015" and section VTPLNF provide rough estimations for the vertical stabilizer.

Section PROPWR includes information on the propeller characteristics, such as diameter, height, and number of blades. Lastly, section SYMFLP contains details on the flap condition, set at 15 degrees here.